2010

Simulation Of Photochromic Compounds Using Density Functional Theory Methods

Pansy Patel
University of Central Florida

SIMULATION OF PHOTOCHROMIC COMPOUNDS USING DENSITY FUNCTIONAL THEORY METHODS

by

PANSY DHILON PATEL

M.Sc. Panjab University, INDIA 2003

A dissertation submitted in partial fulfillment of the requirements
for the degree of Doctor of Philosophy
in the Department of Chemistry
in the College of Sciences
at the University of Central Florida
Orlando, Florida

Spring term

2010

Major Professor: Artëm E. Masunov

ABSTRACT

This Thesis describes the systematic theoretical study aimed at prediction of the essential properties for the functional organic molecules that belong to diarylethene (DA) family of compounds. Diarylethenes present the distinct ability to change color under the influence of light, known as photochromism. This change is due to ultrafast chemical transition from open to closed ring isomers (photocyclization). It can be used for optical data storage, photoswitching, and other photonic applications. In this work we apply Density Functional Theory methods to predict 6 of the related properties: (i) molecular geometry; (ii) resonant wavelength; (iii) thermal stability; (iv) fatigue resistance; (v) quantum yield and (vi) nanoscale organization of the material.

In order to study sensitivity at diode laser wavelengths, we optimized geometry and calculated vertical absorption spectra for a benchmark set of 28 diarylethenes. Bond length alternation (BLA) parameters and maximum absorption wavelengths (λ_{max}) are compared to the data presently available from X-ray diffraction and spectroscopy experiments. We conclude that TD-M05/6-31G*/PCM//M05-2X/6-31G*/PCM level of theory gives the best agreement for both the parameters. For our predictions the root mean square deviation (RMSD) are below 0.014 Å for the BLAs and 25 nm for λ_{max}. The polarization functions in the basis set and solvent effects are both important for this agreement.

Next we consider thermal stability. Our results suggest that UB3LYP and UM05-2X functionals predict the activation barrier for the cycloreversion reaction within 3-4

kcal/mol from experimental value for a set of 7 photochromic compounds. We also study thermal fatigue, defined as the rate of undesirable photochemical side reactions. In order to predict the kinetics of photochemical fatigue, we investigate the mechanism of by-product formation. It has been established experimentally that the by-product is formed from the closed isomer; however the mechanism was not known. We found that the thermal by-product pathway involves the bicyclohexane (BCH) ring formation as a stable intermediate, while the photochemical by-product formation pathway may involve the methylcyclopentene diradical (MCPD) intermediate. At UM05-2X/6-31G* level, the calculated barrier between the closed form and the BCH intermediate is 51.2 kcal/mol and the barrier between the BCH intermediate and the by-product 16.2 kcal/mol.

Next we investigate two theoretical approaches to the prediction of quantum yield (QY) for a set of 14 diarylethene derivatives at the validated M05-2X/6-31G* theory level. These include population of ground-state conformers and location of the pericycylic minimum on the potential energy surface 2-A state.

Finally, we investigate the possibility of nanoscale organization of the photochromic material based on DNA template, as an alternative to the amorphous polymer matrix. Here we demonstrate that Molecular Dynamic methods are capable to describe the intercalation of π-conjugated systems between DNA base pairs and accurately reproduced the available photophysical properties of these nanocomposites.

In summary, our results are in good agreement with the experimental data for the benchmark set of molecules we conclude that Density Functional Theory methods could

be successfully used as an important component of material design strategy in prediction of accurate molecular geometry, absorption spectra, thermal stability of isomers, fatigue resistance, quantum yield of photocyclization and photophysical properties of nanocomposites.

This thesis is dedicated to my grandmother and my parents

ACKNOWLEDGMENTS

I take this opportunity with immense pleasure to express my deep sense of gratitude to Dr. Artëm E. Masunov, Assistant Professor, NanoScience Technology Center and Department of Chemistry, University of Central Florida, my thesis supervisor, for his inspiring guidance and excellent supervision to carry out this research. His inspiration, valuable discussion, cooperation and constant encouragement, which resulted in this work, will remain a lifelong memory. I thank him for his excellent guidance, sincere advice, understanding and unstinted support during all the tough times of my Ph. D. life. I do sincerely acknowledge the freedom rendered to me by him for independent thinking, planning and executing the research. I consider very fortunate for my association with him, which has given a decisive turn and a significant boost in my career.

I would like to thank Dr. Aniket Bhattacharya, Dr. Suren Tatulian, Dr. Lei Zhai, Dr. Andre Gesquiere and Dr. Robert Igarashi, my committee members, for the aspiring discussions and for their timely help and co-operation. I gratefully acknowledge the guidance, training, and support by Dr. Adrian E. Roitberg, Professor, Quantum Theory Project at University of Florida, in training me and teaching me the basics of Molecular Dynamics. Computational Facilities at i2lab and Stokes, UCF and Slater Lab, UF are gratefully acknowledged. Special thanks to all the senior post doctorate scholars, Dr. Ivan A. Mikhailov, Dr. Kyrill Suponitsky and Dr. Talgat Inaerbaev for their invaluable suggestions throughout my research in the lab.

I would like to thank my colleagues Satyender Goel, Shruba Gangopadhyay and Workalemahu Berhanu and undergraduate juniors Andrew, Andy, Richard, Ivan and Angel for maintaining a warm and cheerful atmosphere in the lab. They made working in the lab very enjoyable. Special thanks to my friends Chetak, Korina, Krishnaveni, Erin, Saral, Himanshu Saxena, and Pankaj who made my life memorable at UCF. I also thank my roommates Divya, Swati, Annapurna, Archana and Aishwarya for pleasant, accommodating, supportive and sociable environment. My regards to all my friends, Kishore, Abhijit, Sujit, Bojanna, Prabhu, Bala and all my well wishers.

It is my great pleasure to thank my parents who stood by me during all days of hardships and who shaped me to this status with their vision and selfless agenda in making me a person that I am today. My heartfelt gratitude to my grandmother, whom I miss everyday and who is an inspiration to me in all my endeavors. My special thanks to my little sister for always cheering me, my sister-in-law, brother-in-law and family for their support. I extend my acknowledgment to my parents-in-law, for their never-ending support and trust.

My special thanks to my husband, Dhilon for the care and cooperation throughout my research. For all his sacrifices and going through the same turmoil with patience and endurance during the preparation of thesis. Finally I thank Chairman, Department of Chemistry and Director, NanoScience Technology Center for providing infrastructural facilities to complete my work successfully. I am also thankful to NSF, for the financial assistance.

TABLE OF CONTENTS

LIST OF FIGURES

LIST OF TABLES

LIST OF ABBREVIATIONS

Abbreviation	Full Form
PM	Photochromic Material
DA	Diarylethene
CHD	1,2-cyclohexadiene
cZc-HT	1,3,5-hexatriene
FMO	Frontier Molecular Orbital
MO	Molecular Orbital
CAS	Complete Active Space
SCF	Self-Consistent Field
MP2	Second Order Møller-Plesset Perturbation Theory
IRD	Internal Relaxation Directions
DFT	Density Functional Theory
TD-DFT	Time-Dependent Density Functional Theory
CEO	Coupled Electronic Oscillator
AM1	Austin-Model 1
INDO/S	Intermediate Neglect of Differential Overlap/Screened
CIS	Configuration Interaction with Single substitution
RKS	Restricted Kohn-Sham
UKS	Unrestricted Kohn-Sham
BLA	Bond Length Alternation
NLO	Non-Linear Optics

HOMO	Highest Occupied Molecular Orbital
LUMO	Lowest Unoccupied Molecular Orbital
QY	Quantum Yield
MR-SCI	Multirefrence Single-excitation Configuration Interaction
GGA	Generalized Gradient Approximation
ADSIC	Averaged-Density Self-Interaction Correction
B3LYP	Becke, three-parameter, Lee-Yang-Parr hybrid functional
PBE0	Perdew, Burke and Ernzerhof zero GGA functional
NMR	Nuclear Magnetic Resonance
IR	Infra-Red
ESR	Electron-Spin Resonance
UV-Vis	UltaViolet -Visible
PCM	Polarizable Continuum Model
QY	Quantum Yield
HF	Hartree-Fock
WFT	Wave Function Theory
PM3	Parameterized Model number 3
ZINDO	Zerner's Intermediate Neglect of Differential Overlap
BMK	Boese-Martin functional for kinetics
M05-2X	Minnesota functional 2005 with double exact exchange
BLYP	Becke, Lee-Yang-Parr hybrid functional
TPSS	τ-dependent gradient-corrected functional of Tao, Perdew, Staroverov, and Scuseria

BHandHLYP	Becke, Lee-Yang-Parr Half-and-half Functional
SCRF	Self-Consistent Reaction Field
IEFPCM	Polarizable Continuum Model (PCM) using The Integral Equation Formalism variant
ZPE	Zero Point Vibrational Energies
SOMO	Singly Occupied Molecular Orbital

CHAPTER 1 INTRODUCTION

1.1 Introduction to Photochromism

Photochromism is a non-destructive process involving light initiated rearrangement of chemical bonds accompanied by the change in color and other properties. It often results in reversible transformation of a chemical species from open to closed ring isomers. The simplest example of photochromism is 1,2-cyclohexadiene (CHD) (closed isomer) and 1,3,5-hexatriene (cZc-HT) (open isomer) (**Figure 1.1**).

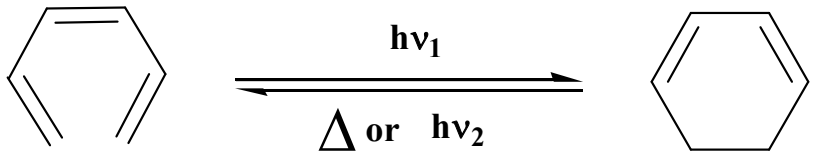

Figure 1.1: Photochromic reversible transformation of hexatriene (left) and cyclohexadiene (right).

The two isomers differ from one another not only in the absorption spectra but also in various physical and chemical properties such as molecular structure, refractive index, dielectric constant and oxidation-reduction potential.[1] The photoswitching in these compounds occurs through conrotatory electrocyclic mechanism Electrocyclic reactions are unimolecular processes which involve the exchange of π-bonds for ring-closing sigma-bonds. Woodward-Hoffmann rules[2] have been used to predict the final product formation of such reactions and the process is understood by the frontier molecular orbital theory (FMO). Accordingly, Upon heating, 1,3,5-hexatriene will undergo an

electrocyclic ring closure to give 1,3-cyclohexadiene (**Figure 1.1**). The correlation diagram for the mechanism of thermal and photochemical ring closure explains that in a thermally excited system, if the terminus of the Highest Occupied Molecular Orbital (HOMO) is superimposed upon the triene system, the end groups must rotate in a disrotatory manner to form the bond (**Figure 1.2a**). On the contrary, in the photoexcited system, the end groups conrotate to form the sigma bond (**Figure 1.2b**).

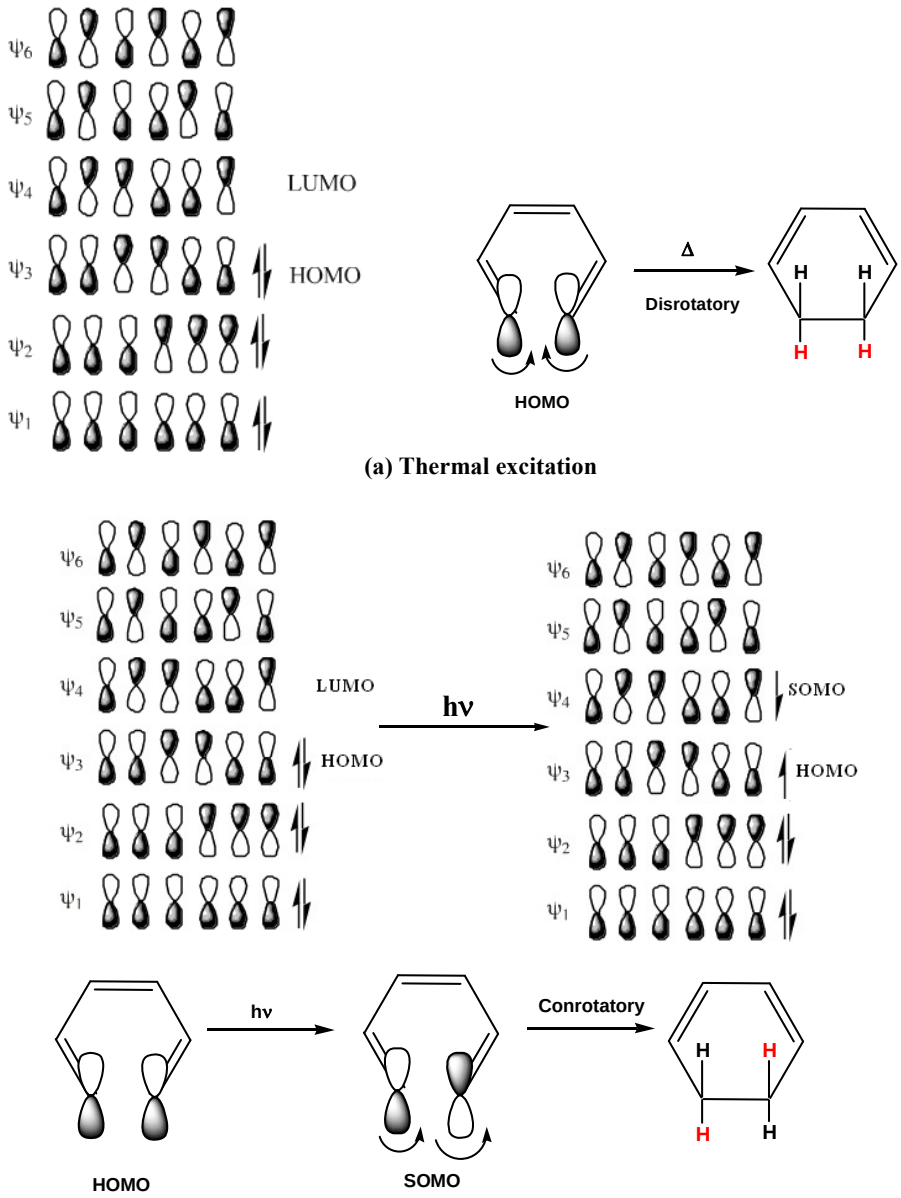

Figure 1.2: Orbital correlation diagrams according to Frontier Molecular Orbital theory depicting a: Thermal excitation and b: photochemical excitation in 1, 3, 5-hexatriene

Photochromic compounds or photochromic materials (PM) can be broadly classified into thermally reversible compounds (T-type or thermally unstable) and

thermally irreversible (P-type or thermally stable) compounds. Typical examples of T-type compounds are Azobenzene and Spiropyran; and Diarylethenes (DAs) and Fulgides belong to thermally irreversible P-type photochromic compounds (**Figure 1.3**). The instant property changes upon photoirradiation can be used in various optoelectronic devices such as optical memory, optical switching, displays and nonlinear optics. Irie and co-workers and the research group of Lehn[3-11] were among the first authors to investigate DAs as a potential candidate for photochromic applications (**Figure 1.3 (c)**). Diarylethenes are an important class of thermally irreversible PMs, which have been extensively investigated to estimate some of the above mentioned properties and their potential application as optical switches.[8, 9, 11-13] In the following project, we review the theoretical efforts directed at prediction of these properties

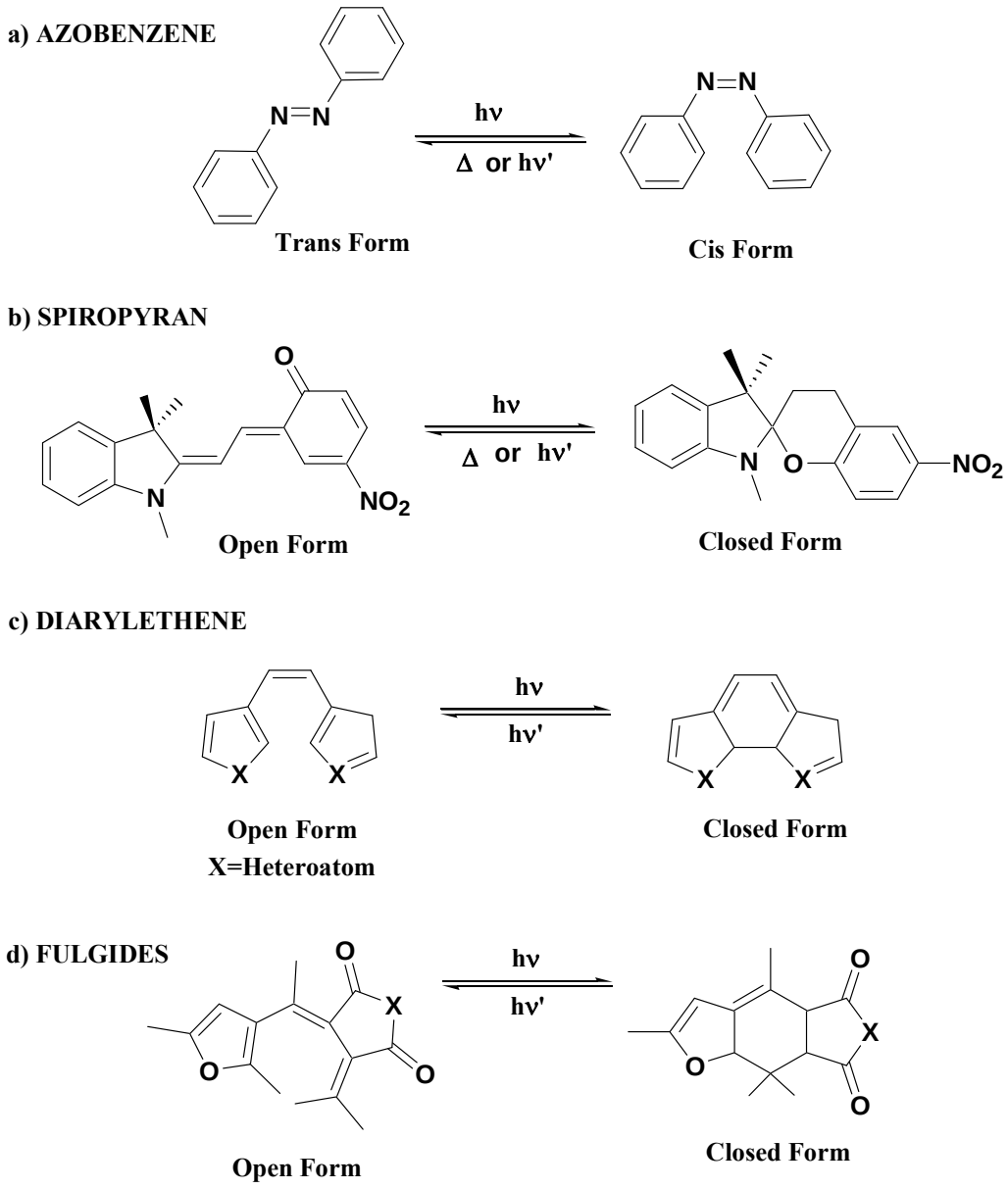

Figure 1.3: a,b: Thermally unstable (T-type) and c,d: thermally irreversible (P-type) photochromics.

The thermal stability of P-type compounds makes them promising materials in design of various optoelectronic devices such as optical memory, optical switching, displays and nonlinear optics. In order to be practically useful, the PM has to satisfy

certain requirements, including: a) Sensitivity at diode laser wavelengths; b) Thermal stability of both isomers; c) Fatigue resistance; d) Efficient photochromic reactivity: high sensitivity, rapid response; e) Non-destructive readout capability and f) High solubility in polymer matrices.[9]

1.2 Computational Studies of Photochromism in Diarylethenes

1.2.1 Thermal Stability

Thermal irreversibility stability of both closed and open isomers is an indispensible property for applications of DAs for optoelectronic devices. According to Irie *et al.*,[9, 14] the molecular design principle of thermally irreversible DAs is the heterocyclic aryl group. In particular to DAs, experiments have suggested that the thermal stability depends on the aryl group substitutions and it is their aromatic stabilization energies which allow conrotatory cycloreversion and hence make the closed ring isomer thermally unstable. It was found that in case of low aromatic stabilization aryl groups like furan, thiophene, selenophene or thiazole rings, the closed-ring isomers are thermally stable and do not return to the open-ring form isomers even at 80°C. While in case of pyrrole, indole, or phenyl rings, having high aromatic stabilization energies, the closed isomers are thermally unstable.[9, 14]

Over the past three decades, Irie and co workers have extensively worked on designing dual-mode optical molecular switches both experimentally[4-5, 12-26] and theoretically.[27-33] Lehn *et al.* [6-8, 34-36] have also synthesized PMs as potential molecular optical switches and investigated the thermal stability as a measure of their half-life time at elevated temperatures. The photoswitching in DAs occurs through conrotatory electrocyclic mechanism. This is a unimolecular stereoselective process and can be easily understood by the Woodward-Hoffmann rules.[37] According to these rules, conrotatory

and disrotatory cyclization proceeds along the pathways conserving different symmetry elements during which Molecular Orbitals (MOs) undergo continuous evolution. When occupied orbitals of the reactant evolve into the occupied orbitals of the product, the potential energy barrier is fairly low, and reaction is thermally allowed. When the occupied orbitals of the reactant evolve into the vacant orbitals of the product and *vice versa*, the reaction is photochemically allowed, and thermally forbidden (have a large activation barrier in the ground state). Cycloreversion reaction in diarylethenes is an example of such thermally forbidden reaction.

The conclusions from Woodward-Hoffmann rules have been confirmed by *ab initio* quantum chemical calculations. In particular, a number of studies were published on the photochemical conversion in the model system of cyclohexadiene (CHD) and 1,3,5-hexatriene (cZc-HT). A complete mechanistic picture of the photochemical ring opening and ring closure occurring on the $^2A_1$ and $^1B_2$ surface after CHD photoexcitation has been drawn by Celani *et al.* [38, 39] using correlated wave function theory methods (complete active space self-consistent-field (CAS-SCF) and CAS-SCF/MP2). Theoretical investigation of the CHD/cZc-HT photochemical interconversion have also been performed at CASPT2[40] and multirefrence- single-excitation configuration interaction (MR-SCI)[41] theory levels to investigate the potential energy surface, find the reaction path, and transition probabilities. Garavelli *et al.* [42] employed the algorithm of steepest decent to compute initial relaxation directions (IRD) from the tip of the conical intersection to predict the mechanism of the product formation for the CHD/cZc-HT photochemical interconversion. Sakai *et al.* [43] calculated the potential energy surfaces for

the electrocyclic reactions of cZc-HT with different *ab initio* molecular orbital methods. The activation energies of two electrocyclic reaction pathways (conrotatory, 47.62 kcal/mol and disrotatory, 37.24 kcal/mol) for cZc-HT were reported at CASPT2/6-311+G** level. Since the latter mechanism allowed by orbital symmetry has a lower energy barrier, the reactant and product with C_s symmetry are unstable. The conrotatory mechanism with a higher energy barrier leads to stable reactant and product with C_2 symmetry, so it is the preferable pathway for ring closure. Unfortunately, the correlated wavefunction theory methods are very demanding computationally, and cannot be performed on the larger molecules of practical interest. For those molecules, semiempirical and Time-Dependent Density Functional Theory (TD-DFT) studies had been reported.

Nakamura and Irie[20] carried out semiempirical calculations on the three types of molecular systems (furyl, pyrrolyl, and thienyl), and have concluded that the energy difference between the ring closed and open forms controls the ease of their conversion as well as thermal stability. They observed that in the case of the thienyl derivative, the ground-state energy difference between the open and closed forms is the lowest, compared to furyl and pyrrolyl derivatives and concluded that the energy barrier in the case of the thienyl derivative would be the largest, which makes cycloreversion reaction less likely.

Semiempirical Hamiltonian Intermediate Neglect of Differential Overlap/Screened (INDO/S) in combination with Coupled Electronic Oscillator (CEO)

formalism was used by Tretiak, Mukamel, and others to study the excited state dynamics for electrocyclic reactions in DA derivatives.[44,45] They were able to explain the slow conversion of the precursor for the ring-opening process that corresponds to the pericyclic minimum on the excited state potential surface into the ground state products by the presence of the potential barrier, separating this minimum from the conical intersection to the ground state.[46]

Another semiempirical study was reported by Cho *et al.*[47] They investigated the thermal stability of 2,3-bis(2,4,5-trimethyl-3-thienyl)maleic anhydride P-type photochromic compound. Both closed form and three open forms were optimized: one parallel and two antiparallel ones. Restricted AM1 calculations were performed to calculate the ground state thermal stability and concluded the energy barrier heights for cyclization and ring-opening are 226kJ/mol and 160kJ/mol respectively. For the S1 state, configuration interaction with single substitutions (CIS) was used. Energy barriers at the S1 state were found to be much lower (33 kJ/mol for cyclization and 13 kJ/mol for the ring-opening). Due to the low accuracy of semiempirical method, no λ_{max} prediction was attempted.

One has to note, however, that TD-DFT has been found to encounter difficulties in the description of potential surfaces in the vicinity of conical intersections.[48] The source of these problems was traced to the poor description of the reference ground state near the pericyclic minimum within the restricted Kohn-Sham (RKS) formalism.[49] The Kohn-Sham formalism of DFT was developed for non-degenerate cases; it breaks down

for systems with strong diradical character and degeneracy of the electronic levels, which happens to be the case for conical intersections. However, static (also called left-right) electron correlation can be taken into account by introducing different orbitals for different spin. This approach, often referred to as broken symmetry, or unrestricted Kohn-Sham formalism (UKS) is known to yield a qualitatively correct description of the bond breaking.[50] During the course of this research project, we could isolate a set of 7 photochromic DA derivatives, where experimental data on the thermal cycloreversion were available. We have employed UKS approach to investigate the activation barriers for cycloreversion of this set of compounds and predict the Thermal Stability of PM in chapter 3 (section 3.2).

1.2.2 Fatigue Resistance

Along with thermal stability, fatigue resistance is yet another important property of the thermally irreversible photochromic compounds for their potential applications as optoelectronic devices. Irie *et al.* [12] investigated the mechanism of fatigue resistance and observed the decline in the absorbance of 1,2-bis(2-methyl-5-phenyl-3-thienyl)perfluorocyclopentene after only a few cycles while the absorbance of its methylated derivative remained constant even after 800 cycles (10^4 cycles for a good candidate). The formation of a colored byproduct was suggested as the possible reason for the decrease in absorbance. They suggested that the methyl substituents at the 4- and 4′-positions are considered to prevent rearrangement of the thiophene rings to the six-membered condensed ring. The authors later also isolated similar two six-membered heterocyclic ring containing byproduct in another compound 1,2-Bis(2,5-dimethyl-3-thienyl)perfluorocyclopentene[51] and suggested two different probable schemes for the mechanistic formation based on the diradical recoupling process formulated by Celani *et al*.[38] In both the cases it was clear that the byproduct formation takes place from the closed isomer since they observed decrease in the yield of the open form. We investigate the reaction mechanism for byproduct formation in chapter 3 (section 3.3).[52]

1.2.3 Molecular Geometry

The distinctly different positions of the maxima on the absorption spectra of the open and closed forms of the PMs determine the differences in their color and had been attributed to the length of the conjugated chain in these systems. In the case of photochromic diarylethenes (**Figure 1.4**), the open form has twisted π-system and is colorless while the closed form with nearly planar π-system is conjugated and colored.

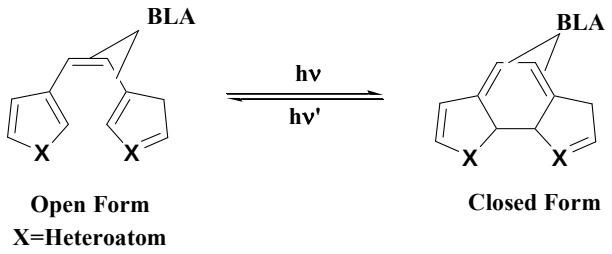

Figure 1.4: Isomeric forms of thermally irreversible (P-type) Diarylethenes depicting the Bond Length Alternation (BLA).

Since geometry is critically important for accurate prediction of electronic spectra, this section is focused on the geometrical aspect of PMs. An important geometrical parameter of any conjugated system is the bond length alternation (BLA), defined as the difference between the lengths of the single and double bonds. For linear chain oligomers it has been shown that the band gap, nonlinear optical (NLO) properties, excitation energies, etc. strongly depend on BLA.[53-58] Thus, the accurate description of the ground state geometry is essential to predict the optical properties of photochromic diarylethenes. The theoretical predictions of BLA for several series of conjugated

oligomers were conducted by Jacquemin and co-workers [59-66] in the past decade. They performed *ab initio* calculations on mainly acyclic conjugated systems and concluded that (1) Second-order Møller Plesset Second order (MP2) values are in good agreement with higher-order electron-correlated wavefunction approaches that include triple excitations; (2) basis set effects are relatively limited, and polarized double-ζ basis is sufficient, at least for DFT calculations; (3) all conventional Generalized Gradient Approximation (GGA) and meta-GGA provide similar BLA, that are much too small and too rapidly decreasing with the chain lengthens; (4) hybrid functionals correct this trends but to a small extent so that quantitative agreement with MP2 values is still far away; (5) the conformation differences do not alter these three latter conclusions; (6) self-interaction corrections included via the averaged-density self-interaction correction (ADSIC) scheme improves BLA evolution obtained by the conventional DFT approaches. For medium-size oligomers ADSIC predicts BLA in better agreement with MP2, than B3LYP or PBE0. However, diarylethene derivatives had not been investigated in that respect. We report our benchmarking study of BLA parameter in the series of PM in chapter 3 (section 3.1).[67]

1.2.4 Sensitivity at Diode Laser Wavelengths

The distinctive absorption spectrum of the two isomeric forms of the photochromic compounds is an essential property of investigation. Experimental absorption spectra (λ_{max}) of such compounds are determined in different solvents for different derivatives. Recently, Nakamura *et al.*[3] reviewed the theoretical studies on photochromic systems aimed at understanding of experimental spectroscopic data (NMR, Raman, IR and ESR). They did not consider the UV-Vis spectra, however. The visible spectra of the closed-ring structures were predicted by Uchida *et al.*[23] using semi-empirical methods, which lack the accuracy.

In their pioneering TD-DFT study Majumdar *et al.* [68] investigated dithienylethene derivatives as potential NLO photoswitches. They reported the open and closed structures, stability, electronic absorption spectra, and hyperpolarizabilities. Other DFT studies soon followed. Jacquemin, Perpete, *et al.* [60,63,64,61,69] investigated several sets of DA derivatives and found that TD-DFT treatment gives much more accurate results than semiempirical approach. The absorption spectra were predicted, while implicitly taking bulk solvent effects into account with polarizable continuum model (PCM). Their work however was restricted only to the closed-ring isomers. Similar studies were extended to both closed and open-ring isomers.[70,66,71]

Chen *et al.*[70] used TD-B3LYP/6-31G* theory level to predict the absorption spectra of closed isomers of 6 different diarylmaleic anhydrides. Perrier *et al.*[66] designed 10 photochromic diarythienyls with different conjugated substitution at the 5 and 5′ position of the thiophene ring and investigated the substituent effect on the optical properties of both the closed-ring and open-ring isomers at B3LYP/6-31G theory level. For both closed and open forms the photoreactive state was the lowest excitation and to have the HOMO-LUMO nature in most cases. Its λ_{max} were predicted and correlated to the HOMO-LUMO energy gap and to the BLA parameter. They concluded that conjugated substituents stabilize LUMO and decrease BLA. However, in most of the cases considered the lowest excitation has low oscillator strength and does not correspond to the brightest optical transition. No comparison with experimental data was reported.

Laurent *et al.*[71] investigated 6 oxazole-diarylethenes (both closed and open forms) using TD-PBE0/6–311+G(2d,p)/PCM//PBE0/6–311G(d,p)/PCM. The theoretical λ_{max} for the brightest states were in a good agreement with experiment. The authors concluded that the larger the experimental λ_{max}, the larger the theory/experiment discrepancy (in nm), and introduced the linear scaling correction to predict the accurate λ_{max}. Direct correlation was reported also between experimental λ_{max} and the HOMO-LUMO gap for the 29 dithienylazoles (closed forms only). Recently, the authors also investigated the effect of substituents on the optical spectra by changing the heteroatom in the aryl ring and also the substituents attached to the aryl ring.[72] They correlated the sensitivity of the closed isomer to the heteroatom substitution in particular to maleic anhydride derivatives of DA. Theoretical investigations on thermally irreversible PMs have also been

conducted by other groups in order to predict other ground-state properties.[47, 68, 73,69] For the current project, we benchmark different Density Functionals for accurate predictions of λ_{max} for both the closed and open isomeric forms of a set of 28 DA derivatives in chapter 3 (section 3.1).[67]

1.2.5 Efficient Photochromic Reactivity and Quantum Yield

Diarylethenes (DAs) are currently under investigation to be used in optoelectronic devices such as optical memories and optical switches.[9] For such applications, large photocyclization quantum yields (QYs) is required. In case of the rewritable optical memory media, the destruction of memory due to irradiation is necessary, so the QY (if wavelength-dependent) should be zero at a certain wavelength during irradiation so that we can write on the device and we can erase the data by the light where the QY is non-zero. There is a scarcity of experimental information on the excited states and the QY is dependent on the excitation of the PM. Therefore the control on the QYs is the most difficult subject. There are a number of experimental studies on the QY of DAs. [9, 11, 13, 14, 24, 26, 74-78] From the time-resolved experimental studies over the years, it has been established that both cyclization and cycloreversion processes take place in the picoseconds time domain.[46, 79-83] It has also been shown that these transformations do not involve the triplet states. Miyasaka *et al.*[84] observed enhancement of the quantum efficiency of the cycloreversion process due to the stepwise multiphoton process.

The quantum yields of DAs have been extensively studied and it is well-known that it is dependent on the substituent attached to the aryl group. [9, 22, 77] The open form of the DAs has two conformations parallel (mirror symmetry) and antiparallel (C_2 symmetry) and it is the latter which can only proceed to photocyclization. The population ratio of the two conformers in general is 1:1; thus the cyclization quantum yield (QY)

cannot exceed 0.5. Almost all photoexcited antiparallel conformations undergo the cyclization reaction. Irie and co-workers suggested introduction of bulky substituents to the thiophene rings, which should increase the ratio of the antiparallel conformation and in turn is expected to increase the QY.[85] Stellaci *et al.*[86] found that the QY increases by incorporating the dithienylethenes into a polymer backbone which is due to the fact that only the antiparallel conformation can exist in the polymer backbone. The inclusion of DAs in confined space is also another approach to increase the antiparallel conformation ratio and hence the QY. [9]

A number of theoretical approaches have been employed to understand the cyclization/ring-opening mechanism in some of the DA derivatives. Cho *et al.*[47] performed semiempirical AM1 calculations on 2,3-bis(2,4,5-trimethyl-3-thienyl)maleic anhydride on the C_2 symmetry constraint. The first excited state was calculated using, configuration interaction with single substitutions (CIS). They suggested that in the S_1 state, the photochromic isomers can easily interconvert over the relatively low energy barrier, which is not possible in the S_0 state, suggesting that the absorption of a photon generated a conrotation of the thienyl rings.

Asano *et al.*[29] studied the photochromic cyclization reactions for 1,2-bis (2-methyl-5-phenyl-3-thienyl) perfluorocyclopentene and 1,2-bis (2-methyl-1-benzothiophen-3-yl) perfluorocyclopentene using DFT calculations. They used canonical Boltzmann statistics for studying the population distribution of the stable structures in solution and correlated it to the quantum yield. The difference of the QYs in crystals and

hexane solution for the these molecules was explained based on their ground state geometries, the relaxation from the Franck–Condon states, the shapes of the potential energy surfaces of the ground state, and the geometry change by the large amplitude motions. They compared the cyclization reactions in crystals versus in solution.

To better understand the reaction mechanism of the proposed stepwise multiphoton process in the cycloreversion process, attempts have been made to project a detailed potential energy surface (PES) in the lowest excited states of some of the photochromic compounds using theoretical methods. Guillaumont and co-workers[30] performed *ab initio* complete active space self-consistent-field (CASSCF) calculations under the C_2 symmetry constraint for some dithienylethene derivatives. They correlated the experimental QY with different properties like calculated energy difference, optimized C—C bond lengths and the natural orbital occupation number of the σ* orbital of the 2A excited state closed isomer. Based on their calculations, Nakamura *et al.*[87] suggested that the thermodynamic stability of the various energy minima on the ground state is primarily important for the cyclization reactions, while a detailed PES analysis of the excited state profile and the locations of the conical intersections are important for the cycloreversion reactions. We test different correlation schemes for QY prediction in chapter 3 (section 3.4)

1.2.6 DNA Templated Nanostructured Photochromic Materials

The association of molecular switches and biomolecules can be advantageous for several reasons. Several studies demonstrating the use of DA based photochromic compounds to reversibly control biochemical reactivity have been done recently. Branda and co-workers [88] have used sulfonamide and copper based dithienylethene derivatives as inhibitors to regulate human carbonic anhydrase I (hCAI) activity. The use of visible light to activate the photoresponsive inhibitor not only allow them to control and reversibility enhance the activity of the enzyme, but it also allows better penetration into the tissue and reduce the amount of damage caused by higher energy UV light. The researchers also investigated the use of PMs in modulation of lewis acidity of Boron and regulation of Bergman cyclization.[88-90] In yet another study it was shown that the photochromic dithienylethene regulates paralysis in *Caenorhabditis elegans*, a simple model nematode. This biological photoswitching suggested that dithienylethene can be processed by living organisms.[91]

Here we will focus on photon-mode rewritable optical memory media in order to develop thermally irreversible PMs. Generally, the photochromic reactions are done in polypeptide matrix films. Recently, Saito *et al.*[92] proposed intercalation of the photochromic compounds between the base pairs of DNA. Their studies involved experimental preparation of open isomer of the diarylethene derivative intercalated in stretched DNA followed by photoirradiation in both parallel as well as perpendicular

direction to the stretched film. The absorbance studies suggested that the DA derivative lies perpendicular to the stretched direction of the DNA film, with probability of one of the aromatic moieties intercalated between the base pairs. Large change in reversible optical rotation was observed and attributed to the interaction of the closed isomer with the chiral liquid-crystalline-like ordered structure of DNA. This study holds a great promise to optimize material properties, (such as photocyclization QY) not by chemical modification of the chromophore but templating and other ways to control material nanostructures.

In order to design DNA intercalated PMs, one needs to select a suitable computational method and validate it against experimental observations. While the data on photochromic chromophores intercalated in DNA are limited, a large body of experimental data is collected on aromatic drug molecules intercalated in DNA. The aromatic drug is cationic in nature while the DNA is polyanionic in aqueous isotonic solution, thus implying the involvement of weak electrostatic attractive forces. Due to planar structure of the drug, it may easily slide into the hydrophobic environment found between the base pairs.

Many simulations have been done to investigate both structural features and energetics of DNA intercalation. Rodgers *et al.* performed molecular dynamics calculations to study multiple DNA binding modes of Anthracene-9-Carbonyl-N Spermine (a spermine derivative terminally substituted with an anthracene moiety) in the poly(dAdT)$_2$ complex[93]. They incorporated preferred binding orientations and locations

(minor groove, major groove, backbone, etc.), base sequence selectivity, association/dissociation kinetics, equilibrium constants for complex formation, etc. They deduced that the ligand can intercalate from both the minor groove and the major groove. In contrast, intercalation with poly(dGdC)$_2$ probably occurs only from the major groove. The studies also suggested a sequential nature to the binding of the ligand to calf thymus DNA, with GC-rich sites being occupied first. More recently Mukherjee *et al.,* [94] performed simulation studies of the intercalation pathway, free energy and structural changes owing to DNA intercalation by anticancer duanomycin drug. The results pointed to a mechanism where the drug first binds to the minor groove and then intercalates into the DNA in an activated process. In chapter 3 (section 3.5), we benchmark predictive capabilities of Molecular Dynamics Simulations in experimentally studied case of spermine bound anthracene DNA intercalators.

1.3 References

1. Bouas-Laurent, H.; Durr, H., Organic photochromism. *Pure and Applied Chemistry* **2001,** 73, (4), 639-665.
2. Hoffmann, R.; Woodward, R. B., Selection rules for concerted cycloadditon reactions. *Journal of the American Chemical Society* **1965,** 87, (9), 2046-&.
3. Nakamura, S.; Yokojima, S.; Uchida, K.; Tsujioka, T.; Goldberg, A.; Murakami, A.; Shinoda, K.; Mikami, M.; Kobayashi, T.; Kobatake, S.; Matsuda, K.; Irie, M., Theoretical investigation on photochromic diarylethene: A short review. *Journal of Photochemistry and Photobiology a-Chemistry* **2008,** 200, (1), 10-18.
4. Yamaguchi, T.; Takami, S.; Irie, M., Photochromic properties of 1,2-bis (6-substitute-2-methyl-1-benzofuran-3-yl) ethene derivatives. *Journal of Photochemistry and Photobiology a-Chemistry* **2008,** 193, (2-3), 146-152.
5. Yamaguchi, T.; Uchida, K.; Irie, M., Photochromic properties of diarylethene derivatives having benzofuran and benzothiophene rings based on regioisomers. *Bulletin of the Chemical Society of Japan* **2008,** 81, (5), 644-652.
6. Gilat, S. L.; Kawai, S. H.; Lehn, J. M., Light-triggered electrical and optical switching devices. *Journal of the Chemical Society-Chemical Communications* **1993**, (18), 1439-1442.
7. Gilat, S. L.; Kawai, S. H.; Lehn, J. M., Light-triggered electrical and optical switching devices. *Molecular Crystals and Liquid Crystals Science and Technology Section a-Molecular Crystals and Liquid Crystals* **1994,** 246, 323-326.
8. Gilat, S. L.; Kawai, S. H.; Lehn, J. M., Light-triggered molecular devices - photochemical switching of optical and electrochemical properties in molecular wire type diarylethene species. *Chemistry-a European Journal* **1995,** 1, (5), 275-284.
9. Irie, M., Photochromism: Memories and switches - introduction. *Chemical Reviews* **2000,** 100, (5), 1683-1683.
10. Irie, M.; Mohri, M., Thermally irreversible photochromic sysytems- reversible photocyclization of diarylethene derivatives. *Journal of Organic Chemistry* **1988,** 53, (4), 803-808.
11. Nakayama, Y.; Hayashi, K.; Irie, M., Thermally irreversible photochromic systems - reversible photocyclization of nonsymmetrical diarylethene derivatives. *Bulletin of the Chemical Society of Japan* **1991,** 64, (3), 789-795.
12. Irie, M.; Lifka, T.; Uchida, K.; Kobatake, S.; Shindo, Y., Fatigue resistant properties of photochromic dithienylethenes: By-product formation. *Chemical Communications* **1999**, (8), 747-748.
13. Kobatake, S.; Shibata, K.; Uchida, K.; Irie, M., Photochromism of 1,2-bis(2-ethyl-5-phenyl-3-thienyl)perfluorocyclopentene in a single-crystalline phase. Conrotatory thermal cycloreversion of the closed-ring isomer. *Journal of the American Chemical Society* **2000,** 122, (49), 12135-12141.
14. Irie, M.; Mohri, M., Thermally irreversible photochromic systems - reversible photocyclization of diarylethene derivatives. *Journal of Organic Chemistry* **1988,** 53, (4), 803-808.
15. Irie, M., Photochromism of diarylethene single crystals and single molecules. *Molecular Crystals and Liquid Crystals* **2005,** 430, 1-+.
16. Kobatake, S.; Matsumoto, Y.; Irie, M., Conformational control of photochromic reactivity in a diarylethene single crystal. *Angewandte Chemie-International Edition* **2005,** 44, (14), 2148-2151.
17. Kobatake, S.; Uchida, K.; Tsuchida, E.; Irie, M., Single-crystalline photochromism of diarylethenes: Reactivity-structure relationship. *Chemical Communications* **2002**, (23), 2804-2805.
18. Kobatake, S.; Yamada, T.; Uchida, K.; Kato, N.; Irie, M., Photochromism of 1,2-bis(2,5-dimethyl-3-thienyl)perfluorocyclopentene in a single crystalline phase. *Journal of the American Chemical Society* **1999,** 121, (11), 2380-2386.
19. Matsuda, K.; Irie, M., Diarylethene as a photo switching unit. *Journal of Photochemistry and Photobiology C-Photochemistry Reviews* **2004,** 5, (2), 169-182.
20. Nakamura, S.; Irie, M., Thermally irreversible photochromic systems - a theoretical-study. *Journal of Organic Chemistry* **1988,** 53, (26), 6136-6138.

21. Saita, K.; Kobatake, S.; Fukaminato, T.; Nanbu, S.; Irie, M.; Sekiya, H., Raman spectroscopic study on isomers of photochromic 1,2-bis(2,5-dimethy1-3-thienyl) perfluorocyclopentene in crystal and stability of the closed-ring forms in the open-ring forms. *Chemical Physics Letters* **2008,** 454, (1-3), 42-48.
22. Uchida, K.; Kido, Y.; Yamaguchi, T.; Irie, M., Thermally irreversible photochromic systems. Reversible photocyclization of 2-(1-benzothiophen-3-yl)-3-(2 or 3-thienyl)maleimide derivatives. *Bulletin of the Chemical Society of Japan* **1998,** 71, (5), 1101-1108.
23. Uchida, K.; Nakamura, S.; Irie, M., Thermally irreversible photochromic systems - substituent effect on the absorption wavelength of 11,12-dicyano-5a,5b-dihydro-5a,5b-dimethylbenzo(1,2-b-6,5-b')bis[1]benzo thiophene. *Bulletin of the Chemical Society of Japan* **1992,** 65, (2), 430-435.
24. Uchida, K.; Nakayama, Y.; Irie, M., Thermally irreversible photochromic systems - reversible photocyclization of 1,2-bis(benzo[b]thiophen-3-yl)ethene derivatives. *Bulletin of the Chemical Society of Japan* **1990,** 63, (5), 1311-1315.
25. Yamada, T.; Kobatake, S.; Irie, M., Single-crystalline photochromism of diarylethene mixtures. *Bulletin of the Chemical Society of Japan* **2002,** 75, (1), 167-173.
26. Yamada, T.; Muto, K.; Kobatake, S.; Irie, M., Crystal structure-reactivity correlation in single-crystalline photochromism of 1,2-bis(2-methyl-5-phenyl-3-thienyl)perfluorocyclopentene. *Journal of Organic Chemistry* **2001,** 66, (18), 6164-6168.
27. Abe, Y.; Okada, S.; Horii, T.; Nakao, R.; Irie, M., Mndo-pm3 mo studies on the thermal enantiomerization of 1 ',3 ',3 '-trimethyl-6-nitrospiro[2h-l-benzopyran-2,2 '-indoline]. *Molecular Crystals and Liquid Crystals* **2000,** 345, 419-424.
28. Asano, Y.; Murakami, A.; Kobayashi, T.; Goldberg, A.; Guillaumont, D.; Yabushita, S.; Irie, M.; Nakamura, S., Theoretical study on the photochromic cycloreversion reactions of dithienylethenes; on the role of the conical intersections. *Journal of the American Chemical Society* **2004,** 126, (38), 12112-12120.
29. Asano, Y.; Murakami, A.; Kobayashi, T.; Kobatake, S.; Irie, M.; Yabushita, S.; Nakamura, S., Theoretical study on novel quantum yields of dithienylethenes cyclization reactions in crystals. *Journal of Molecular Structure-Theochem* **2003,** 625, 227-234.
30. Guillaumont, D.; Kobayashi, T.; Kanda, K.; Miyasaka, H.; Uchida, K.; Kobatake, S.; Shibata, K.; Nakamura, S.; Irie, M., An ab initio mo study of the photochromic reaction of dithienylethenes. *Journal of Physical Chemistry A* **2002,** 106, (31), 7222-7227.
31. Uchida, K.; Guillaumont, D.; Tsuchida, E.; Mochizuki, G.; Irie, M.; Murakami, A.; Nakamura, S., Theoretical study of an intermediate, a factor determining the quantum yield in photochromism of diarylethene derivatives. *Journal of Molecular Structure-Theochem* **2002,** 579, 115-120.
32. Yoshioka, Y.; Irie, M., Ab initio study of 3-furyl fulgide .1. Molecular structures and relative stabilities of three isomers. *Electronic Journal of Theoretical Chemistry* **1996,** 1, 183-190.
33. Yoshioka, Y.; Irie, M., Ab initio study of 3-furyl fulgide .2. Substituent effects on photochemical reactions. *Electronic Journal of Theoretical Chemistry* **1996,** 1, 191-198.
34. Kawai, S. H.; Gilat, S. L.; Lehn, J. M., Dual-mode optical-electrical molecular switching device. *Journal of the Chemical Society-Chemical Communications* **1994**, (8), 1011-1013.
35. Kawai, S. H.; Gilat, S. L.; Ponsinet, R.; Lehn, J. M., A dual-mode molecular switching device - bisphenolic diarylethenes with integrated photochromic and electrochromic properties. *Chemistry-a European Journal* **1995,** 1, (5), 285-293.
36. Tsivgoulis, G. M.; Lehn, J. M., Photonic molecular devices - reversibly photoswitchable fluorophores for nondestructive readout for optical memory *Angewandte Chemie-International Edition in English* **1995,** 34, (10), 1119-1122.
37. Hoffmann, R.; Woodward, R. B., Selection rules for concerted cycloadditon reactions. *Journal of the American Chemical Society* **1965,** 87, (9), 2046-2048.
38. Celani, P.; Ottani, S.; Olivucci, M.; Bernardi, F.; Robb, M. A., What happens during the picosecond lifetime of 2a(1) cyclohexa-1,3-diene - a cas-scf study of the cyclohexadiene hexatriene photochemical interconversion. *Journal of the American Chemical Society* **1994,** 116, (22), 10141-10151.
39. Celani, P.; Bernardi, F.; Robb, M. A.; Olivucci, M., Do photochemical ring-openings occur in the spectroscopic state? B-1(2) pathways for the cyclohexadiene/hexatriene photochemical interconversion. *Journal of Physical Chemistry* **1996,** 100, (50), 19364-19366.

40. Garavelli, M.; Page, C. S.; Celani, P.; Olivucci, M.; Schmid, W. E.; Trushin, S. A.; Fuss, W., Reaction path of a sub-200 fs photochemical electrocyclic reaction. *Journal of Physical Chemistry A* **2001,** 105, (18), 4458-4469.
41. Tamura, H.; Nanbu, S.; Nakamura, H.; Ishida, T., A theoretical study of cyclohexadiene/hexatriene photochemical interconversion: Multireference configuration interaction potential energy surfaces and transition probabilities for the radiationless decays. *Chemical Physics Letters* **2005,** 401, (4-6), 487-491.
42. Garavelli, M.; Celani, P.; Fato, M.; Bearpark, M. J.; Smith, B. R.; Olivucci, M.; Robb, M. A., Relaxation paths from a conical intersection: The mechanism of product formation in the cyclohexadiene/hexatriene photochemical interconversion. *Journal of Physical Chemistry A* **1997,** 101, (11), 2023-2032.
43. Sakai, S.; Takane, S., Theoretical studies of the electrocyclic reaction mechanisms of hexatriene to cyclohexadiene. *Journal of Physical Chemistry A* **1999,** 103, (15), 2878-2882.
44. Ern, J.; Bens, A.; Martin, H. D.; Mukamel, S.; Schmid, D.; Tretiak, S.; Tsiper, E.; Kryschi, C. In *Femtosecond reaction dynamics of a photochromic dithienylethene derivative*, 2000; Elsevier Science Bv: 2000; pp 742-744.
45. Ern, J.; Bens, A. T.; Martin, H. D.; Mukamel, S.; Tretiak, S.; Tsyganenko, K.; Kuldova, K.; Trommsdorff, H. P.; Kryschi, C., Reaction dynamics of a photochromic fluorescing dithienylethene. *Journal of Physical Chemistry A* **2001,** 105, (10), 1741-1749.
46. Ern, J.; Bens, A. T.; Martin, H. D.; Mukamel, S.; Schmid, D.; Tretiak, S.; Tsiper, E.; Kryschi, C., Reaction dynamics of photochromic dithienylethene derivatives. *Chemical Physics* **1999,** 246, (1-3), 115-125.
47. Cho, H. G.; Cheong, B. S., Theoretical investigation of 2,3-bis(2,4,5-trimethyl-3-thienyl)maleic anhydride: A thermally irreversible photochromic system. *Bulletin of the Korean Chemical Society* **1998,** 19, (3), 308-313.
48. Levine, B. G.; Ko, C.; Quenneville, J.; Martinez, T. J., Conical intersections and double excitations in time-dependent density functional theory. *Molecular Physics* **2006,** 104, (5-7), 1039-1051.
49. Mikhailov, I. A.; Belfield, K. D.; Masunov, A. E., Dft-based methods in the design of two-photon operated molecular switches. *Journal of Physical Chemitsry A* **2009**, Accepted.
50. Gunnarsson, O.; Lundqvist, B. I., Exchange and correlation in atoms, molecules, and solids by spin-density functional formalism. *Physical Review B* **1976,** 13, (10), 4274-4298.
51. Higashiguchi, K.; Matsuda, K.; Kobatake, S.; Yamada, T.; Kawai, T.; Irie, M., Fatigue mechanism of photochromic 1,2-bis(2,5-dimethyl-3-thienyl)perfluorocyclopentene. *Bulletin of the Chemical Society of Japan* **2000,** 73, (10), 2389-2394.
52. Patel, P. D.; Mikhailov, I. A.; Belfield, K. D.; Masunov, A. E., Theoretical study of photochromic compounds, part 2: Thermal mechanism for byproduct formation and fatigue resistance of diarylethenes used as data storage materials. *International Journal of Quantum Chemistry* **2009,** 109, (15), 3711-3722.
53. Bartkowiak, W.; Zalesny, R.; Leszczynski, J., Relation between bond-length alternation and two-photon absorption of a push-pull conjugated molecules: A quantum-chemical study. *Chemical Physics* **2003,** 287, (1-2), 103-112.
54. BlanchardDesce, M.; Alain, V.; Bedworth, P. V.; Marder, S. R.; Fort, A.; Runser, C.; Barzoukas, M.; Lebus, S.; Wortmann, R., Large quadratic hyperpolarizabilities with donor-acceptor polyenes exhibiting optimum bond length alternation: Correlation between structure and hyperpolarizability. *Chemistry-a European Journal* **1997,** 3, (7), 1091-1104.
55. Bourhill, G.; Bredas, J. L.; Cheng, L. T.; Marder, S. R.; Meyers, F.; Perry, J. W.; Tiemann, B. G., Experimental demonstration of the dependence of the 1st hyperpolarizability of donor-acceptor-substituted polyenes on the ground-state polarization and bond-length alternation. *Journal of the American Chemical Society* **1994,** 116, (6), 2619-2620.
56. Choi, C. H.; Kertesz, M.; Karpfen, A., The effects of electron correlation on the degree of bond alternation and electronic structure of oligomers of polyacetylene. *Journal of Chemical Physics* **1997,** 107, (17), 6712-6721.

57. Kirtman, B.; Champagne, B.; Bishop, D. M., Electric field simulation of substituents in donor-acceptor polyenes: A comparison with ab initio predictions for dipole moments, polarizabilities, and hyperpolarizabilities. *Journal of the American Chemical Society* **2000,** 122, (33), 8007-8012.
58. Meyers, F.; Marder, S. R.; Pierce, B. M.; Bredas, J. L., Electric-field modulated nonlinear-optical properties of donor-acceptor polyenes - sum-over-states investigation of the relationship between molecular polarizabilities (alpha, beta, and gamma) and bond-length alternation. *Journal of the American Chemical Society* **1994,** 116, (23), 10703-10714.
59. Jacquemin, D.; Femenias, A.; Chermette, H.; Ciofini, I.; Adamo, C.; Andre, J. M.; Perpete, E. A., Assessment of several hybrid dft functionals for the evaluation of bond length alternation of increasingly long oligomers. *Journal of Physical Chemistry A* **2006,** 110, (17), 5952-5959.
60. Jacquemin, D.; Perpete, E. A., Ab initio calculations of the colour of closed-ring diarylethenes: Td-dft estimates for molecular switches. *Chemical Physics Letters* **2006,** 429, (1-3), 147-152.
61. Jacquemin, D.; Perpete, E. A.; Chermette, H.; Ciofini, I.; Adamo, C., Comparison of theoretical approaches for computing the bond length alternation of polymethineimine. *Chemical Physics* **2007,** 332, (1), 79-85.
62. Jacquemin, D.; Perpete, E. A.; Ciofini, I.; Adamo, C., Assessment of recently for the evaluation of the developed density functional approaches bond length alternation in polyacetylene. *Chemical Physics Letters* **2005,** 405, (4-6), 376-381.
63. Perpete, E. A.; Jacquemin, D., An ab initio scheme for quantitative predictions of the visible spectra of diarylethenes. *Journal of Photochemistry and Photobiology a-Chemistry* **2007,** 187, (1), 40-44.
64. Perpete, E. A.; Maurel, F.; Jacquemin, D., Td-dft investigation of diarylethene dyes with cyclopentene, dihydrothiophene, and dihydropyrrole bridges. *Journal of Physical Chemistry A* **2007,** 111, (25), 5528-5535.
65. Perrier, A.; Maurel, F.; Aubard, J., Theoretical study of the electronic and optical properties of photochromic dithienylethene derivatives connected to small gold clusters. *Journal of Physical Chemistry A* **2007,** 111, (39), 9688-9698.
66. Perrier, A.; Maurel, F.; Aubard, J., Theoretical investigation of the substituent effect on the electronic and optical properties of photochromic dithienylethene derivatives. *Journal of Photochemistry and Photobiology a-Chemistry* **2007,** 189, (2-3), 167-176.
67. Patel, P. D.; Masunov, A. E., Theoretical study of photochromic compounds. 1. Bond length alternation and absorption spectra for the open and closed forms of 29 diarylethene derivatives. *Journal of Physical Chemistry A* **2009,** 113, (29), 8409-8414.
68. Majumdar, D.; Lee, H. M.; Kim, J.; Kim, K. S.; Mhin, B. J., Photoswitch and nonlinear optical switch: Theoretical studies on 1,2-bis-(3-thienyl)-ethene derivatives. *Journal of Chemical Physics* **1999,** 111, (13), 5866-5872.
69. Maurel, F.; Perrier, A.; Perpete, E. A.; Jacquemin, D., A theoretical study of the perfluoro-diarylethenes electronic spectra. *Journal of Photochemistry and Photobiology a-Chemistry* **2008,** 199, (2-3), 211-223.
70. Chen, D. Z.; Wang, Z.; Zhao, X.; Hao, Z. L., Theoretical study on geometric electronic structures and absorption wavelengths of closed-ring isomers of diarylmaleic anhydrides. *Journal of Molecular Structure-Theochem* **2006,** 774, (1-3), 77-81.
71. Laurent, A. D.; Andre, J. M.; Perpete, E. A.; Jacquemin, D., Photochromic properties of dithienylazoles and other conjugated diarylethenes. *Journal of Photochemistry and Photobiology a-Chemistry* **2007,** 192, (2-3), 211-219.
72. Laurent, A. D.; Assfeld, X.; Jacquemin, D.; Andre, J. M.; Perpete, E. A., Substitution effects on the optical spectra of diarylethene photochroms: Ab initio insights. *Molecular Simulation* **2010,** 36, (1), 74-78.
73. Williams, R. V.; Edwards, W. D.; Mitchell, R. H.; Robinson, S. G., A dft study of the thermal, orbital symmetry forbidden, cyclophanediene to dihydropyrene electrocyclic reaction. Predictions to improve the dimethyldihydropyrene photoswitches. *Journal of the American Chemical Society* **2005,** 127, (46), 16207-16214.
74. Fukaminato, T.; Kawai, T.; Kobatake, S.; Irie, M., Fluorescence of photochromic 1,2-bis(3-methyl-2-thienyl)ethene. *Journal of Physical Chemistry B* **2003,** 107, (33), 8372-8377.

75. Hanazawa, M.; Sumiya, R.; Horikawa, Y.; Irie, M., Thermally irreversible photochromic systems - reversible photocyclization of 1,2-bis(2-methylbenzo[b]thiophen-3-yl)perfluorocycloalkene derivatives. *Journal of the Chemical Society-Chemical Communications* **1992**, (3), 206-207.
76. Irie, M.; Lifka, T.; Kobatake, S.; Kato, N., Photochromism of 1,2-bis(2-methyl-5-phenyl-3-thienyl)perfluorocyclopentene in a single-crystalline phase. *Journal of the American Chemical Society* **2000,** 122, (20), 4871-4876.
77. Irie, M.; Sakemura, K.; Okinaka, M.; Uchida, K., Photochromism of dithienylethenes with electron-donating substituents. *Journal of Organic Chemistry* **1995,** 60, (25), 8305-8309.
78. Yamaguchi, T.; Irie, M., Photochromism of bis(2-alkyl-1-benzofuran-3-yl)perfluorocyclopentene derivatives. *Journal of Organic Chemistry* **2005,** 70, (25), 10323-10328.
79. Ern, J.; Bens, A.; Martin, H. D.; Mukamel, S.; Schmid, D.; Tretiak, S.; Tsiper, E.; Kryschi, C., Femtosecond reaction dynamics of a photochromic dithienylethene derivative. *Journal of Luminescence* **2000,** 87-9, 742-744.
80. Ern, J.; Bens, A. T.; Bock, A.; Martin, H. D.; Kryschi, C., Femtosecond transient absorption studies on photochromism of dithienylethene derivates. *Journal of Luminescence* **1998,** 76-7, 90-94.
81. Miyasaka, H.; Nobuto, T.; Itaya, A.; Tamai, N.; Irie, M., Picosecond laser photolysis studies on a photochromic dithienylethene in solution and in crystalline phases. *Chemical Physics Letters* **1997,** 269, (3-4), 281-285.
82. Tamai, N.; Miyasaka, H., Ultrafast dynamics of photochromic systems. *Chemical Reviews* **2000,** 100, (5), 1875-1890.
83. Tamai, N.; Saika, T.; Shimidzu, T.; Irie, M., Femtosecond dynamics of a thiophene oligomer with a photoswitch by transient absorption spectroscopy. *Journal of Physical Chemistry* **1996,** 100, (12), 4689-4692.
84. Miyasaka, H.; Murakami, M.; Itaya, A.; Guillaumont, D.; Nakamura, S.; Irie, M., Multiphoton gated photochromic reaction in a diarylethene derivative. *Journal of the American Chemical Society* **2001,** 123, (4), 753-754.
85. Uchida, K.; Matsuoka, T.; Sayo, K.; Iwamoto, M.; Hayashi, S.; Irie, M., Thermally reversible photochromic systems. Photochromism of a dipyrrolylperfluorocyclopentene. *Chemistry Letters* **1999**, (8), 835-836.
86. Stellacci, F.; Bertarelli, C.; Toscano, F.; Gallazzi, M. C.; Zotti, G.; Zerbi, G., A high quantum yield diarylethene-backbone photochromic polymer. *Advanced Materials* **1999,** 11, (4), 292-295.
87. Nakamura, S.; Kobayashi, T.; Takata, A.; Uchida, K.; Asano, Y.; Murakami, A.; Goldberg, A.; Guillaumont, D.; Yokojima, S.; Kobatake, S.; Irie, M., Quantum yields and potential energy surfaces: A theoretical study. *Journal of Physical Organic Chemistry* **2007,** 20, (11), 821-829.
88. Vomasta, D.; Hogner, C.; Branda, N. R.; Konig, B., Regulation of human carbonic anhydrase i (hcai) activity by using a photochromic inhibitor. *Angewandte Chemie-International Edition* **2008,** 47, (40), 7644-7647.
89. Lemieux, V.; Spantulescu, M. D.; Baldridge, K. K.; Branda, N. R., Modulating the lewis acidity of boron using a photoswitch. *Angewandte Chemie-International Edition* **2008,** 47, (27), 5034-5037.
90. Sud, D.; Wigglesworth, T. J.; Branda, N. R., Creating a reactive enediyne by using visible light: Photocontrol of the bergman cyclization. *Angewandte Chemie-International Edition* **2007,** 46, (42), 8017-8019.
91. Al-Atar, U.; Fernandes, R.; Johnsen, B.; Baillie, D.; Branda, N. R., A photocontrolled molecular switch regulates paralysis in a living organism. *Journal of the American Chemical Society* **2009,** 131, (44), 15966-15967.
92. Saito M, Y. Y., Yokoyama Y Reversible change in optical rotation by photochromism of diarylethenes in the stretched DNA-quaternary ammonium ion complex films. *Chemistry Letters* **2003,** 32, (9), 806-807.
93. Rodger, A.; Taylor, S.; Adlam, G.; Blagbrough, I. S.; Haworth, I. S., Multiple DNA-binding modes of anthracene-9-carbonyl-n-1 spermine. *Bioorganic & Medicinal Chemistry* **1995,** 3, (6), 861-872.
94. Mukherjee, A.; Lavery, R.; Bagchi, B.; Hynes, J. T., On the molecular mechanism of drug intercalation into DNA: A simulation study of the intercalation pathway, free energy, and DNA structural changes. *Journal of the American Chemical Society* **2008,** 130, (30), 9747-9755.

CHAPTER 2 METHODS OF CALCULATION

2.1 Density Functional Theory

For calculation of many-body electronic structure problems, the nuclei of the treated molecules are considered fixed (Born-Oppenheimer approximation) and so it is this static potential around which the electronics are moving.[1, 2] The stationary Schrödinger equation for such a system is:

$$\hat{H}\Psi = \left[\hat{T}+\hat{V}+\hat{U}\right]\Psi = \left[\sum_{i}^{N} -\frac{\hbar^2}{2m}\nabla_i^2 + \sum_{i}^{N} V(\vec{r}_i) + \sum_{i<j}^{N} U(\vec{r}_i,\vec{r}_j)\right]\Psi = E\Psi \qquad \text{(eq. 1)}$$

Here $\Psi(\vec{r}_i,.....,\vec{r}_N)$ is the wavefunction describing the stationary electronic state, $\hat{H}$ is the electronic molecular Hamiltonian, N is the number of electrons, $\hat{T}$ is the N-electron kinetic energy, $\hat{V}$ is the N-electron potential energy from the external field and $\hat{U}$ is the electron-electron interaction energy for N-electron system. Out of these three operators, $\hat{V}$ is system dependent while both $\hat{T}$ and $\hat{U}$ depend only on electron distribution. There are many sophisticated methods for solving the many-body Schrödinger equation based on the expansion of the wavefunction in Slater determinants.

Many properties of the molecules in their electronic ground states are can be described in the mean field approximation, also known as Hartree-Fock (HF) theory. In this approximation each electron is assigned a wave function called an orbital, shaped in

the mean field created by the density distribution of all other electrons. Total electron wavefunction is expressed as antisymmetrized product (called Slater determinant) of these orbitals. Electron repulsion is then composed of two terms: classical Coulomb energy and exchange energy EHFX, resulting from quantum nature of electrons. Single Slater determinants can be used for description of electronically excited states in similar manner. Electron correlation effects are missing from this picture. However, they are present in the ground and excited states to a different degree, making mean field approximation inaccurate for spectroscopic purposes.

Traditionally, post-HF ab initio Wavefunction Theory (WFT) is used to describe electronic excited states more accurately than mean field approximation. Although WFT tools are capable to provide quantitative predictions of nearly experimental quality, they are often computationally prohibitive. For this reason WFT methods are often combined with semiempirical Hamiltonians (AM1, PM3, CS-INDO, ZINDO, etc.) to guide the experimental work.3,4,5 As a result of semiempirical parameterization, the accuracy varies from one class of the compounds to another, and at best only quantitative picture is obtained.

An alternative to WFT methods one can use Density Functional Theory (DFT) approach.[6, 7] There, the key variable is the particle density and which is given by:

$$n(\vec{r}) = N\int d^3r_2 \int d^3r_3 .....\int d^3r_N \Psi^*(\vec{r},\vec{r}_2,.....,\vec{r}_N)\Psi(\vec{r}_1,\vec{r}_2,.....,\vec{r}_N) \qquad \text{(eq. 2)}$$

It is possible to calculate ground-state observables using this density, in particular ground-state energy E_0, which is also a functional of n_0 :

$$E_0 = E[n_0] = \langle \Psi[n_0] | \hat{T} + \hat{V} + \hat{U} | \Psi[n_0] \rangle \quad \text{(eq. 3)}$$

And the final energy can be minimized as:

$$E[n] = T[n] + U[n] + \int V(\vec{r}) n(\vec{r}) d^3 r \quad \text{(eq. 4)}$$

The Kohn-Sham equations[8] to solve for non-interacting particles, are given by

$$\left[-\frac{\hbar^2}{2m} \nabla^2 + V_s(r) \right] \phi_i = \varepsilon_i \phi_i \quad \text{(eq. 5)}$$

$$n(\vec{r}) = \sum_i |\phi_i(r)|^2 \quad \text{(eq. 6)}$$

Which yields the orbitals ϕ_i ; and the effective single-particle potential V_s can be written in more detail as:

$$V_s(\vec{r}) = V(\vec{r}) + \int \frac{e^2 n_s(\vec{r}')}{|\vec{r} - \vec{r}'|} d^3 r' + V_{XC}[n_s(\vec{r})] \quad \text{(eq. 7)}$$

Here the second term denotes the so-called Hartree term describing the electron-electron Coulomb repulsion, while the last term V_{XC} is called the exchange-correlation potential, which replaces exact exchange in HF method and includes all the many-particle interactions. The KS equations (eq.5) are a solved self-consistently for orbitals until convergence is reached.

2.2 Time-Dependent Density Functional Theory

Time-Dependent DFT (TD-DFT) is an approximation method to solve time-dependent Schrödinger equation. It is analogous to DFT in replacing wave function with the density, except this time the electron density changes with time.[9, 10] The corresponding KS equations in TD-DFT can be written as:

$$\left[-\frac{\hbar^2}{2m}\nabla^2 + \upsilon_s(r,t)\right]\phi_i(r,t) = i\frac{\partial}{\partial t}\phi_i(r,t) \qquad \text{(eq. 8)}$$

$$n_s(r,t) = \sum_{i=1}|\phi_i(r,t)|^2 \qquad \text{(eq. 9)}$$

The typically used TD-DFT implementation[11] is based on the linear response approximation within DFT, and is used to investigate the excited state properties of many-body systems. Instead of increasing complexity of the molecular wavefunction, the electron correlation in DFT is introduced in terms of exchange-correlation functional E_{XC}, replacing exact exchange E_{HFX} in HF theory without increase in computational expense. Some empirical parameter fitting is typically involved in the design of the exchange-correlation functional in this formalism; it is largely system-independent. Although exact exchange is non-local and orbital-dependent, in DFT the functional E_{XC} is expressed in terms of the total electron density and its gradients (respectively local and semi-local approximation). Unlike exact exchange, E_{XC} includes repulsion of electron from its own density and does not vanish for one-electron system. This property is known as self-

interaction error, and it has both negative and positive effects. As negative result, in DFT bonds are too weak, while electrons are over-delocalized and do not interact with Coulomb asymptotic ~1/r at large separations. On a positive site, self interaction is mimicking non-local part of electron correlation and should be retained to some degree when improvements to E_{XC} are made.

Practically useful step in balancing self-interaction error was made by Becke,[12] who suggested to include a fraction of HF exchange energy a in E_{XC} functional:

$$E_{XC} = aE_{HFX} + (1-a)E_{DFX} + E_C \qquad \text{(eq. 10)}$$

where a is empirical parameter, E_{DFX} and E_C are exchange and correlation functionals including local and semi-local terms.

Theoretical description of the light absorption by conjugated photochromic compounds is an important component in photochemical and photophysical studies of these molecules, essential for both experimental design and interpretation. The original (B3LYP)[12] as well as more recent hybrid functionals often achieve chemical accuracy in predictions of properties.[13,14,15] Moderate computational costs brings hopes for TD-DFT to be a good candidate for universal black-box approach of spectroscopic accuracy. However, extensive testing revealed various drawbacks in the commonly used TD-DFT implementations, and necessitated further improvements (see recent review[16] for more details).

2.3 Functionals and Basis sets

For the current research project, all the calculations have been performed using GAUSSIAN 2003 package.[17] We predict the maxima on the experimental absorption spectra (λ_{max}) for both closed- and open-ring isomers, include the solvent effects, and compare them with the benchmark set of experimental data. In order to make the accurate predictions of the spectral properties we ensure that the molecular geometry is in agreement with the experimental X-ray crystal structures, available for some of DA derivatives. We validate different DFT methods to predict the ground state geometry for the open and closed isomers as well as for some by-products. The optimized structures were further used to predict the excitation spectrum of each molecule with TD-DFT formalism. Out of several excited states predicted by TD-DFT only the one with the maximal oscillator strength (which was not the lowest excited state) was used for comparison with the experimental spectra. The polarizable continuum model used in this study was non-equilibrium solvation self-consistent reaction field theory as implemented in GAUSSIAN 2003 (keyword SCRF=IEFPCM)[18] with default empirical parameters, including atomic and solvent radii, fast ε_∞ and slow ε_0 dielectric constants. Solvents used for this work were selected according to the particular solvent used to record the benchmark experimental data: benzene (Bz), dichloromethane (DCM), acetonitrile (ACN) and heptane (Hep) in place of hexane.[19]

Photochromic effect involves the photochemical pericyclic reactions proceeding on the excited state potential surfaces, and thermal cycloreversion reactions following the ground state potential energy surface. Thus, both the relative energies and the transition states of the conformers need to be described equally well. Only a few exchange-correlation functionals were designed to give accurate energies for both transition state and equilibrium geometries. They accomplished this by combining the increased fraction of Hartree-Fock exchange with dependence on kinetic energy density. Among them are Boese-Martin functional for kinetics (BMK)[20] and Minnesota functional 2005 with double exact exchange (M05-2X), developed by Zhao and Truhlar.[21] While organic reaction barriers were excluded from the training set used in parameterization of BMK, the M05-2X functional was designed with organic reactions in mind, and was shown to perform better than other functionals for a wide range of organic reactions and molecular properties.[22, 23] For these reasons we used M05 and M05-2X functionals for the detailed study.

Several different functionals have been tested namely B3LYP,[24] BLYP,[25] BHandHLYP,[26] PBE0,[27] TPSS,[28] BMK,[20] M05,[29] and M05-2x[30] to predict the thermal stability, and fatigue resistance.[31] Calculations were performed at semi-empirical AM1,[32-35] HF and DFT methods.[36, 37] Hybrid exchange-correlation functionals including various fraction of Hartree-Fock exchange were used (20% for B3LYP,[38-40] 42% for BMK,[20] and 56% for M05-2X[21]) in combination with MIDI! and 6-31G* basis sets. In order to follow UKS solution, the broken symmetry guess was generated and followed using keyword Guess(Mix,NoExtra). The stability of the Kohn-Sham orbitals was tested before and after

geometry optimization using the keyword Stable=Opt. If cases where instability was found, the geometry optimization was repeated with the stable set of orbitals used as initial guess. The transition state search for the cycloreversion barrier was performed by using Opt=TS keyword while the transition state search for the fatigue resistance profile was performed by employing the *Synchronous Transit-Guided Quasi-Newton* (STQN) method[41, 42] as implemented in the GAUSSIAN 2003 package. This method uses a linear synchronous transit or quadratic synchronous transit approach to get closer to the quadratic region around the transition state and then uses a quasi-Newton or eigenvector-following algorithm to complete the optimization. This method will converge efficiently to the actual transition structure using an empirical estimate of the Hessian and suitable starting structures for the reactants and intermediates. To characterize each stationary point as a minimum or a transition state and to estimate the zero point vibrational energies (ZPE) and vibrational frequencies for all optimized species were computed at all levels.

The potential energy profile of diarylethene set of compounds was predicted with non-standard TD-ΔSCF formalism. In ΔSCF approach, the lowest excited state is approximated with single Slater determinant with two singly occupied orbitals $HOMO^1$ and $LUMO^1$. In order for ΔSCF to converge to the excited state, it must have different symmetry from the ground state. In TD-ΔSCF one applies TD-DFT formalism to this ΔSCF as the reference state and obtains both ground and double-excited states as single excitations (**Scheme 1**).

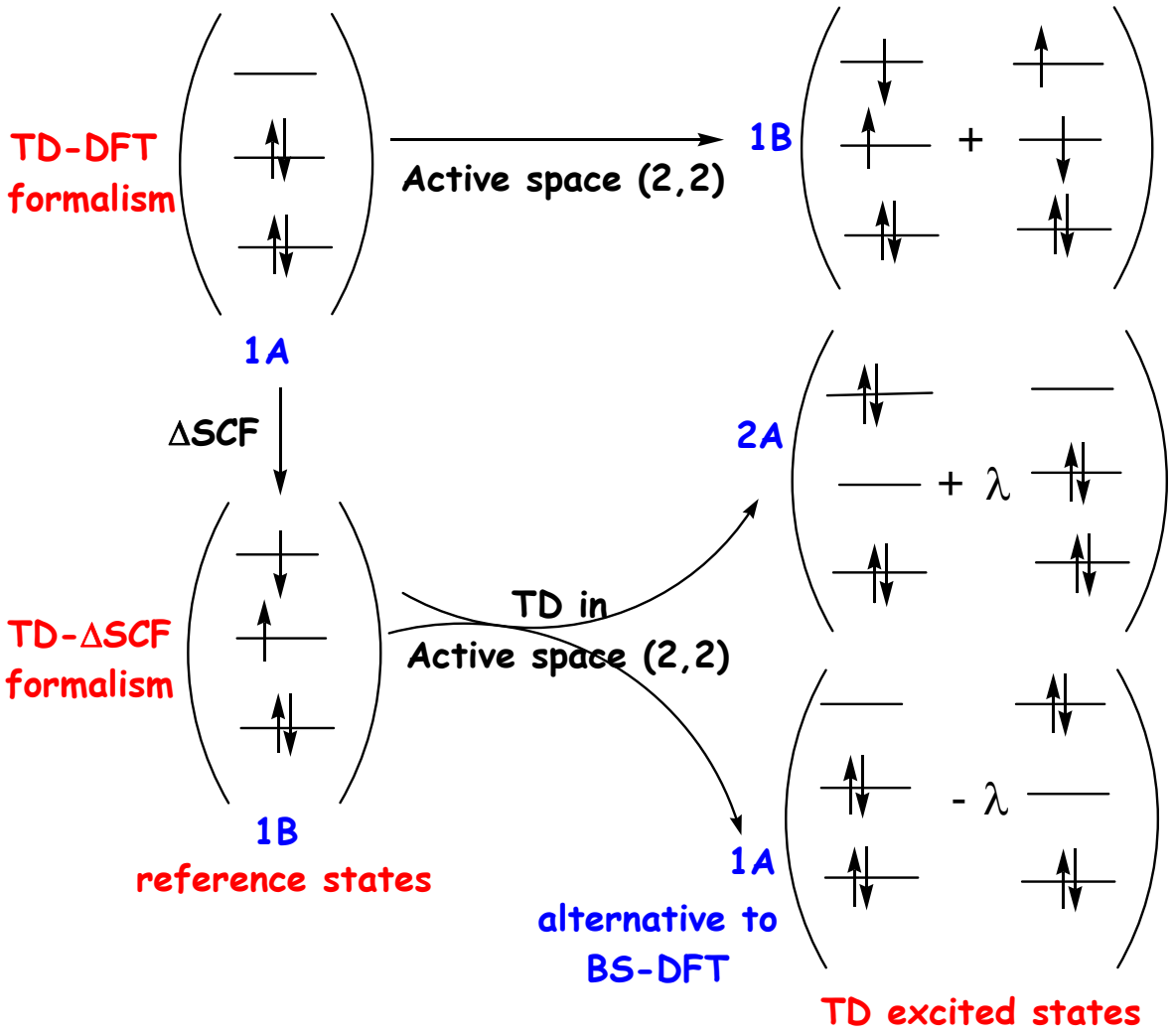

Scheme 1: Comparison of the conventional TD-DFT (top) and TD-ΔSCF formalism (bottom) for locating the pericyclic minimum.

All the calculations were performed at UM05-2X method and ΔSCF reference was obtained using 'Guess=Alter' keyword, which allowed us to singly occupy both HOMO and LUMO. We restricted the active space to two orbitals and thus obtained a lower energy 1A state and a higher energy 2A state, the latter was optimized to the pericyclic minimum.

2.4 Molecular Dynamics

Molecular Dynamics (MD) is a computer simulation technique where the time evolution of a set of interacting atoms is followed by integrating their equations of motion. [43, 44] In MD simulations we follow the laws of classical mechanics, and most notably Newton's law for each atom *i* in a system constituted by *N* atoms:

$$F_i = m_i a_i \qquad \text{(eq. 11)}$$

Here, m_i is the atom mass, a_i is its acceleration, and F_i the force acting upon it, due to the interactions with other atoms. MD is a statistical mechanics technique and during a typical MD simulation, the initial set of positions and velocities is given and succeeding time evolution is obtained. When visualizing such a simulation, one would see the atoms moving around and bumping into each other, oscillating etc. representing more or less the actual macroscopic experimental set up. This is done by calculating a 6N-dimentional space comprised of 3N positions and 3N momenta. Basically, we obtain a set of configurations distributed according to some statistical distribution function, or statistical ensemble. The inclusion of collisions and friction forces between the solute and its environment, along with the potential forces is done by using Langevin or Brownian dynamics[45]. Equation 11 then becomes a stochastic differential equation with the forces on its right side expressed by equation 12:

$$F_i = -\nabla r_i U(r_1, r_2, ...r_N) - m_i \gamma_i V_i + R_i(t) \qquad i = 1,2,....., N \qquad \text{(eq. 12)}$$

where $\boldsymbol{V_i}$ and γi are the velocity and the friction coefficient of atom i, respectively; U is the potential energy of the system ($-\nabla r_i U$ being the potential force acting on atom i); and $\mathbf{R}_i(t)$ is the vector of random forces arising from the collision of atom i with the molecules of the environment (solvent) that are not considered explicitly. $\mathbf{R}_i(t)$ has zero mean (equation 13), and the $\mathbf{R}_i$ is taken at different times are δ-correlated (equation 14):

$$R_i(t) = 0 \qquad \text{(eq. 13)}$$

$$R_i(t) \bullet R_i(t') = 2m_i\gamma_i k_B T\delta(t-t') \qquad \text{(eq. 14)}$$

Here T is the absolute temperature of the system, k_B is the Boltzmann constant, and $\delta(x)$ is the Dirac δ-function. According to statistical physics, physical quantities are represented by averages over configurations distributed according to a certain statistical ensemble. A trajectory obtained by MD simulation provides such a set of configurations. Therefore, a measurement of a physical quantity by simulation is simply obtained as an arithmetic average of the various instantaneous values assumed by that quantity during the MD run. MD allows studying the dynamics of large macromolecules, including biological systems such as proteins, nucleic acids (DNA, RNA), membranes, etc.[46]

The relative free energy of solvation of a bound state and an unbound state of solvated molecular systems or comparison of free energy of two different solvated conformations of the same molecule can be calculated using equation 15.

$$[A]_{aq} + [B]_{aq} \rightarrow [AB]_{aq}$$

$$\Delta G^0_{b,solv} = \Delta G^0_{complexAB,solv} - (\Delta G^0_{A,solv} + \Delta G^0_{B,solv}) \qquad \text{(eq. 15)}$$

However, in case of MD simulations of such solvated systems, the solvent-solvent interactions provide major energy contributions, which would yield large fluctuations in total energy, and the calculation will be computationally expensive. The molecular mechanics combined with Poisson–Boltzmann and surface area calculations (MMPBSA) is an effective method to calculate free energy of binding by dividing up the calculation as follows.

$$\Delta G^0_{b,solv} = \Delta G^0_{bind,vacuum} + \Delta G^0_{solv,complex}\left(\Delta G^0_{solv,ligand} + \Delta G^0_{solv,receptor}\right) \qquad \text{(eq. 16)}$$

The free energy of solvation is calculated by first solving the linearized Poisson Boltzmann equation for each of the three states (ligand, receptor and the complex). This will provide the electrostatic contribution to the solvation free energy. The hydrophobic contributions are then added:

$$\Delta G^0_{solv} = G^0_{electrostatic,\varepsilon=80} - G^0_{electrostatic,\varepsilon=1} + \Delta G^0_{hydrophobic} \qquad \text{(eq. 17)}$$

The $\Delta G_{bind,vacuum}$ is obtained by calculating the average interaction energy between the receptor and the ligand and calculating the entropy change upon binding. [47] For the current work, we carried put MD simulations to model ligand-DNA intercalation process. For this project, 8 different polycationic anthracene pharmacophore conjugated with polyamine chains (ant-PA) and 1 neutral anthracene (ant) were constructed and optimized at B3LYP/6-31G* level of theory using GAUSSIAN 2003 package[48]. The 12-mer 5′(GCGCGCGCGCGC)$_2$3′ Z-DNA was built using w3DNA, a web-based interface to

the 3DNA software package [49, 50]. The ant-PA-DNA intercalated complexes were constructed using Sirius visualization program.[51] The four terminal base pairs on each DNA end were chosen as CG base pairs (G-7-C-8 and G-17-C-18) in the minor grove between which the ligand (ant or ant-PA) was intercalated.

2.5 References

1. Szabo, A. O., N. S., *Modern Quantum Chemistry*. Dover Publishing: Mineola, New York, 1996.
2. Levine, I. N., *Quantum Chemistry*. Prentice Hall: New Jersey 191.
3. Matsuura, A.; Sato, H.; Sotoyama, W.; Takahashi, A.; Sakurai, M., Am1, Pm3, And Pm5 Calculations Of The Absorption Maxima Of Basic Organic Dyes. *Journal Of Molecular Structure-Theochem* **2008,** 860, (1-3), 119-127.
4. Baraldi, I.; Momicchioli, F.; Ponterini, G.; Vanossi, D., A Recent Development Of The Csindo Model. Treatment Of Solvent Effects On Structures And Optical Properties Of Organic Dyes. In *Advances In Quantum Chemistry, Vol 36*, Academic Press Inc: San Diego, 2000; Vol. 36, Pp 121-150.
5. Jacquemin, D.; Beljonne, D.; Champagne, B.; Geskin, V.; Bredas, J. L.; Andre, J. M., Analysis Of The Sign Reversal Of The Second-Order Molecular Polarizability In Polymethineimine Chains. *Journal Of Chemical Physics* **2001,** 115, (14), 6766-6774.
6. W. Koch, M. C. H., *A Chemist's Guide To Density Functional Theory* Wiley-Vch, Weinheim,: 2002.
7. R. G. Parr, W. Y., *Density-Functional Theory Of Atoms And Molecules* Oxford University Press, : New York, 1989.
8. Kohn, W.; Sham, L. J., Self-Consistent Equations Including Exchange And Correlation Effects. *Physical Review* **1965,** 140, (4a), 1133-&.
9. Hohenberg, P. K., W., Inhomogeneous Electron Gas. *Physical Review B* **1964,** 136, (3b), 864-865.
10. Runge, E.; Gross, E. K. U., Density Functional Theory For Time-Dependent Systems. *Physical Review Letters* **1984,** 52, (12), 997-1000.
11. Casida, M. E., Time-Dependent Density Functional Response Theory For Molecules. In *Recent Advances In Density Functional Methods*, Chong, D. A., Ed. World Scientific: Singapore, 1995; Vol. 3 Of Part I, Pp 155-192.
12. Becke, A. D., Density-Functional Thermochemistry .3. The Role Of Exact Exchange. *Journal Of Chemical Physics* **1993,** 98, (7), 5648-5652.
13. Sousa, S. F.; Fernandes, P. A.; Ramos, M. J., General Performance Of Density Functionals. *Journal Of Physical Chemistry A* **2007,** 111, (42), 10439-10452.
14. Zhao, Y.; Truhlar, D. G., Exploring The Limit Of Accuracy Of The Global Hybrid Meta Density Functional For Main-Group Thermochemistry, Kinetics, And Noncovalent Interactions. *Journal Of Chemical Theory And Computation* **2008,** 4, (11), 1849-1868.
15. Jacquemin, D.; Wathelet, V.; Perpete, E. A.; Adamo, C., Extensive Td-Dft Benchmark: Singlet-Excited States Of Organic Molecules. *Journal Of Chemical Theory And Computation* **2009,** 5, (9), 2420-2435.
16. Casida, M. E., Time-Dependent Density-Functional Theory For Molecules And Molecular Solids. *Journal Of Molecular Structure-Theochem* **2009,** 914, (1-3), 3-18.
17. Frisch Mj, T. G., Schlegel Hb, Scuseria Ge, Robb Ma, Cheeseman Jr., Zakrzewski Vg, Montgomery Ja Jr., Stratmann Re, Burant Jc, Dapprich S, Millam Jm, Daniels Ad, Kudin Kn, Strain M. C, Farkas O, Tomasi J, Barone V, Cossi M, Cammi R, Mennucci B, Pomelli C, Adamo C, Clifford S, Ochterski J, Petersson Ga, Ayala Py, Cui Q, Morokuma K, Malick Dk, Rabuck Ad, Raghavachari K, Foresman Jb, Cioslowski J, Ortiz J. V, Baboul A. G, Stefanov B. B, Liu G, Liashenko A, Piskorz P, Komaromi I, Gomperts R, Martin Rl, Fox Dj, Keith T, Al-Laham Ma, Peng Cy, Nanayakkara A, Gonzalez C, Challacombe M, Gill Pmw, Johnson B, Chen W, Wong Mw, Andres Jl, Gonzalez C, Head-Gordon M, Replogle Es, And Pople Ja, , Gaussian03, Rev.E In 2003.
18. Tomasi, J.; Mennucci, B.; Cances, E., The Ief Version Of The Pcm Solvation Method: An Overview Of A New Method Addressed To Study Molecular Solutes At The Qm Ab Initio Level. *Journal Of Molecular Structure-Theochem* **1999,** 464, (1-3), 211-226.
19. Patel, P.; Masunov, A. E., Theoretical Study Of Photochromic Compounds: 1. Bond Lengths Alternation And Absorption Spectra Of The Open And Closed Isomers Of Diarylethene *Journal Of Physical Chemistry A* **2009,** Accepted.

20. Boese, A. D.; Martin, J. M. L., Development Of Density Functionals For Thermochemical Kinetics. *Journal Of Chemical Physics* **2004,** 121, (8), 3405-3416.
21. Zhao, Y.; Schultz, N. E.; Truhlar, D. G., Design Of Density Functionals By Combining The Method Of Constraint Satisfaction With Parametrization For Thermochemistry, Thermochemical Kinetics, And Noncovalent Interactions. *Journal Of Chemical Theory And Computation* **2006,** 2, (2), 364-382.
22. Wodrich, M. D.; Corminboeuf, C.; Schreiner, P. R.; Fokin, A. A.; Schleyer, P. V., How Accurate Are Dft Treatments Of Organic Energies? *Organic Letters* **2007,** 9, (10), 1851-1854.
23. Zhao, Y.; Truhlar, D. G., Assessment Of Density Functionals For Pi Systems: Energy Differences Between Cumulenes And Poly-Ynes; Proton Affinities, Bond Length Alternation, And Torsional Potentials Of Conjugated Polyenes; And Proton Affinities Of Conjugated Shiff Bases. *Journal Of Physical Chemistry A* **2006,** 110, (35), 10478-10486.
24. Becke, A. D., Density-Functional Exchange-Energy Approximation With Correct Aymptotic - Behavior. *Physical Review A* **1988,** 38, (6), 3098-3100.
25. Iikura, H.; Tsuneda, T.; Yanai, T.; Hirao, K., A Long-Range Correction Scheme For Generalized-Gradient-Approximation Exchange Functionals. *Journal Of Chemical Physics* **2001,** 115, (8), 3540-3544.
26. Becke, A. D., A New Mixing Of Hartree-Fock And Local Density Functional Theories. *Journal Of Chemical Physics* **1993,** 98, (2), 1372-1377.
27. Adamo, C.; Barone, V., Toward Reliable Density Functional Methods Without Adjustable Parameters: The Pbe0 Model. *Journal Of Chemical Physics* **1999,** 110, (13), 6158-6170.
28. Tao, J. M.; Perdew, J. P.; Staroverov, V. N.; Scuseria, G. E., Climbing The Density Functional Ladder: Nonempirical Meta-Generalized Gradient Approximation Designed For Molecules And Solids. *Physical Review Letters* **2003,** 91, (14), 4.
29. Zhao, Y.; Schultz, N. E.; Truhlar, D. G., Exchange-Correlation Functional With Broad Accuracy For Metallic And Nonmetallic Compounds, Kinetics, And Noncovalent Interactions. *Journal Of Chemical Physics* **2005,** 123, (16), 4.
30. Zhao, Y.; Truhlar, D. G., A New Local Density Functional For Main-Group Thermochemistry, Transition Metal Bonding, Thermochemical Kinetics, And Noncovalent Interactions. *Journal Of Chemical Physics* **2006,** 125, (19), 18.
31. Patel, P. D.; Mikhailov, I. A.; Belfield, K. D.; Masunov, A. E., Theoretical Study Of Photochromic Compounds, Part 2: Thermal Mechanism For Byproduct Formation And Fatigue Resistance Of Diarylethenes Used As Data Storage Materials. *International Journal Of Quantum Chemistry* **2009,** 109, (15), 3711-3722.
32. Davis, L. P.; Guidry, R. M.; Williams, J. R.; Dewar, M. J. S.; Rzepa, H. S., Mndo Calculations For Compounds Conatining Aluminum And Boron. *Journal Of Computational Chemistry* **1981,** 2, (4), 433-445.
33. Dewar, M. J. S.; Mckee, M. L.; Rzepa, H. S., Mndo Parametere For 3rd Period Elements. *Journal Of The American Chemical Society* **1978,** 100, (11), 3607-3607.
34. Dewar, M. J. S.; Reynolds, C. H., An Improved Set Of Mndo Parameters For Sulfur. *Journal Of Computational Chemistry* **1986,** 7, (2), 140-143.
35. Dewar, M. J. S.; Zoebisch, E. G.; Healy, E. F.; Stewart, J. J. P., The Development And Use Of Quantum-Mechanical Molecular-Models .76. Am1 - A New General Purpose Quantum-Mechanical Molecular-Model. *Journal Of The American Chemical Society* **1985,** 107, (13), 3902-3909.
36. Bartolotti, L. J. F. K., *Reviews In Computational Chemistry*. Vch Publishers: New York, 1996.
37. Parr, R. G. Y., Weitao T., *Density Functional Theory Of Atoms And Molecules*. Oxford University Press: New York, 1989.
38. Becke, A. D., Density-Functional Thermochemistry .3. The Rolr Of Exact Exchange. *Journal Of Chemical Physics* **1993,** 98, (7), 5648-5652.
39. Lee, C. T.; Yang, W. T.; Parr, R. G., Development Of The Colle-Salvetti Correlation-Energy Formula Into A Functional Of The Electron-Density *Physical Review B* **1988,** 37, (2), 785-789.
40. Perdew, J. P.; Wang, Y., Accurate And Simple Analytic Representation Of The Electron-Gas Correlation-Energy. *Physical Review B* **1992,** 45, (23), 13244-13249.

41. Peng, C. Y.; Ayala, P. Y.; Schlegel, H. B.; Frisch, M. J., Using Redundant Internal Coordinates To Optimize Equilibrium Geometries And Transition States. *Journal Of Computational Chemistry* **1996,** 17, (1), 49-56.
42. Peng, C. Y.; Schlegel, H. B., Combining Synchronous Transit And Quasi-Newton Methods To Find Transition-States. *Israel Journal Of Chemistry* **1993,** 33, (4), 449-454.
43. Ciccotti, G. A. H., W. G. , *Molecular Dynamics Simulation Of Statistical-Mechanical Systems*. North-Holland: 1986.
44. Heermann, D. W., *Computer Simulation Methods*. Springer: 1986.
45. Vangunsteren, W. F.; Berendsen, H. J. C., Algorithms For Brownian Dynamics. *Molecular Physics* **1982,** 45, (3), 637-647.
46. Berendsen, H. J. C., Biophysical Applications Of Molecular-Dynmaics. *Computer Physics Communications* **1987,** 44, (3), 233-242.
47. Steinbrecher, R. W. T. Http://Ambermd.Org/Tutorials/Advanced/Tutorial3/
48. Frisch Mj, T. G., Schlegel Hb, Scuseria Ge, Robb Ma, Cheeseman Jr., Zakrzewski Vg, Montgomery Ja Jr., Stratmann Re, Burant Jc, Dapprich S, Millam Jm, Daniels Ad, Kudin Kn, Strain M. C, Farkas O, Tomasi J, Barone V, Cossi M, Cammi R, Mennucci B, Pomelli C, Adamo C, Clifford S, Ochterski J, Petersson Ga, Ayala Py, Cui Q, Morokuma K, Malick Dk, Rabuck Ad, Raghavachari K, Foresman Jb, Cioslowski J, Ortiz J. V, Baboul A. G, Stefanov B. B, Liu G, Liashenko A, Piskorz P, Komaromi I, Gomperts R, Martin Rl, Fox Dj, Keith T, Al-Laham Ma, Peng Cy, Nanayakkara A, Gonzalez C, Challacombe M, Gill Pmw, Johnson B, Chen W, Wong Mw, Andres Jl, Gonzalez C, Head-Gordon M, Replogle Es, And Pople Ja, , Gaussian03. In 2003.
49. Olson, X.-J. L. A. W. K., 3dna: A Software Package For The Analysis, Rebuilding And Visualization Of Three-Dimensional Nucleic Acid Structures *Nucleic Acids Research* **2003,** 31, (17), 5108-5121.
50. Olson, X.-J. L. W. K., 3dna: A Versatile, Integrated Software System For The Analysis, Rebuilding And Visualization Of Three-Dimensional Nucleic-Acid Structures. *Nature Protocols 3, - 1213 - 1227 (2008)* **2008,** 3, 1213-1227.
51. Sasha Buzko, S.-H. P., Ashton Taylor *Sirius Visualization System* 1.2; San Diego, 2009.

CHAPTER 3 RESULTS AND DISCUSSION

3.1 Bond Length Alternation and Absorption Maxima

3.1.1 Data Set

A benchmark set of 28 diarylethene derivative photochromic compounds was used to predict equilibrium geometry. They can be broadly classified into three data sets based on the bridging functional group (**Figure 3.1**): a) Dicyano derivatives (DCN), b) Maleicanhydride derivatives (MA) and c) Perfluorocyclopentene derivative (PFC)

a) Dicyano derivatives

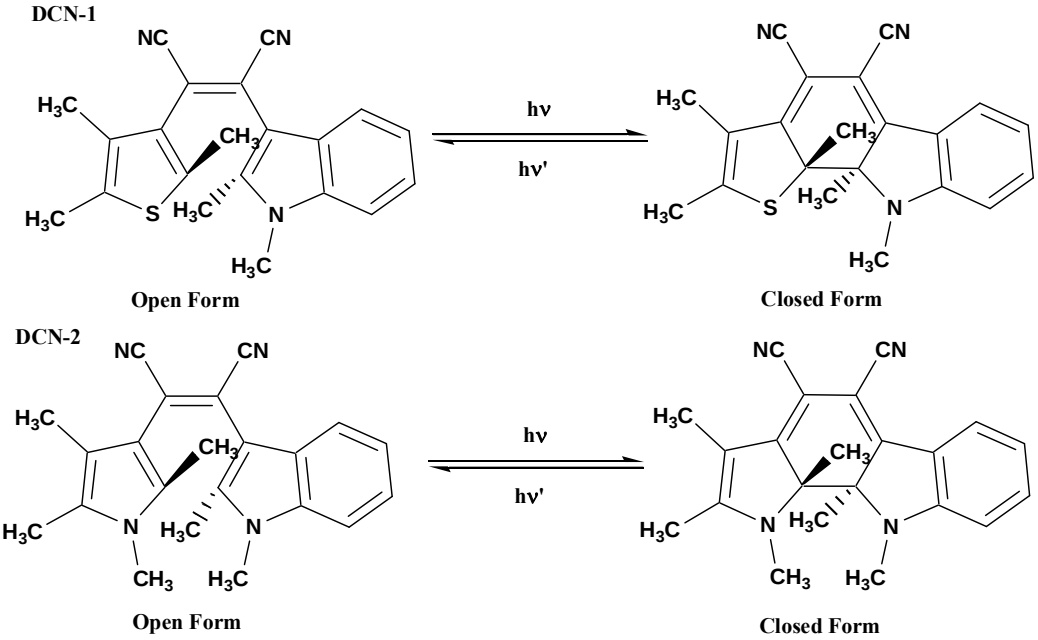

b) Maleicanhydride derivatives

MA-1

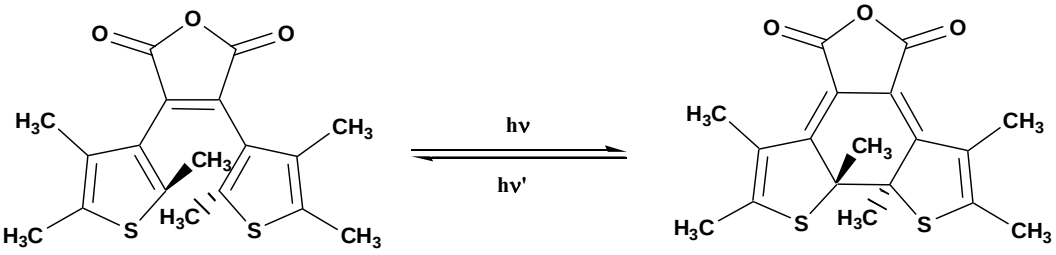

Open Form　　Closed Form

MA-1-A

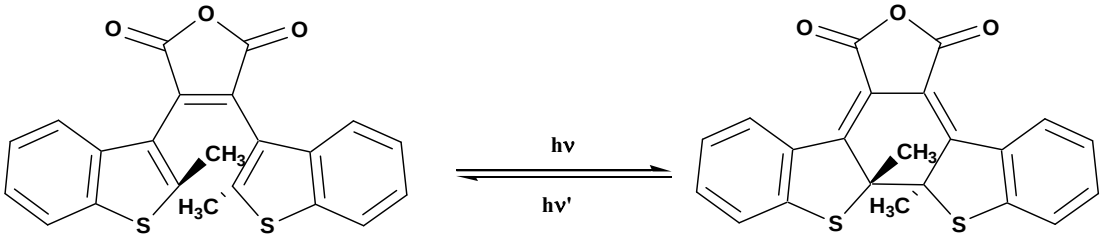

Open Form　　Closed Form

MA-2

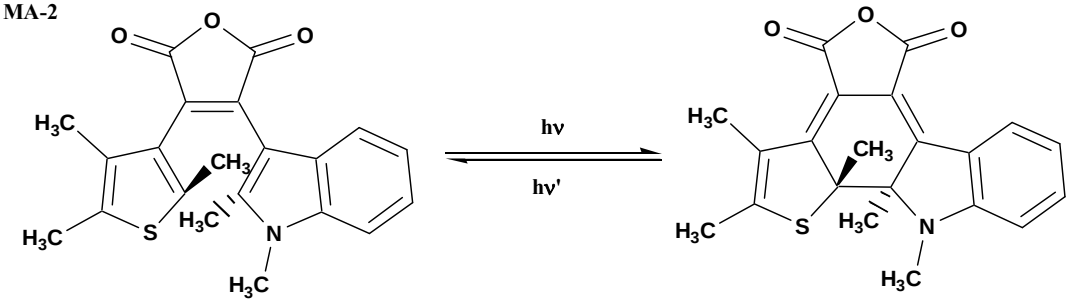

Open Form　　Closed Form

MA-2-A

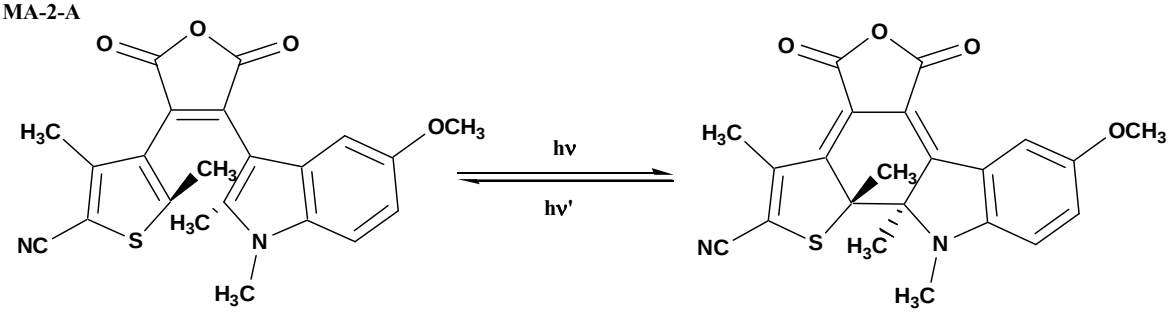

Open Form　　Closed Form

MA-2-B

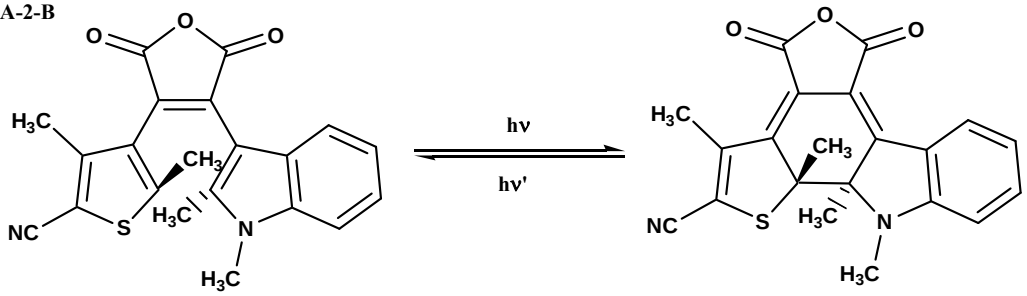

Open Form　　Closed Form

MA-3

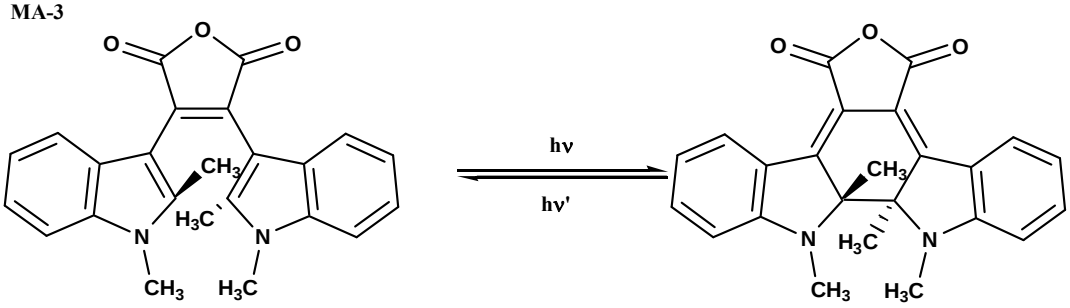

Open Form　　Closed Form

MA-hit

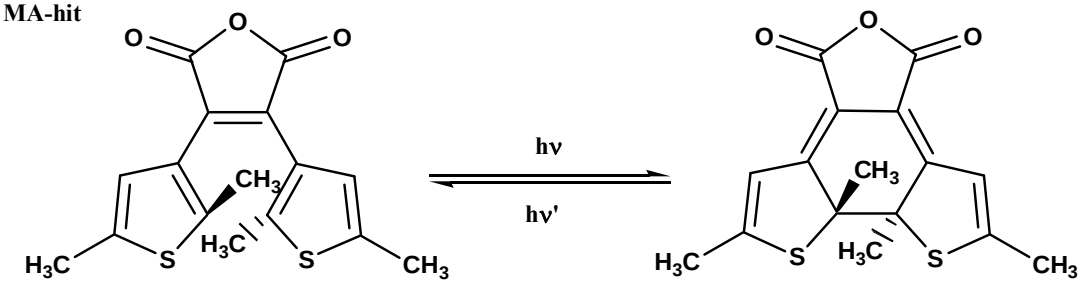

Open Form　　Closed Form

MI

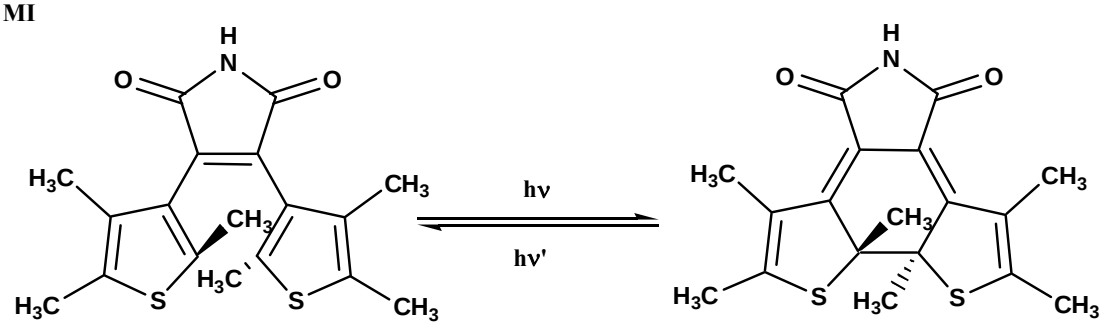

Open Form　　Closed Form

c) Perfluorocyclopentene derivatives

PFC-1

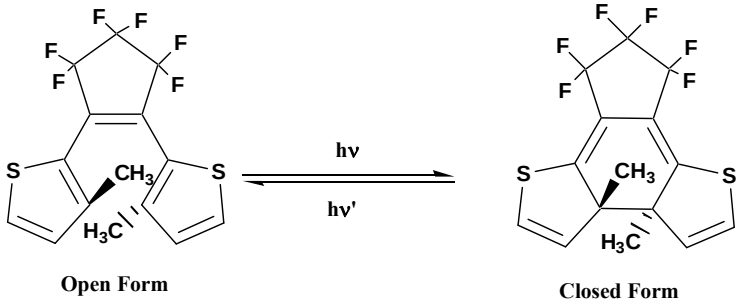

PFC-1-A

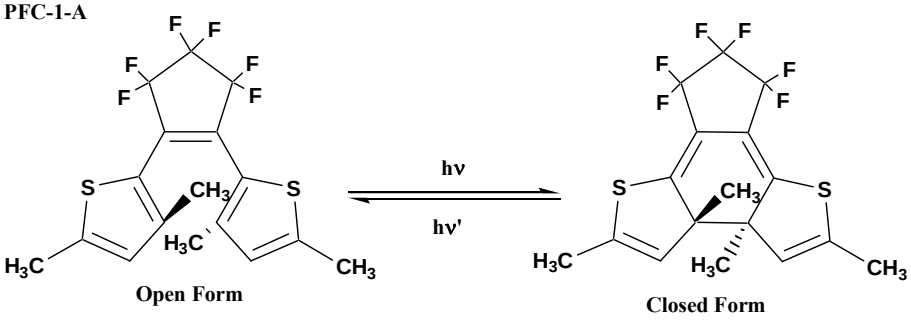

PFC-1-B

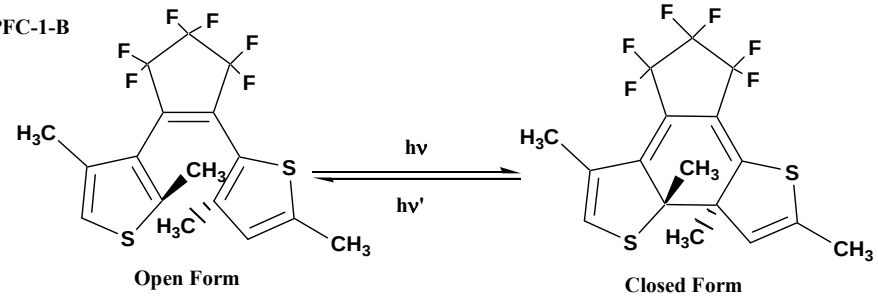

PFC-1-C

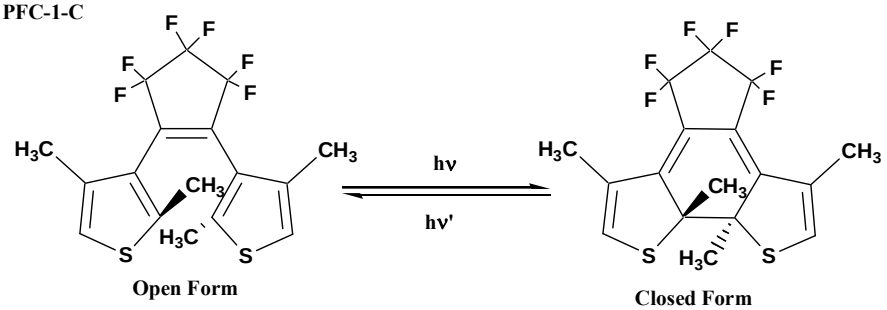

PFC-1-D

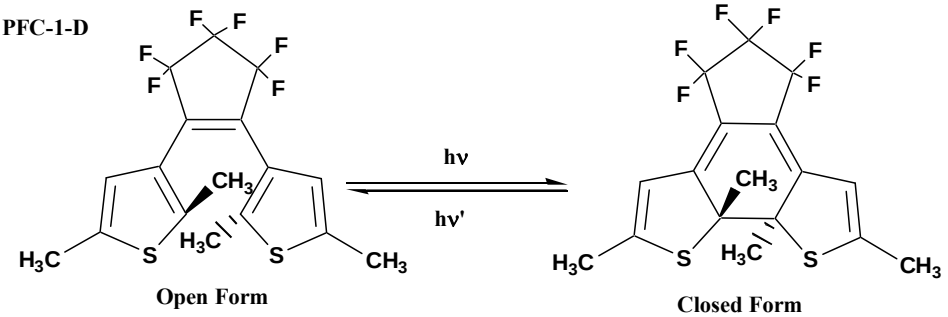

PFC-1-E

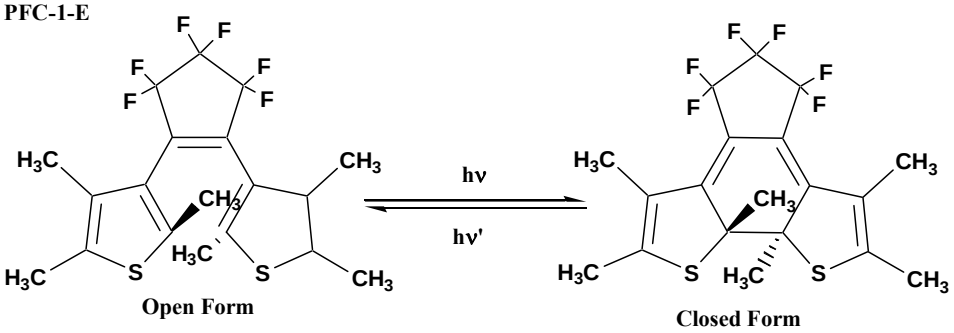

PFC-2

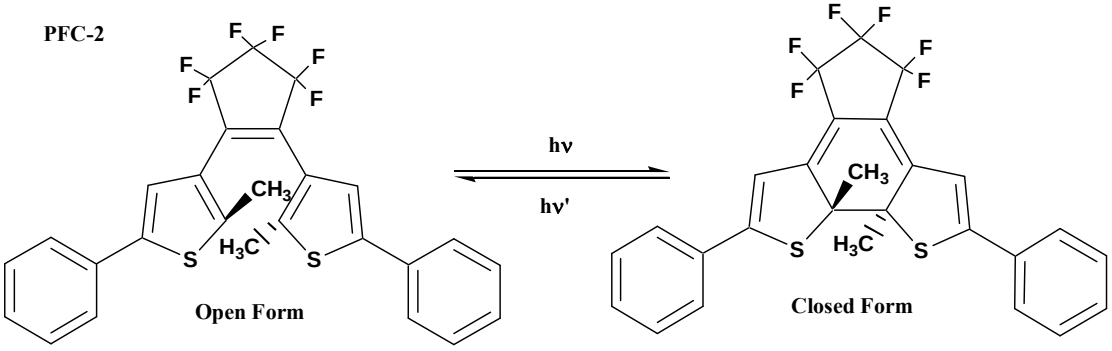

PFC-2-A

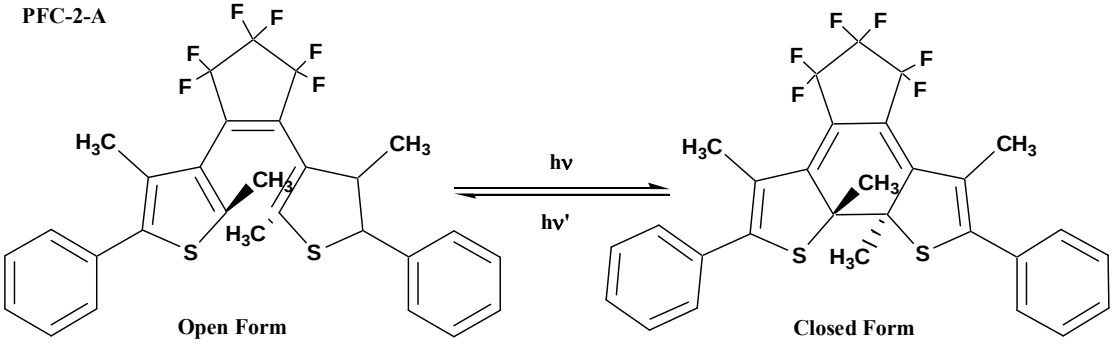

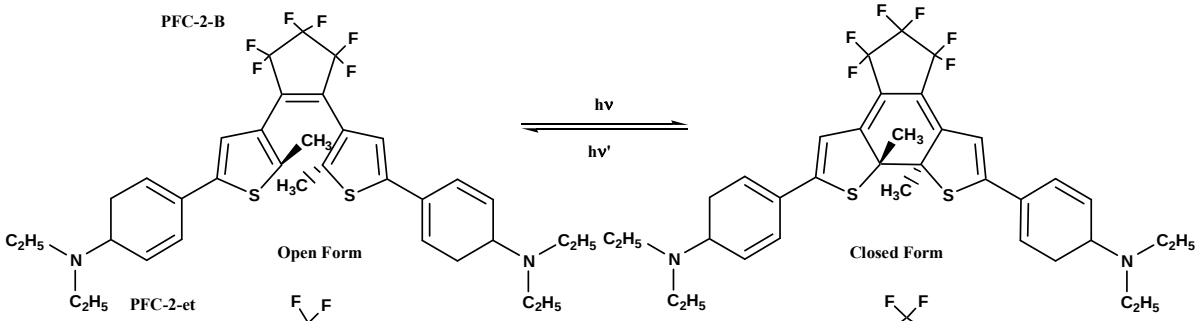
PFC-2-B
hν
hν'
Open Form
Closed Form
PFC-2-et
hν
hν'
Open Form
Closed Form

PFC-3

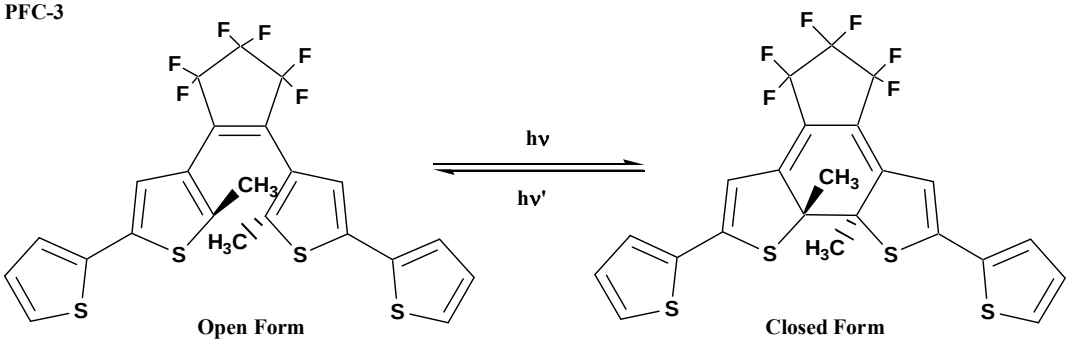
hν
hν'
Open Form
Closed Form

PFC-4

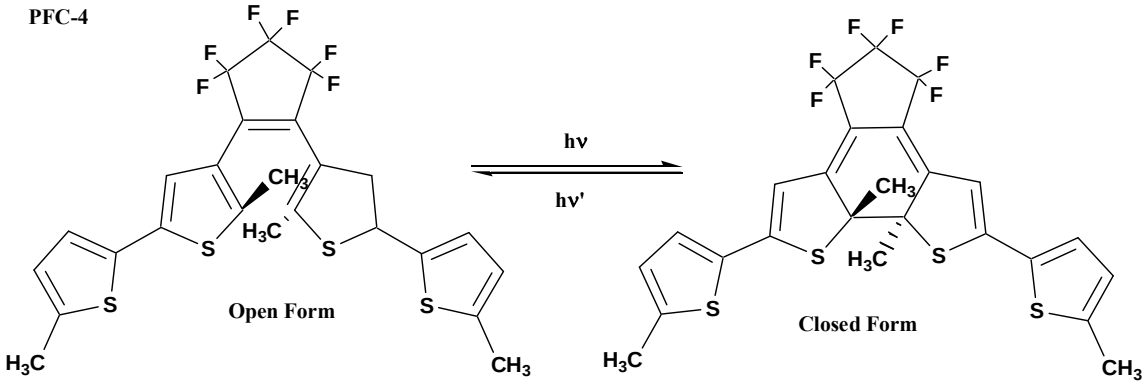
hν
hν'
Open Form
Closed Form

PFC-5

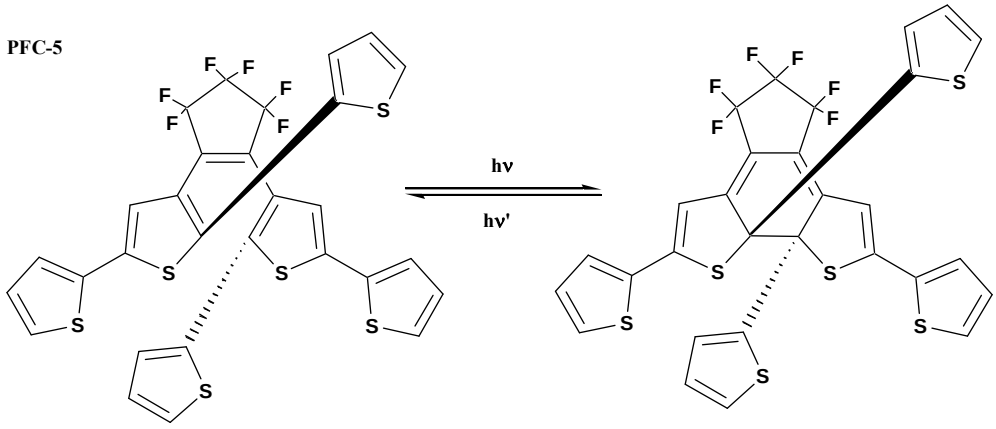

Open Form Closed Form

PFC-6

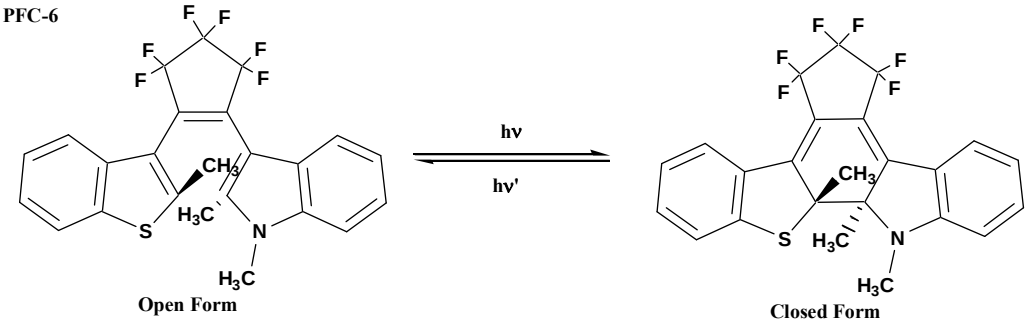

Open Form Closed Form

PFC-6-A

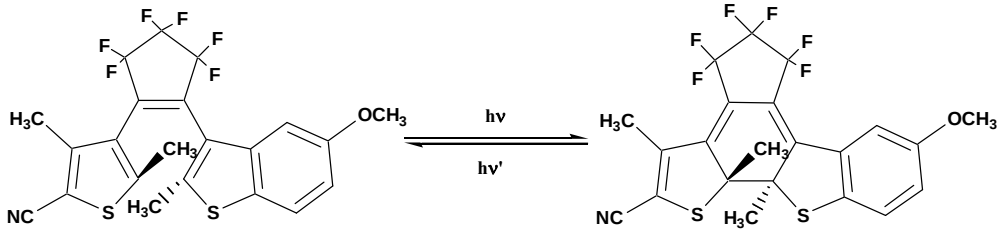

Open Form Closed Form

PFC-7

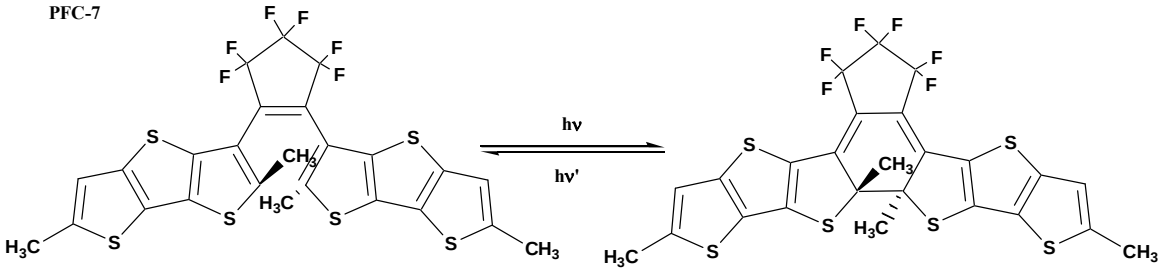

Open Form Closed Form

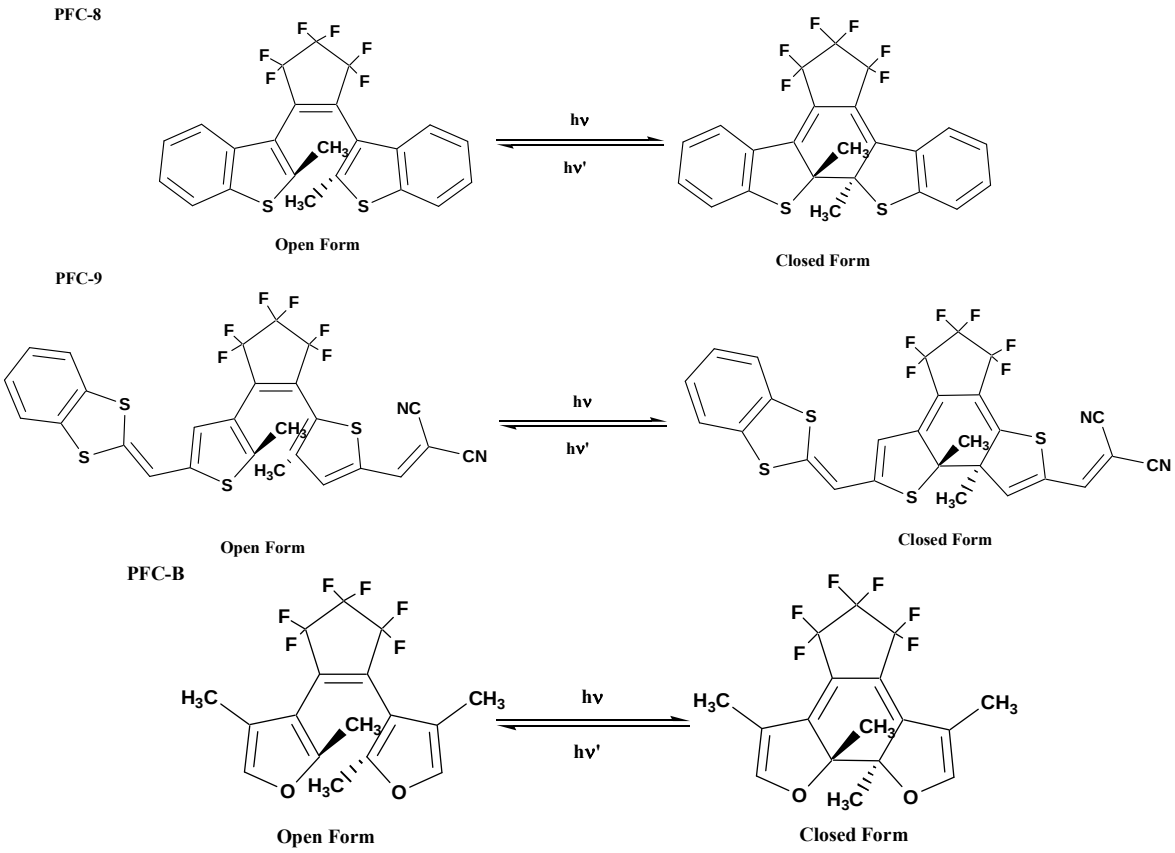

Figure 3.1: Benchmark set of open and closed-ring isomers studied in this work: Dicyano (DCN), Maleicanhydride (MA), Maleimide (Mi) derivatives and Perfluorocyclopentene derivatives (PFC)

3.1.2 Results

Table 3.1 reports the results obtained with different TD-DFT exchange-correlation functionals (BMK, B3LYP, M05-2X and M05) and basis sets (MIDI! and 6-31G*) for prediction of the absorption spectra at the experimental X-ray geometry of 1,2-bis(2-methyl-5-phenyl-3-thienyl)perfluorocyclopentene (PFC-2). For fair comparison with experimental absorption spectrum, recorded in hexane we use PCM implicit solvation model.

Table 3.1: Wavelength of the maxima on the absorption spectra (λ_{max}, nm) and the deviation ($\Delta\lambda$, nm) for bis(2,5-dimethyl-3-thienyl)perfluorocyclopentene (PFC-2) calculated at different theory levels with and without solvent (heptane) compared to the experimental data (in hexane).

PFC-2	**Closed**		**Open A**		**Open B**	
	λ_{max}	$\Delta\lambda$	λ_{max}	$\Delta\lambda$	λ_{max}	$\Delta\lambda$
Experiment	575		280		280	
TD-BMK/6-31G*//EXP	540	35	267	13	263	17
TD-BMK/6-31G*/PCM//EXP	555	20	271	9	266	14
TD-B3LYP/MIDI!//EXP	575	0	274	6	278	2
TD-B3LYP/MIDI!/PCM//EXP	590	-15	284	-4	280	0
TD-B3LYP/6-31G*//EXP	586	-11	291	-11	286	-6
TD-B3LYP/6-31G*/PCM//EXP	603	-28	294	-14	289	-9
TD-M05-2X/6-31G*/PCM//EXP	549	16	265	15	260	20
TD-M05/6-31G*/PCM//EXP	607	-32	289	-9	284	-4

It is evident from the results above that in order to accurately predict the λ_{max}, implicit solvent is essential. Although B3LYP/MIDI! performs slightly better for the closed-ring isomers, the M05/6-31G* was selected as it reproduced λ_{max} for both open and closed isomers consistently. **Table 3.2** contains the predictions obtained using other theoretical methods: AM1, HF and DFT with different exchange-correlated functionals

(B3LYP, BHandHLYP, PBE1PBE, BMK, M05, and M05-2x) and two basis sets (MIDI! and 6-31G*) for both BLA and spectral maxima of bis(2,5-dimethyl-3-thienyl)perfluorocyclopentene (PFC-2). In addition to the detailed study of PFC-2, we also investigated a representative of a different class of diarylethenes, 1,2-bis(2,5-dimethyl-3-thienyl)maleicanhydride (MA-hit). This is the only maleic anhydride derivative with available X-ray data (open isomer only).[1] TD-BMK/6-31G*/PCM//BMK/6-31G*/PCM predictions which were in agreement with experiment in case of PFC-2, were not so accurate in case of MA-hit. The only method with good agreement for BLA as well as absorption spectra prediction for PFC-2 and MA-hit was TD-M05/6-31G*/PCM//M05-2X/6-31G*/PCM.

Table 3.2: Bond length alternation (BLA, Å) and wavelength of the maxima on the absorption spectra (λ_{max}, nm) for bis(2,5-dimethyl-3-thienyl)perfluorocyclopentene (PFC-2) and 1,2-bis(2,5-dimethyl-3-thienyl)maleicanhydride (MA-hit) calculated at different theory level and compared to the experimental data (solvent for PFC-2 – heptane and for Ma-hit – benzene). See Figure 1.4 for definition of BLA1 and BLA2.

PFC-2	**Closed**				**Open**			
	BLA1	**BLA2**	**λ_{max}**	**$\Delta\lambda$**	**BLA1**	**BLA2**	**λ_{max}**	**$\Delta\lambda$**
Experiment	0.085	0.055	575		-0.112	0.050	276	
TD-B3LYP/MIDI!//AM1	0.103	0.085	605	-30	-0.093	0.052	269	7
TD-B3LYP/ MIDI!//HF/STO-3G	0.147	0.141	514	61	-0.173	0.116	274	2
TD-B3LYP/MIDI!//B3LYP/ MIDI!	0.089	0.056	588	-13	-0.096	0.067	290	-14
TD-B3LYP/MIDI!/PCM//B3LYP/MIDI!	0.089	0.056	605	-30	-0.096	0.067	296	-20
TD-B3LYP/MIDI!/PCM//PBE0/MIDI!	0.089	0.056	605	-30	-0.092	0.061	296	-20
TD-B3LYP/MIDI!/PCM//B1B95/MIDI!	0.092	0.059	599	-24	-0.095	0.060	298	-22
TD-B3LYP/MIDI!//BMK/MIDI!	0.110	0.080	564	11	-0.117	0.082	289	-13
TD-B3LYP/MIDI!/PCM//BHandHLYP/MIDI!	0.107	0.075	572	3	-0.106	0.073	289	-13
TD-B3LYP/MIDI!//HF/MIDI!	0.134	0.102	525	50	-0.129	0.058	272	4
TD-B3LYP/6-31G*//BMK/6-31+G*	0.098	0.072	573	2	-0.116	0.072	276	0
TD-B3LYP/6-31G*//BMK/6-311G*	0.100	0.076	558	17	-0.121	0.074	272	4
TD-B3LYP/6-31G*//B3LYP/6-31G*	0.082	0.057	602	-27	-0.111	0.065	283	-7
TD-B3LYP/MIDI!/PCM//BMK/6-31G*	0.098	0.074	590	-15	-0.116	0.074	298	-22
TD-B3LYP/6-31G*/PCM//BMK/6-31G*	0.100	0.074	590	-15	-0.117	0.073	299	-23
TD-B3LYP/6-31G*/PCM//BMK/6-31G*/PCM	0.083	0.057	620	-45	-0.110	0.066	298	-22
TD-BMK/6-31G*/PCM//BMK/6-31G*/PCM	0.083	0.057	566	9	-0.110	0.066	274	2
TD-B3LYP/6-31G*/PCM//B3LYP/6-31G*/PCM	0.085	0.058	615	-40	-0.100	0.079	302	-26
TD-B3LYP/6-31G*/PCM//M05-2X/6-31G*/PCM	0.100	0.076	581	-6	-0.114	0.068	292	-16
TD-M05-2X/6-31G*/PCM//M05-2X/6-31G*/PCM	0.100	0.076	521	54	-0.114	0.068	262	14
TD-M05/6-31G*/PCM//M05-2X/6-31G*/PCM	0.100	0.076	585	-10	-0.114	0.068	287	-11
MA-hit	**Closed**				**Open**			
	BLA1	**BLA2**	**λ_{max}**	**$\Delta\lambda$**	**BLA1**	**BLA2**	**λ_{max}**	**$\Delta\lambda$**
Experiment			510		-0.109	0.082	403	
TD-BMK/6-31G*/PCM//BMK/6-31G*/PCM	0.092	0.078	477	33	-0.101	0.087	383	20
TD-B3LYP/6-31G*/PCM//BMK/6-31G*	0.092	0.080	519	-9	-0.113	0.087	446	-43
TD-B3LYP/6-31G*/PCM//M05-2X/6-31G*/PCM	0.091	0.077	519	-9	-0.102	0.071	447	-44
TD-M05/6-31G*/PCM//M05-2X/6-31G*/PCM	0.091	0.077	520	-10	-0.102	0.071	423	-20

From the results presented in the **Tables 3.1** and **3.2** it follows, that each of the methods that predicts the BLA accurately, does not appear accurate in the spectral predictions. This is most likely to be a consequence of the implied adiabatic

approximation to TD-DFT. In rigorous theory, frequency-dependent exchange-correlation kernels are required.[2-4] In practice, however, one may simplify this frequency dependence to a step-function and use one exchange-correlation functional to describe the ground state, while using another frequency-independent functional to describe all the low-lying excited states. After a number of functionals were considered, the ones with higher (42-56%) fraction of HF exchange (BMK and M05-2X) were found to better predict the ground state geometry. On the other hand, the functionals with the lower (~20%) fraction of HF exchange, predicted the excitation energies accurately, when combined with linear response adiabatic TD-DFT. Finally, we selected the combination of TD-M05/6-31G*/PCM//MO52x/6-31G*/PCM to be the best in prediction of BLA as well as λ_{max} values for both open and closed conformers for different DA derivatives with consistent accuracy.

Furthermore, BLA and the maxima on the absorption spectra were predicted on a set of DAs, whose X-ray structure had been elucidated, using implicit solvent model for both closed and open isomers (**Table 3.3**) at TD-M05/6-31G*/PCM//M05-2X/6-31G*/PCM. The results from this study also concluded that TD-M05/6-31G* method predicts both BLA and λ_{max} values for both open and closed conformers in best agreement with the experimental parameters for various diarylethene derivatives with consistent accuracy.

Table 3.3: Bond length alternation (BLA, Å) and wavelength of the maxima on the absorption spectra (λ_{max}, nm) for a subset of diarylethenes calculated at TD-M05/6-31G*/PCM//M05-2X/6-31G*/PCM theory level and compared to experimental data.

	Closed isomer			**Open isomer**		
	BLA1	**BLA2**	**λ_{max}**	**BLA1**	**BLA 2**	**λ_{max}**
PFC-1-d						
Experiment[a]	0.095	0.091	505	-0.112	0.089	303
Theory	0.106	0.087	505	-0.113	0.080	316
PFC-1-e						
Experiment[b]			529	-0.132	0.095	
Theory	0.113	0.093	526	-0.117	0.089	279
PFC-2						
Experiment[c]	0.085	0.055	575	-0.112	0.050	276
Theory	0.100	0.076	585	-0.114	0.068	287
PFC-2-et						
Experiment[d]	0.089	0.059	600	-0.115	0.068	286
Theory	0.101	0.075	611	-0.116	0.067	284
PFC-B						
Experiment[e]	0.113	0.055	469	-0.120	0.053	274
Theory	0.119	0.045	476	-0.102	0.057	251
PFC-5						
Experiment[f]			632	-0.133	0.062	320
Theory	0.101	0.071	611	-0.116	0.060	332
MA-hit						
Experiment[g]			510	-0.109	0.082	403
Theory	0.091	0.077	520	-0.102	0.071	423
RMSD	0.011	0.014	11	0.011	0.009	15

[a)]Ref.[5], [b)] Ref. [6], [c)] Ref. [7], [d)] Ref. [8], [e)] Ref. [9], [f)] Ref. [10], [g)] Ref. [1]

Table 3.4: Maximum absorption wavelengths (λ_{max}, nm) measured experimentally and predicted at two theory levels: TD-B3LYP/6-31G*/PCM (T1) and TD-M05/6-31G*/PCM (T2), both use geometry optimized at M05-2X/6-31G*/PCM level for open and closed isomers of diarylethenes in solution. Deviations of the theoretical values from the experimental ones ($\Delta\lambda_{max}$, nm) are also reported.

		Closed					**Open**				
		λ			**Δλ**		**λ**			**Δλ**	
Molecule	**Solvent**	Exp	**T1**	**T2**	**T1**	**T2**	Exp	**T1**	**T2**	**T1**	**T2**
DCN-1[a]	**Bz**	547	552	531	-5	16	412	457	433	-45	-21
DCN-2[a]	**Bz**	574	556	533	18	41	390	480	377	-90	13
MA-1[b]	**Bz**	560	525	531	35	29	335	397	380	-62	-45
MA-1-A[c]	**Bz**	544	538	531	6	13	417	504	475	-87	-58
MA-2[a]	**Bz**	595	563	545	32	50	450	507	481	-57	-31
MA-2-A[d]	**Bz**	680	683	644	-3	36	-	498	493	-	-
MA-2-B[d]	**Bz**	628	624	598	4	30	-	504	481	-	-
MA-3[e]	**Bz**	620	595	565	25	55	470	540	508	-70	-38
Mi[f]	**Bz**	512	496	500	16	12	370	391	374	-21	-4
MA-hit[g]	**Bz**	510	519	520	-9	-10	403	446	423	-43	-20
PFC-1[h]	**Hep**	432	428	436	4	-4	316	342	332	-26	-16
PFC-1-a[i]	**Hep**	425	421	425	4	0	336	357	345	-21	-9
PFC-1-b[i]	**Hep**	469	462	466	7	3	312	311	322	1	-10
PFC-1-c[j]	**Hep**	534	522	528	12	6	234	288	280	-54	-46
PFC-1-d[i]	**Hep**	505	499	505	6	0	303	326	316	-23	-13
PFC-1-e[k]	**Hep**	529	517	505	12	24	-	285	266	-	-
PFC-2[l]	**Hep**	575	590	585	-15	-10	280	298	287	-18	-7
PFC-2-a[j]	**Hep**	562	576	575	-14	-13	262	294	280	-32	-18
PFC-2-b[j]	**Hep**	597	602	593	-5	4	305	324	308	-19	-3
PFC-2-et[m]	**Hep**	600	613	611	-13	-11	286	303	288	-17	-2
PFC-3[n]	**ACN**	605	610	604	-5	1	312	315	304	-3	8
PFC-4[n]	**ACN**	612	619	610	-7	2	320	321	312	-1	8
PFC-5[o]	**DCM**	632	629	611	3	21	320	356	332	-36	-12
PFC-6[p]	**ACN**	565	552	534	13	31	340	368	356	-28	-16
PFC-6-A[d]	**Hep**	665	653	625	12	40	-	375	355	-	-
PFC-7[p]	**ACN**	612	596	585	16	27	290	334	327	-44	-37
PFC-8[q]	**Hep**	517	523	521	-6	-4	258	269	261	-11	-3
PFC-9[r]	**Bz**	828	787	792	41	36	354	379	358	-25	-4
PFC-B[s]	**Hep**	469	491	476	-22	-7	274	258	251	16	23
RMSD					16	24				42	24

[a]Ref.[11], [b]Ref.[12], [c]Ref-[13], [d]Ref.[14], [e]Ref.[15], [f]Ref.[16], [g]Ref.[1], [h]Ref.[17], [i]Ref.[18], [j]Ref.[19], [k]Ref.[6], [l]Ref.[7], [m]Ref.[8], [n]Ref.[20], [o]Ref.[10], [p]Ref.[21], [q]Ref.[22], [r]Ref.[23], [s]Ref.[9].

For the rest of the molecules in the benchmark set single crystal X-ray diffraction data were not available. We report their maximum absorption wavelengths at two theory levels: TD-M05/6-31G*/PCM and TD-B3LYP/6-31G*/PCM (with geometry optimized at M05-2X/6-31G*/PCM level) and compare our predictions with the experimental λ_{max} values in **Table 3.4**. From the **Table 3.4** one can see that the average deviations in the maximum wavelengths obtained with M05 functional is 24 nm for both open and closed forms, and maximum signed errors are 55 nm (closed) and -58 nm (open), while for B3LYP the average deviations are 42 nm (open) and 16 nm (closed), maximum signed errors are 41 nm (closed) and -90 nm (open). The overall average predicted with B3LYP functional is only slightly higher than that for M05 functional. However, B3LYP error is more than twice larger for the open than for the closed isomer. Apparently, B3LYP overestimates the degree of electronic conjugation across the twisted torsional angles in the open form. Thus, we elected to use M05 functional that produces acceptable λ values for both the isomers and gives consistent agreement with experiment for all subclasses of diarylethenes considered in this work: maleic anhydrides, perfluorocyclopentenes, and dicyanodiarylethenes.

3.1.3 Conclusions

Several exchange-correlation functionals in combination with TD-DFT formalism were evaluated for predictions of the absorption spectra for both closed and open isomers of diarylethene photochromic compounds. Bond length alternation descriptors were employed to select suitable exchange-correlation functional to predict the equilibrium geometry in these compounds. We found that a) the most accurate equilibrium geometry based on BLA parameters is calculated at M05-2x/6-31G*/PCM level; b) the spectral data is best reproduced at TD-M05/6-31G*/PCM level with the root mean square deviation from the observed values in the range of 25 nm; c) use of polarization functions in the basis set is important to obtain the best geometry; d) solvent effects as described by polarizable continuum model (PCM) are important for the accurate predictions of the spectral data with TD-DFT. We recommend TD-M05/6-31G*/PCM//M05-2X/6-31G*/PCM theory level for prediction of geometrical and spectral parameters (BLA and λ_{max} values) for both closed and open isomers of diarylethene derivatives.

We have shown that accurate molecular structure and solvent environment are important for predictions of the optical properties in this class of molecules. We intend to use the established protocol in computational design of the new photochromic materials. However, in order to describe other properties and function of the photochromic compounds, one has to go beyond the equilibrium geometry and stationary properties.

3.2 Thermal Stability

3.2.1 Data Set

For the prediction of energy barrier for thermal cycloreversion process in diarylethenes, we selected benchmark set of 7 diarylethene perfluorocyclopentenes (**Figure 3.2**) for which thermal cycloreversion kinetics data is available from the literature.[8, 11, 23, 24]

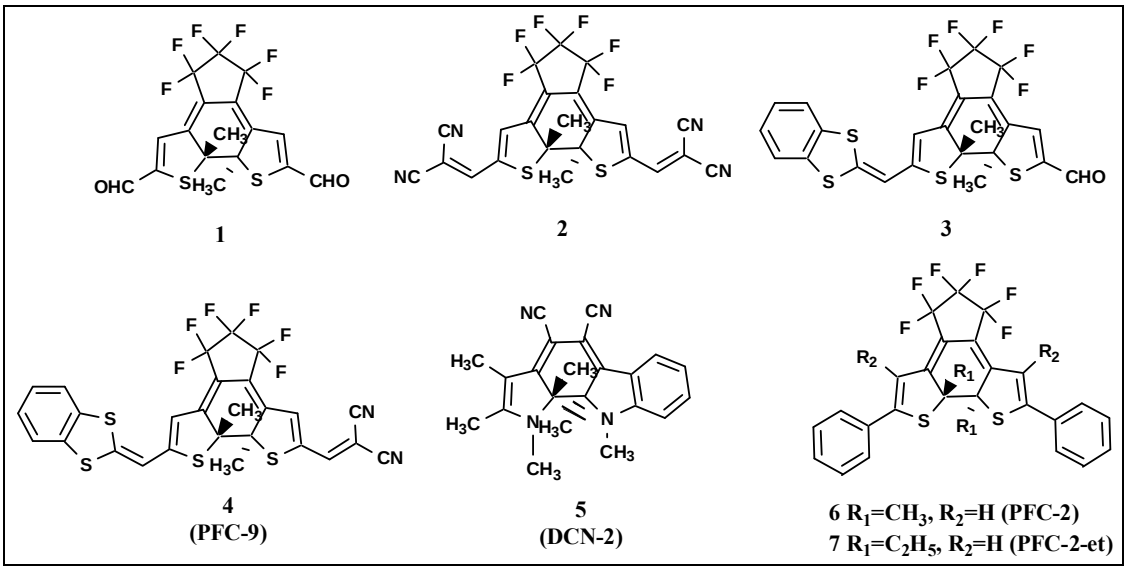

Figure 3.2: Benchmark set of molecules with documented thermal stability.

3.2.2 Activation Energy Determination

Experiments have suggested that thermal stability of the DAs depends on the specific aryl substituents. Their aromatic stabilization energies allow conrotatory cycloreversion and hence make the closed ring isomer thermally unstable. The half-lives for the thermal opening process at elevated temperatures were reported in the literature.[8, 14, 23, 24] The electrocyclic cycloreversion is a unimolecular reaction, therefore, for a given half-life ($t_{1/2}$) the rate constant can be calculated as:

$$k = \frac{-0.693}{t_{1/2}} \qquad \text{(eq. 18)}$$

Using the eq.(18) and from the data published by Irie *et al.*[7] for molecule **6** (PFC-2) ($t_{1/2}$=3.3hr at T=423K and E_a=139kJ/mol), we calculated the rate constant to be k=-0.21hr^{-1}. In order to estimate the activation barrier for these systems we used Arrhenius equation:

$$k = A\exp\frac{-E_a}{RT} \qquad \text{(eq. 19)}$$

Where k is the rate constant, A is the pre-exponential factor, E_a is the activation energy, R is the universal gas constant and T is the temperature. For molecule **6** (PFC-2), the activation barrier was available at two different temperatures and we calculated the pre-exponential factor A to be $-2.968\cdot10^{16}$. Since the cycloreversion process is a unimolecular process, we assumed the value of A to be similar for all the molecules in

Figure 3.2, and used this value for the pre-exponential factor to calculate the experimental activation energy for other molecules, whose $t_{1/2}$ was reported,[8, 11, 23, 24] and used the activation barrier values to benchmark the theoretical predictions (**Table 3.5**).

Table 3.5: Experimental activation barriers for thermal cycloreversion process from closed to open isomers (1-7) using the Arrhenius equation.

Molecule	$t_{1/2}$ (min)	K^{-1} (min^{-1})	Ea (kJ/Mol)	Ea (kCal/Mol)
1[a]	573	-0.07	112.3	26.8
2[a]	3.3	-12.60	98.0	23.4
3[a]	16300	-0.003	121.5	29.0
4[a]	186	-0.224	109.2	26.1
5[b]	----	-0.023	115.5	27.6
6[c]	198	-0.210	139.0	33.2
7[d]	----	-----	120.0	28.7

[a]Ref[23]; [b] Ref[11];[c] Ref[7];[d] Ref[8]

3.2.3 Results

The transition state (TS) in thermally forbidden cycloreversion reactions is expected to have a strong diradical character. The Kohn-Sham or Molecular Orbital description of singlet diradical uses unrestricted formalism where different orbitals are assigned to the electrons of opposite spin (a pair of SOMO, singly occupied molecular orbital). The single determinant with a pair of SOMO is not an eigenvector of the spin operator. Instead, it is an equal mix of singlet and triplet spin states, characterized by the average value of S^2 operator to be close to 1 for most DFT functionals studied. However, UAM1 and UHF determinants remained unrestricted along the reaction path from the open to the closed form, while UKS solution was found to collapse to the restricted determinant soon after the system moved away from the TS. This discontinuity on the potential surface presented the main technical difficulty and required to generate new unrestricted guess on each optimization step with Guess(Always,Mix) keyword. In order to avoid this difficulty we initially combined UHF or UAM1 geometry with single point energy evaluation at DFT level of theory. However, UHF geometry was found to be unsatisfactory at equilibrium (diradical-like), and was not considered further.

Table 3.6: Activation barriers for thermal cycloreversion process from closed to open isomers (in kcal/mol).

	Molecules								
	1	**2**	**3**	**4**	**5**	**6**[a]	**7**[b]	**MAD**	**RMSD**
Experiment	26.8	23.4	29.0	26.1	27.6	33.2	28.7		
UAM1	29.5	29.8	29.9	30.1	24.3	27.1	24.8	6.4	4.8
UB3LYP/MIDI!//UAM1	24.6	22.4	28.6	28.9	38.2	30.0	27.8	10.6	5.9
RM05-2X/MIDI!//UAM1	29.8	26.6	36.2	33.6	45.8	43.1	52.7	24.0	15.6
UM05-2X/MIDI!//UAM1	27.5	26.2	32.1	30.6	39.6	33.1	32.3	12.0	6.9
UHF/MIDI!	27.9	29.5	30.2	30.2	28.2	30.0	27.7	6.1	3.9
B3LYP/MIDI!//UHF/MIDI!	29.2	26.3	33.9	31.7	38.7	37.3	33.6	11.1	7.1
UB3LYP/MIDI!//UHF/MIDI!	27.1	25.2	31.4	30.1	33.4	33.3	30.0	5.8	3.7
BMK/MIDI!//UHF/MIDI!	35.2	31.8	40.5	38.0	45.4	44.8	42.1	17.8	13.6
UBMK/MIDI!//UHF/MIDI!	35.2	31.8	40.4	37.8	39.8	44.5	42.1	13.4	11.8
UB3LYP/6-31G*	28.8	21.8	36.1	29.4	32.6	33.3	29.9	7.0	3.6
UB3LYP/6-31G*(ZPE corr)	26.8	19.8	35.1	27.6	29.3	30.6	27.5	6.0	3.0
UBMK/6-31G*	34.7	28.3	37.5	34.6	38.4	40.6	38.0	10.8	8.3
UBMK/6-31G*(ZPE corr)	32.6	26.0	34.5	33.0	34.8	38.4	34.9	7.2	5.8
UM05-2X/6-31G*	31.4	25.1	34.5	31.5	39.3	38.2	35.8	11.7	6.5
UM05-2X/6-31G*(ZPE corr)	29.3	22.8	32.1	29.4	35.6	35.3	32.9	8.0	4.0
RB3LYP/6-31G*/UB3LYP/6-31G*	31.3	24.1	34.2	30.4	38.9	37.4	34.2	11.3	5.9
RB3LYP/6-31G*/UB3LYP/6-31G*(ZPE corr)	29.8	22.6	33.2	29.0	35.8	35.2	32.1	8.2	4.1
RM05-2X/6-31G*/UM05-2X/6-31G*	35.1	28.7	37.7	33.8	45.6	42.9	40.3	18.0	10.6
RM05-2X/6-31G*/UM052-X/6-31G*(ZPE corr)	33.6	27.1	36.0	32.2	42.5	40.5	37.9	14.9	8.5

[a]Ref[7];[b]Ref[8], MAD: Mean Average Deviation, RMSD: Root Mean Square Deviation

As one can see from the **Table 3.6** the unrestricted KS methods (UB3LYP, UBMK or UM05-2X) give lower energy for the transition state than the restricted ones (RB3LYP or RM05-2X), and are closer to the experimental values in all cases. Zero point energy (ZPE) correction improves the agreement with experiment. After ZPE correction, UB3LYP and UM05-2X methods were found to give the best agreement with experimental activation barriers. The root mean square deviations are 3, 4, and 6 kcal/mol for UB3LYP, UM05-2X, and UBMK respectively. The poor performance of BMK

method is surprising in view of the fact that it was specifically designed to describe chemical kinetics. This may be due to the fact that organic molecules were excluded from the training set used in BMK parameterization.[25] In the contrast, the M05-2X functional was designed with organic reactions in mind.[26] It was shown to perform considerably better than other functionals for a wide range of organic reactions and molecular properties.[27, 28] The systematic plot of the comparison of the calculated activation energy barrier for thermal cycloreversion process in two of the benchmark molecules 6 and 7 with their corresponding experimental barrier (**Figure 3.3**) suggested that UM05-2X functional overestimates over the experimental barrier by ~2-4 kCal/mol. On the other hand, UB3LYP method underestimates the barrier.

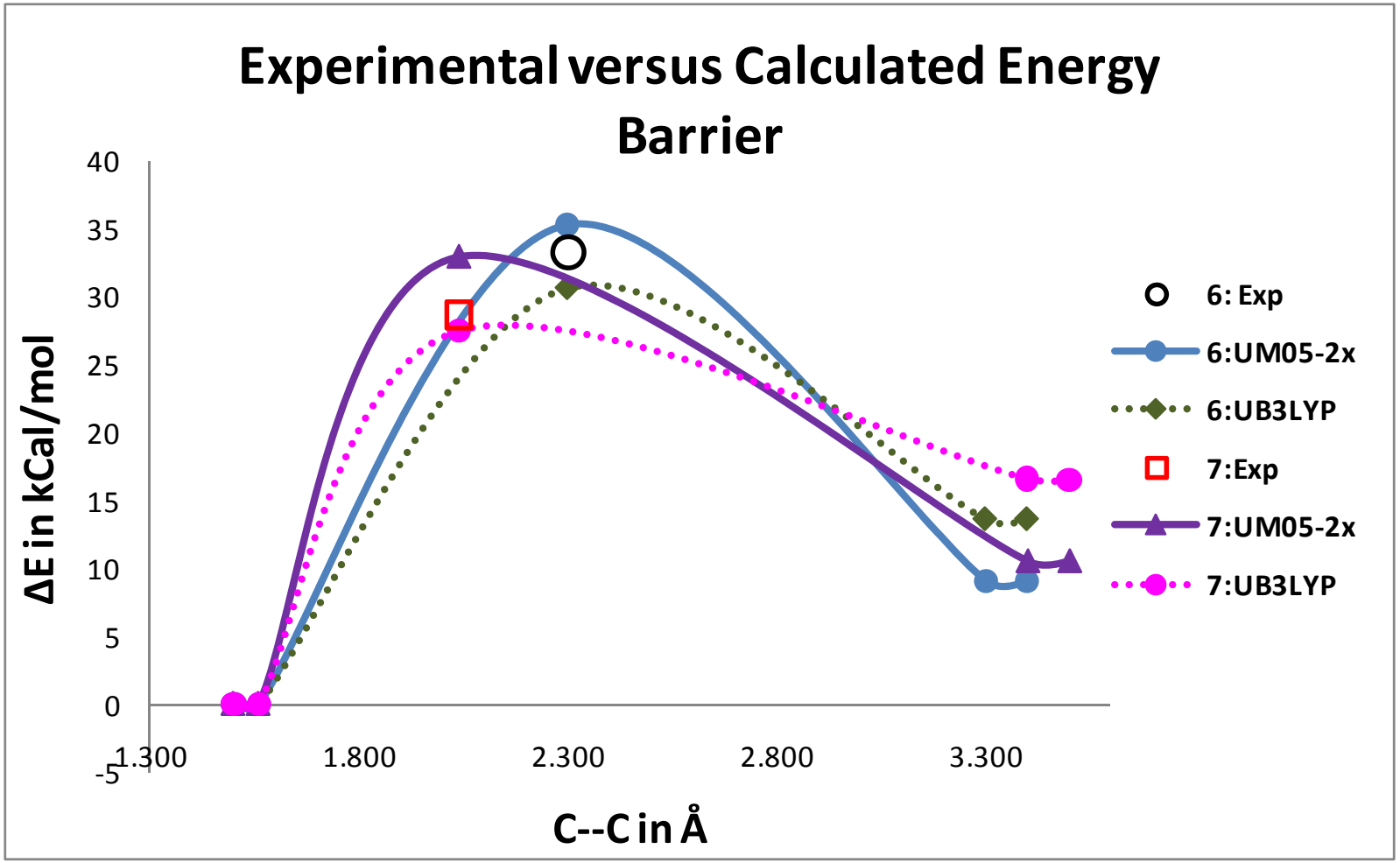

Figure 3.3: Plot of comparison of Experimental activation barrier for thermal cycloreversion with the calculated UM05-2X and UB3LYP data for molecules 6 and 7.

3.2.4 Conclusions

The kinetics of cycloreversion was studied for the benchmark set of seven diarylethene derivatives using Density Functional Theory methods. The activation energies were calculated from the published experimental data, based on the assumption of equal pre-exponential factors in the Arrhenius equation. The geometries of the closed and open isomers, as well as transition states between them were optimized with B3LYP, BMK, and M05-2X methods using MIDI! and 6-31G* basis sets. The predicted activation energies were compared with experimental ones. The use of unrestricted formalism and zero-point energy correction were important in achieving better agreement with experiment. Our results suggest that B3LYP and M05-2X functionals predict the activation barrier for the cycloreversion reaction within 3-4 kcal/mol from experimental value, while BMK overestimates it by 6 kcal/mol on average.

3.3 Fatigue Resistance

3.3.1 Data Set

In this chapter we investigate the mechanism for byproduct formation in the ground state of PFC-2, using unrestricted DFT formalism. We also investigate the activation barriers for the byproduct formation in two other photochromic compounds, PFC-2-A and PFC-1-D, where experimental data are available (**Figure 3.4**). Our study is based on the assumption that photosystem may arrive to the ground state potential energy surface through the conical intersection as MCPD diradical, described by Celani *et al.*[29]

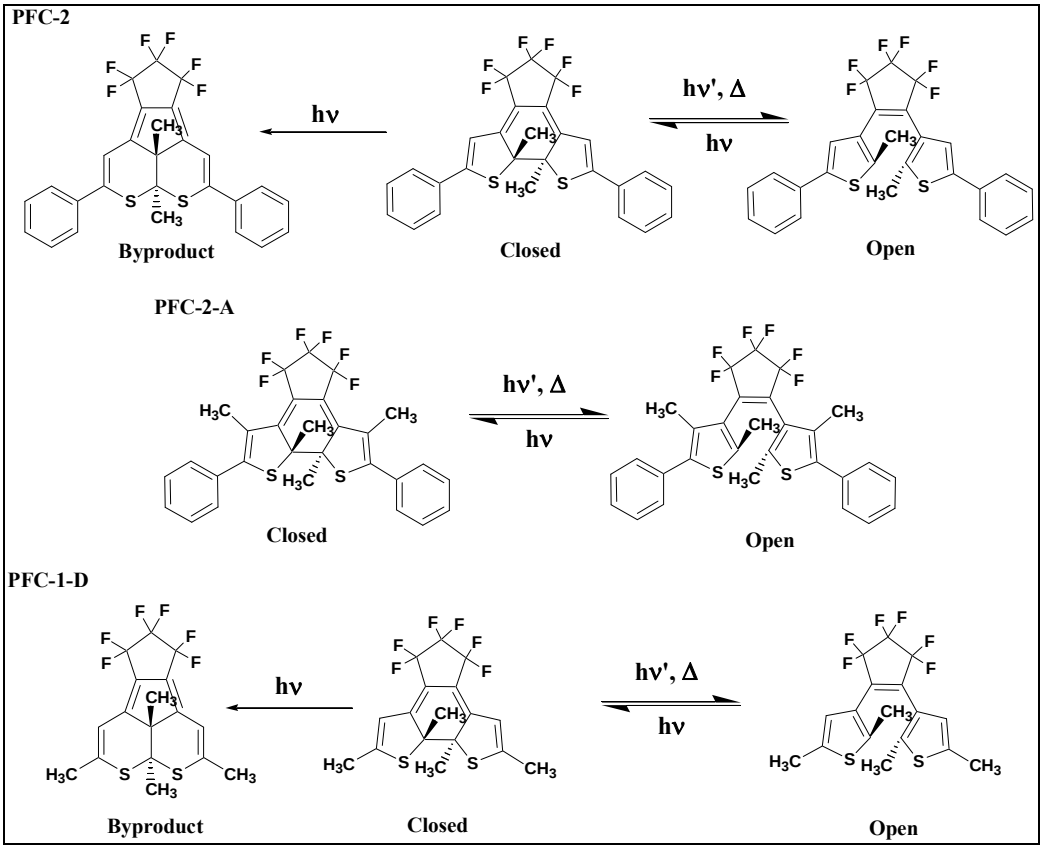

Figure 3.4: Isomeric forms of PFC-2, PFC-2-A and PFC-1-D

3.3.2 Nature of the Excited States in Isomers of 1,2-bis(2-methyl-5-phenyl-3-thienyl)perfluorocyclopentene.

The absorption spectra for the three different isomers (closed, open and byproduct) of PFC-2 (**Figure 3.5**) were predicted using the TD-M05/6-31G*/PCM//M05-2X/6-31G*/PCM level of theory using heptane as implicit solvent. One can see that the predicted spectra are in good agreement with the experiment for all three isomers, considering that vibronic structure was not taken into account and the spectra were broadened with Gaussian line shapes of 0.1 eV empirical widths.

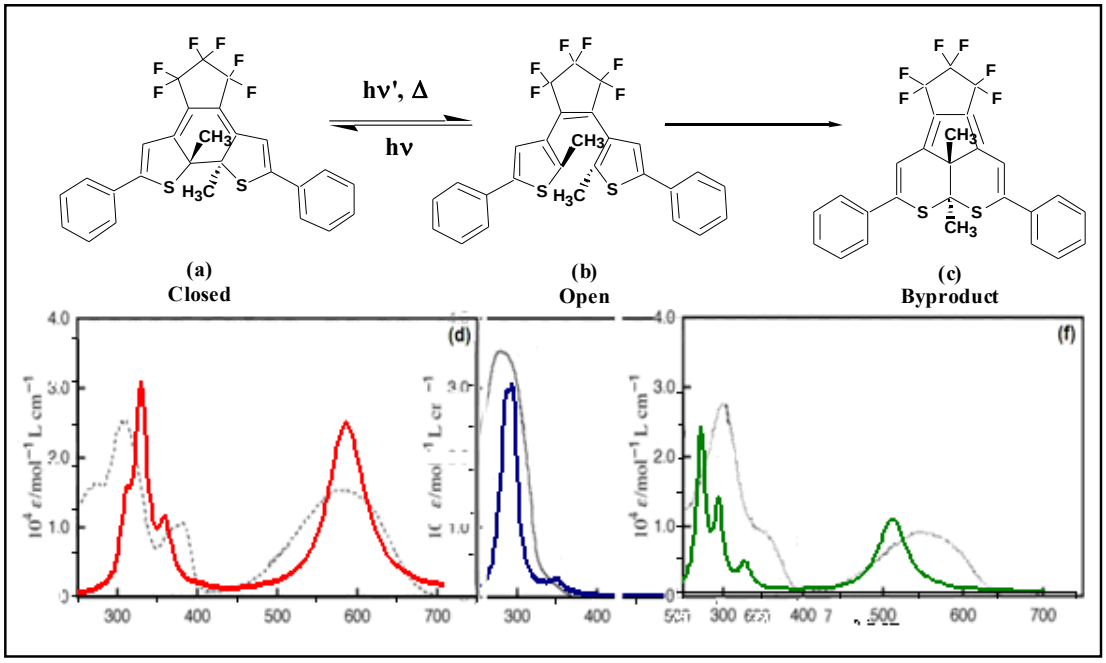

Figure 3.5: (a-c) Isomers of 1 and (d-f) their absorption spectra: experimental (faint lines) and predicted at TD-M05/6-31G*/PCM// M05-2X/6-31G*/PCM level of theory (bold lines). Experimental/theoretical λ_{max} (nm) for the isomers are 575/585 (closed), 276/287 (open) and 547/546 (byproduct).

The detailed description of the electronic excitations in the open and closed forms is presented on **Table 3.7**, and the KS orbitals involved in these excitations are plotted on **Figures 3.6, 3.7 and 3.8**.

Table 3.7: Closed ring, open ring and byproduct isomers of 1: state, energy of the state (E), calculated wavelength (λ), oscillator strength (f), description of the electronic transition and amplitude (amp) of the transition.

closed					
State	**E (eV)**	**λ(nm)**	**f**	**Description**	**amp**
1	**2.12**	**585**	**0.4614**	**HOMO→LUMO**	**0.645**
2	3.26	380	0.0245	HOMO-1→LUMO	0.629
3	3.54	350	0.2237	HOMO→LUMO+1	0.579
4	**3.96**	**313**	**0.6662**	**HOMO-2→LUMO**	**0.676**
5	4.02	308	0.0172	HOMO→LUMO+2	0.567
open					
State	**E (eV)**	**λ(nm)**	**f**	**Description**	**amp**
1	3.73	333	0.0998	HOMO→LUMO	0.671
2	3.98	311	0.0146	HOMO-1→LUMO	0.678
3	**4.33**	**287**	**1.3662**	**HOMO→LUMO+2**	**0.568**
4	4.39	282	0.0382	HOMO→LUMO+1	0.604
5	4.54	273	0.2323	HOMO-2→LUMO	0.658
byproduct					
State	**E (eV)**	**λ(nm)**	**f**	**Description**	**amp**
1	**2.18**	**568**	**0.2768**	**HOMO→LUMO**	**0.653**
2	3.38	367	0.0511	HOMO-1→LUMO	0.654
3	3.85	322	0.3263	HOMO→LUMO+1	0.615
4	**4.12**	**301**	**0.4428**	**HOMO-3→LUMO**	**0.679**
5	4.17	297	0.1753	HOMO-2→LUMO	0.661

The λ_{max} is the transition with the large oscillator strength. In case of the closed isomer there are two bright states, and the lower energy one was found to be of the HOMO→LUMO nature. This state is the one comparable to the reported experimental value (**Figure 3.6**). In case of the open isomer the brightest state is of HOMO→LUMO+2 nature and hence the λ_{max} is 287 nm. The byproduct also has two

bright states, out of which the lower energy one was of the HOMO→LUMO nature (**Figure 3.8**). From the analysis of the KS orbitals for the open isomer in **Figure 3.7**, one can see that the HOMO has antibonding character with respect to the new C—C bond, and LUMO has a bonding character. Therefore, the photocyclization will take place upon the excitation from HOMO to LUMO. However, the optical transition proceeds to the state with large oscillator strength, which corresponds to the brightest optical band. Apparently, some vibrational relaxation from the higher-lying photoabsorbing state to the lowest photoreactive state has to occur before the photocyclic transformation.

HOMOs	LUMOs
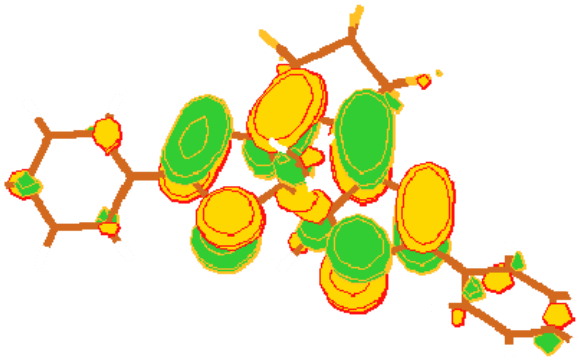 HOMO	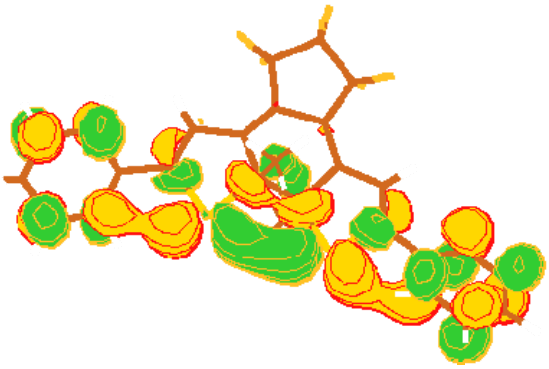 LUMO+2
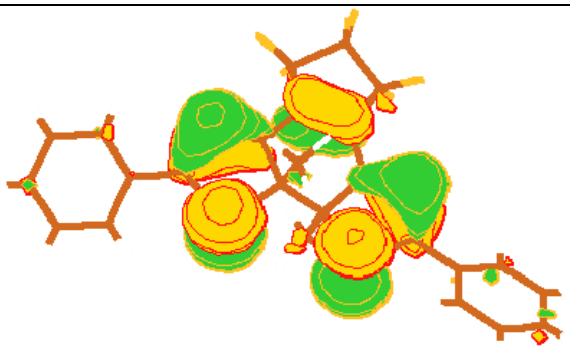 HUMO-1	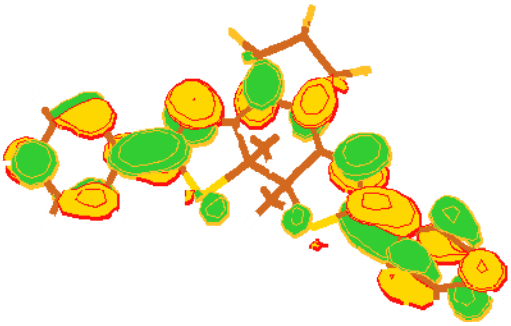 LUMO+1
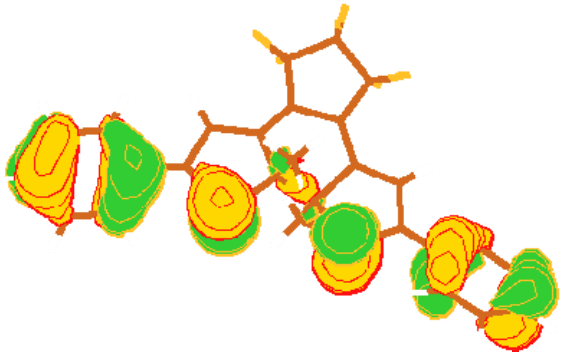 HOMO-2	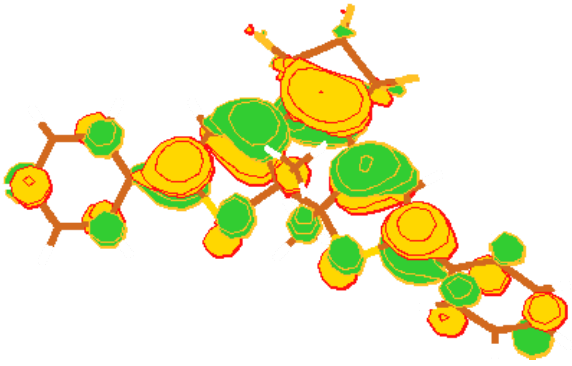 LUMO

Figure 3.6: Essential Kohn-Sham orbital plots for the closed isomer of PFC-2.

HOMOs	LUMOs
 HOMO	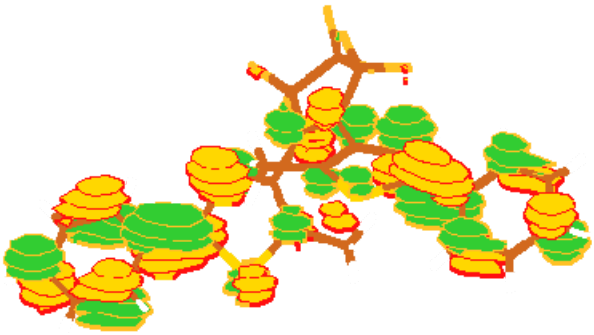 LUMO+2
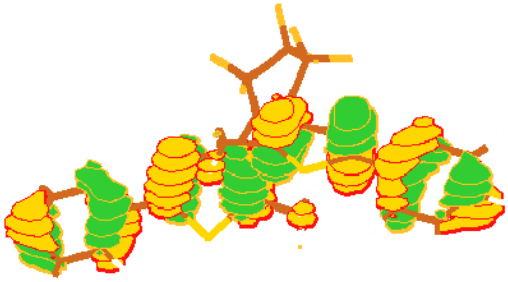 HOMO-1	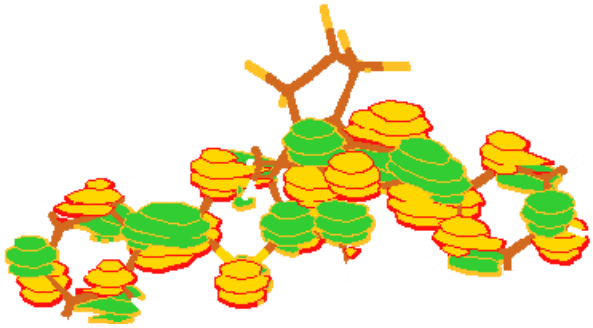 LUMO+1
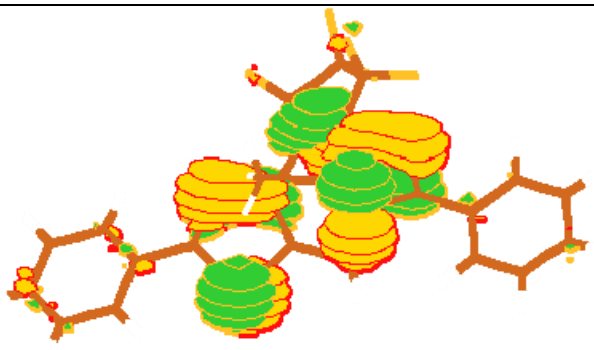 HOMO-2	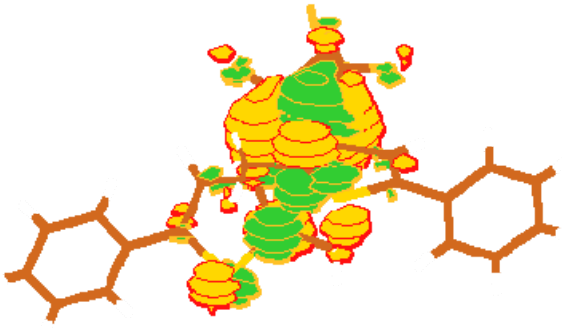 LUMO

Figure 3.7: Essential Kohn-Sham orbital plots for the open isomer of PFC-2.

HOMOs	LUMOs
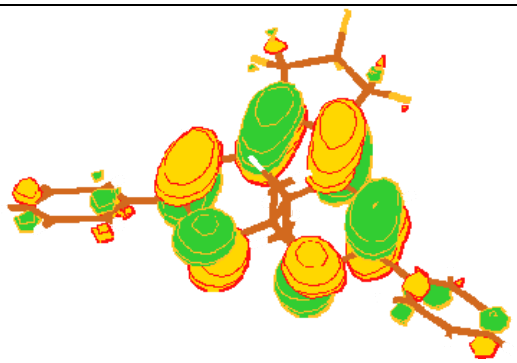 HOMO	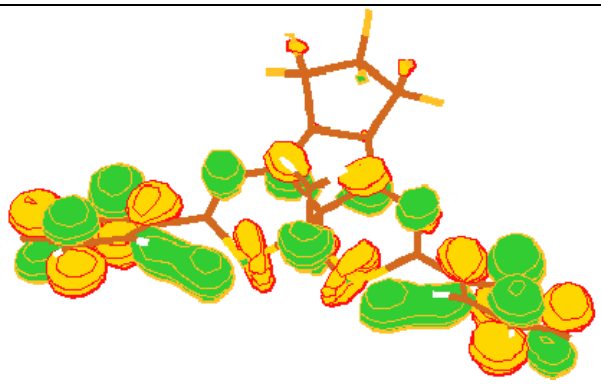 LUMO+2
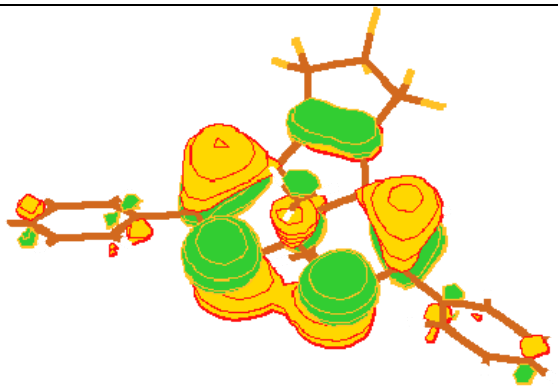 HUMO-1	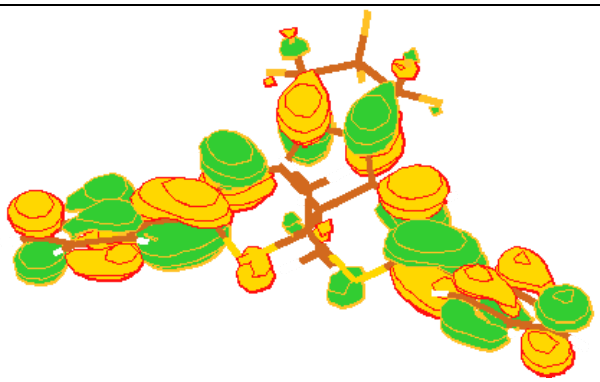 LUMO+1
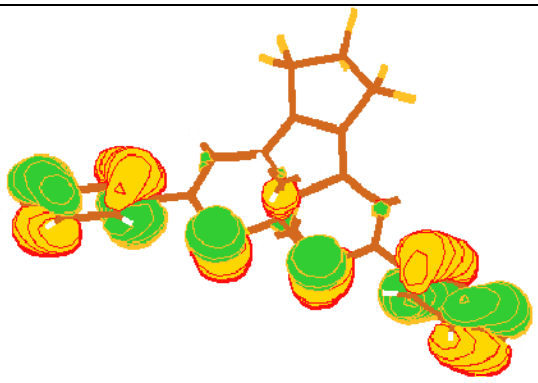 HOMO-2	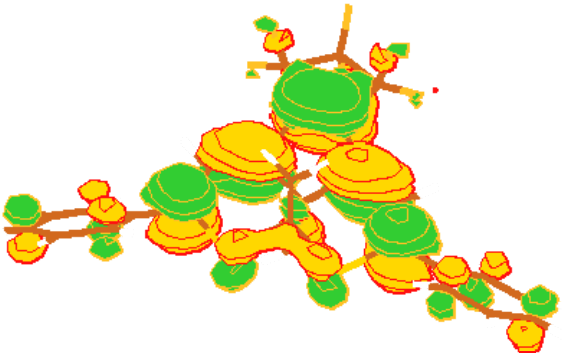 LUMO

Figure 3.8: Essential Kohn-Sham orbital plots for the byproduct isomer of PFC-2.

3.3.3 Mechanism of Byproduct Formation

Celani *et al.*[29] investigated the prototypical electrocyclic photoreaction from cyclohexadiene (CHD) to all-cis 1,3,5-hexatriene (cZc-HXT). They found that after the excitation to the Franck-Condon region on the excited state potential surface, the system descends to the pericyclic minimum, and funnels to the ground state potential surface through the conical intersection (CIX) region, where the ground and excited state surfaces are nearly degenerate. They suggested three possible routes for electron recoupling process from the CIX region: one to the closed form, another one to the open form and the third one to the ground-state methylcyclopentene diradical (MCPD) intermediate. They stated that this intermediate is unstable and may undergo radical pairing to form bicyclohexane (BCH) or the 1,2-hydrogen shift to form methylenecyclopentene. Later Irie *et al*.[30] investigated this reaction experimentally, and established that the byproduct formation takes place from the closed isomer. They suggested two different schemes to describe the formation of byproduct in PFC-1-D. One of them starts with homolytic cleavage of the C—S bond, and proceeds to the BCH intermediate. Another one goes through electrocyclic CIX and also proceeds to BCH intermediate, described by Celani *et al.*

We explored the ground state potential energy surface in three diarylethene derivatives: PFC-2, PFC-2-A and PFC-1-D (**Figure 3.4**), which had their fatigue resistant properties reported experimentally.[24, 30] In our calculations we could identify two

different intermediates to the byproduct formation, similar to the ones, described by Celani *et al*: one is MCPD and another one BCH intermediate, both depicted on **Scheme 2**. Unlike Celani's work, which described MCPD as unstable, in our calculations it is found to be an energy minimum. One can envision four distinctly different transition states connecting the closed form, MCPD, BCH, and the byproduct (**Scheme 2**). However, the extensive search on the ground state potential energy surface using state-of-the-art STQN algorithms did not locate transition states TS4 and TS5. We characterized, however, two other transition states: one leading to BCH from the closed form, and another one connecting BCH to the final byproduct.

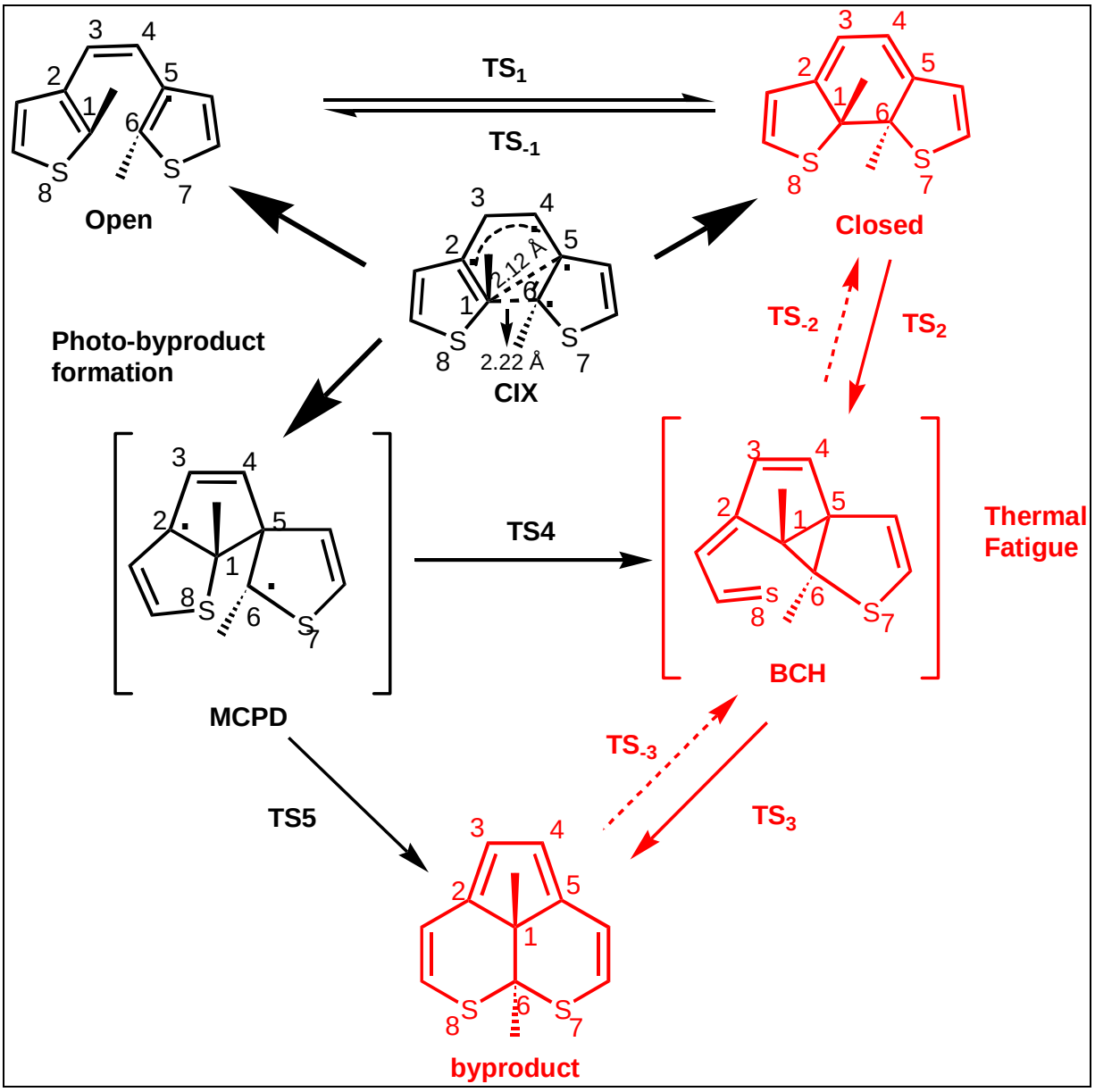

Scheme 2. Proposed mechanistic routes for the thermal and photochemical byproduct formation in dithienylethene derivatives

Based on our findings, we constructed an energy diagram for PFC-2 depicted in **Scheme 3.** TS_1 corresponds to the transition state between the open and closed forms

(C1—C6 bond breaking), TS_2 is the transition state between the closed form and BCH (corresponds to the concurrent C1—C5 bond formation and C1—S8 bond breaking), and TS_3 is the transition state from BCH to the byproduct (corresponds to the formation of C6—S8 bond and breaking of C5—C6 bond).

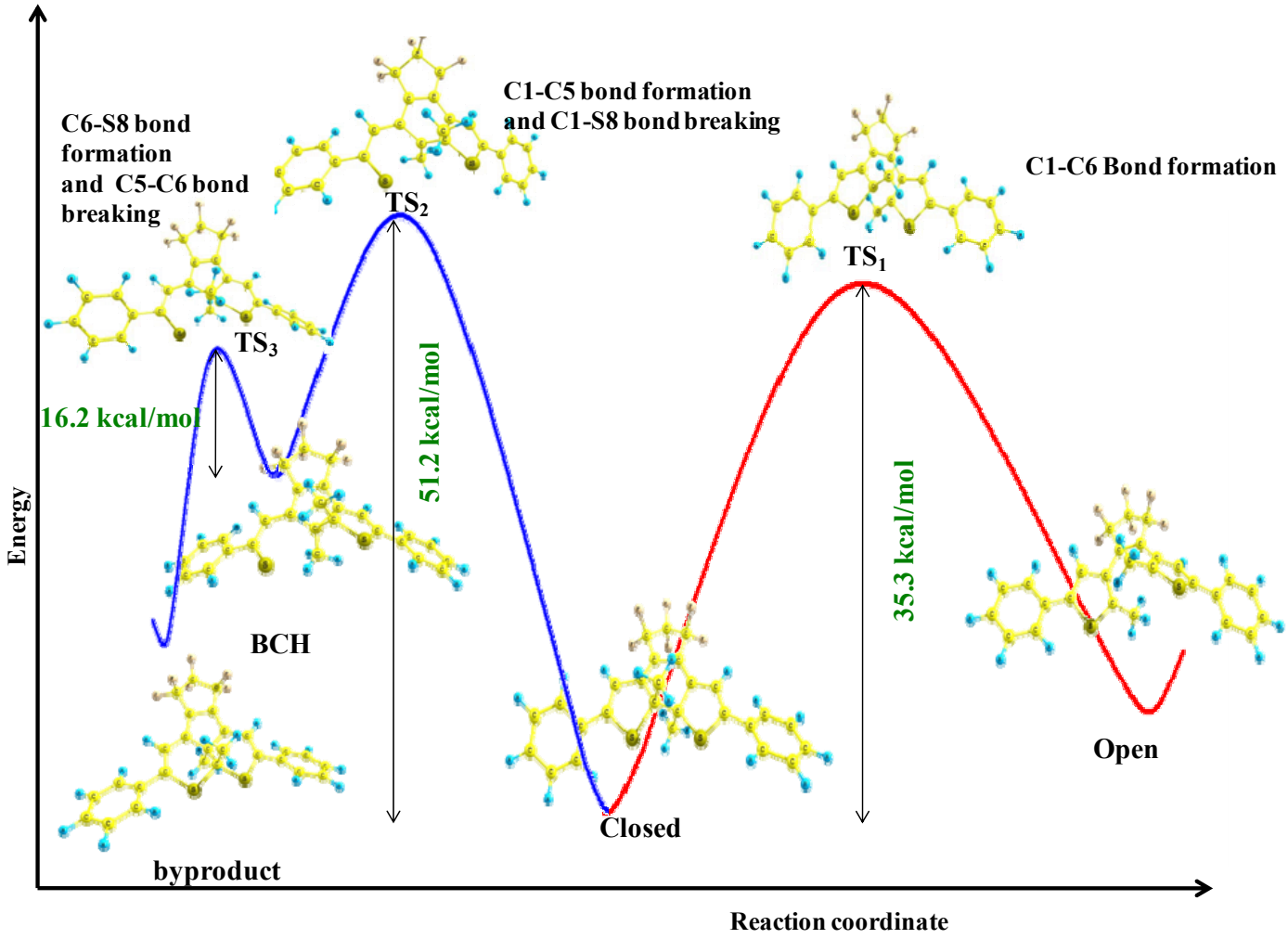

Scheme 3. Energy profile for thermal cycloreversion and the byproduct formation in PFC-2

3.3.4 Results

The **Table 3.8** reports the values of the energy barriers for thermal cycloreversion and the byproduct formation processes evaluated at UM05-2X/6-31G* theory levels for the compounds PFC-2, PFC-2-A and PFC-1-D. The UB3LYP/6-31G* values are also given for comparison.

Table 3.8: Energy barriers for thermal cycloreversion and thermal byproduct formation processes evaluated at UB3LYP/6-31G* and UM05-2X/6-31G* theory levels for 1, 2 and 3 in kcal/mol.

Transition State	TS_1	TS_2	TS_3	TS_{-1}	TS_{-2}	TS_{-3}
		PFC-2				
EXP	33.2					
UM05-2X/6-31G*	38.2	53.4	17.3	46.7	16.5	42.7
UM05-2X/6-31G*(ZPE corr)	35.3	51.2	16.2	44.4	15.1	40.5
UB3LYP/6-31G*	33.3	45.9		45.7	12.2	
UB3LYP/6-31G*(ZPE corr)	30.6	43.9		44.2	11.2	
		PFC-2-A				
UM05-2X/6-31G*	39.6	52.5	22.1	48.9	18.5	46.5
UM05-2X/6-31G*(ZPE corr)	36.9	49.9	21.2	47.4	17.3	44.3
UB3LYP/6-31G*	36.0	46.7	20.0	49.7	15.2	39.9
UB3LYP/6-31G*(ZPE corr)	33.3	44.1	19.1	48.6	14.1	37.9
		PFC-1-D				
UM05-2X/6-31G*	42.3	55.8	16.7	49.3	18.3	43.1
UM05-2X/6-31G*(ZPE corr)	39.3	53.3	16.0	47.1	17.1	40.7
UB3LYP/6-31G*	37.1	47.7	11.3	48.9	14.5	32.4
UB3LYP/6-31G*(ZPE corr)	34.1	45.1	10.4	47.1	13.1	30.3

The TS_2 barrier for both PFC-2 and PFC-1-D (51.2 and 53.3 kcal/mol) is slightly higher than that of PFC-2-A (49.9 kcal/mol). However, the compound PFC-2-A was resistant to fatigue in experimental study.[24, 30] This suggests that BCH intermediate is

inaccessible by thermal mechanism from the closed form, and BCH is probably reached photochemically from the excited state. In the contrast, the transition state TS_3 corresponds to a much lower barrier of 16.2 and 16.0 kcal/mol for compounds PFC-2 and PFC-1-D respectively. The same barrier is much higher at a value of 21.2 kcal/mol for PFC-2-A**.** This clearly correlates with fatigue resistance properties of these compounds, suggesting transformation from BCH to be the rate limiting process. The only difference in molecular structures of PFC-2 and PFC-2-A are hydrogen atom versus. methyl group at the 4 and 4′ position of th ethiophene ring. Apparently, steric repulsion between this methyl group and fluorine atoms of the perfluorocyclopentene group disturbs the planarity, reduces the conjugation and destabilizes the transition state.

3.3.5 Conclusions

The orbital structure of five lowest excited states in open and closed forms of PFC-2 was analyzed and the vibrational relaxation from the higher-lying photoabsorbing state to the lowest photoreactive state was found to be necessary for the photocyclic transformation to occur. The mechanism of the byproduct formation for the compounds PFC-2, PFC-2-A and PFC-1-D was investigated to predict the photofatigue of these molecules. We found the activation energy leading to byproduct from bicyclohexyl intermediate to be 5 kcal/mol higher for the methylated derivative PFC-2-A, and used this fact to explain its higher fatigue resistance. This protocol may become a part of the rational design strategy for the new photochromic materials used in photoswitching and optical data storage applications.

3.4 Quantum Yield

3.4.1 Data Set

For the prediction of Quantum Yield, the data set included 14 compounds for which the quantum yield was experimentally measured (**Figure 3.9**).

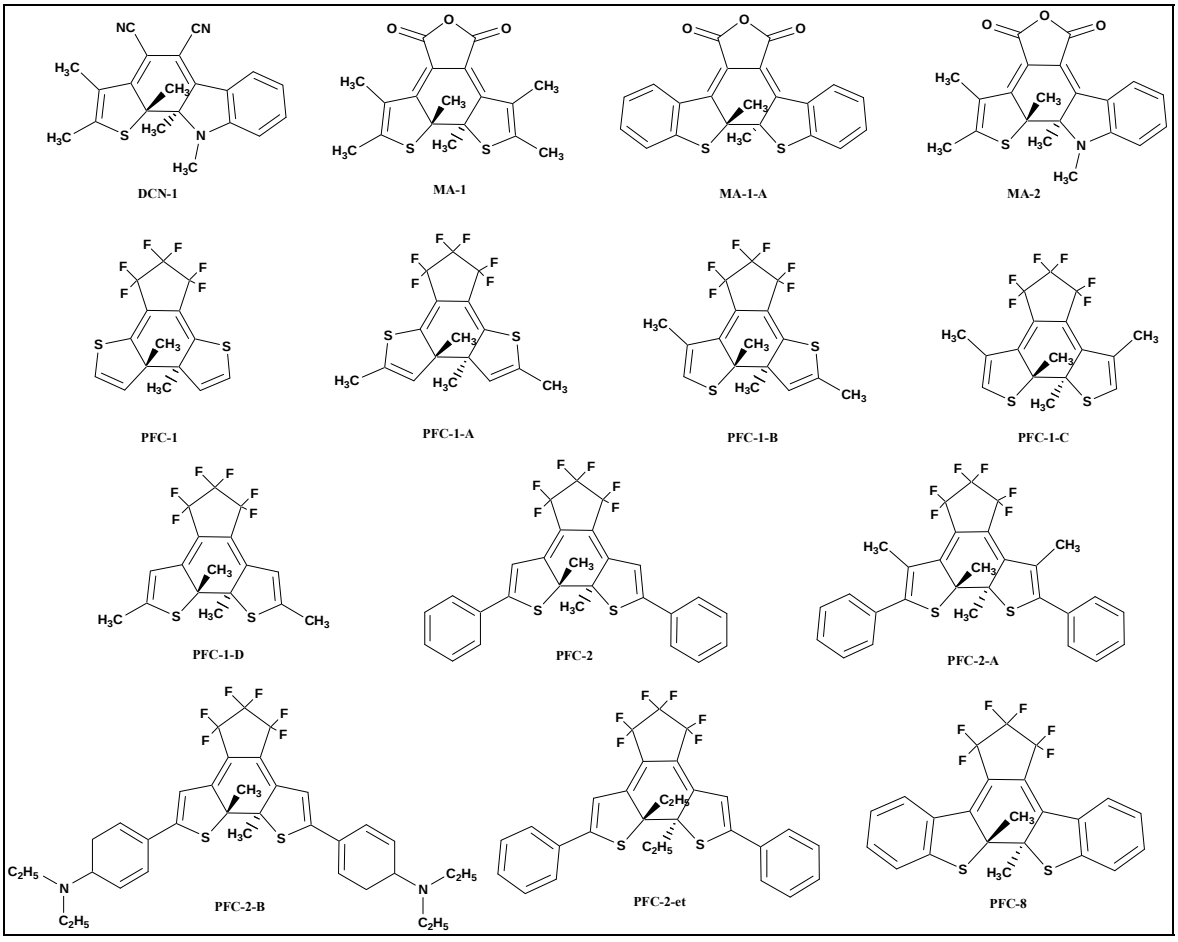

Figure 3.9: Data set of diarylethenes for prediction of quantum yield.

3.4.2 Theoretical Methods for Quantum Yield Prediction

Photochemical transformations are among the most complicated processes in chemistry. Their description involves both electronic transitions and nuclear motions, as well as coupling between the two. The photophysical processes often can be accurately described within Born-Oppenheimer adiabatic approximation, where stationary electronic and nuclear wavefunctions can be separated, and transition probabilities are determined by the product of respective matrix elements (Frank-Condon formalism). In contrast, in most photochemical processes, the nuclear wavefunction is time-dependent (non-stationary) and wavepacket dynamics is often needed for the accurate description. In addition, the ground and excited state potential energy surfaces may approach each other so that the resonance transition frequencies for electronic and nuclear motion become comparable, Born-Oppenheimer approximation fails and non-adiabatic dynamics becomes necessary. Clearly, solution for this quantum problem is feasible for only very small systems, and certain approximation must be made including separation of few nuclear degrees of freedom to be treated quantum-mechanically, while the rest is treated classically.[31]

Next level of approximation involves "surface hopping", where classical motion of the nuclei is combined with quantum transitions between potential energy surfaces according to well-defined probabilities.[32] The classical trajectories can be replaced (at the next level of approximation) with single reaction pathway, or line of steepest descent. Then transition state theory can be used to determine the rate of elementary steps related

to the heights of the potential barriers. When applied to the excited electronic states, the conical intersection plays the role of the transition states between two potential surfaces. Unfortunately, the search for conical intersections is a tedious task in itself, and for this reason we made further simplifications.

In this section, we test three levels of approximations according to these hypotheses (**Scheme 4**):

a) The ground state is the mixture of all formations, only one of which is reactive. Then QY is determined by the fraction of reactive conformation, determined by the Boltzmann distribution. [33]
b) The excited state relaxes fast to the pericyclic minimum on potential energy surface, then leaks slowly to the slope on the ground state surface, QY is determined by the relative position of the pericyclic minimum and transition state on the excited and ground state potential energy surface respectively.
c) There may be a barrier on the excited state pathway from Frank-Condon region to the pericyclic minimum. QY is large when this barrier is absent. In the following section we test these hypotheses.

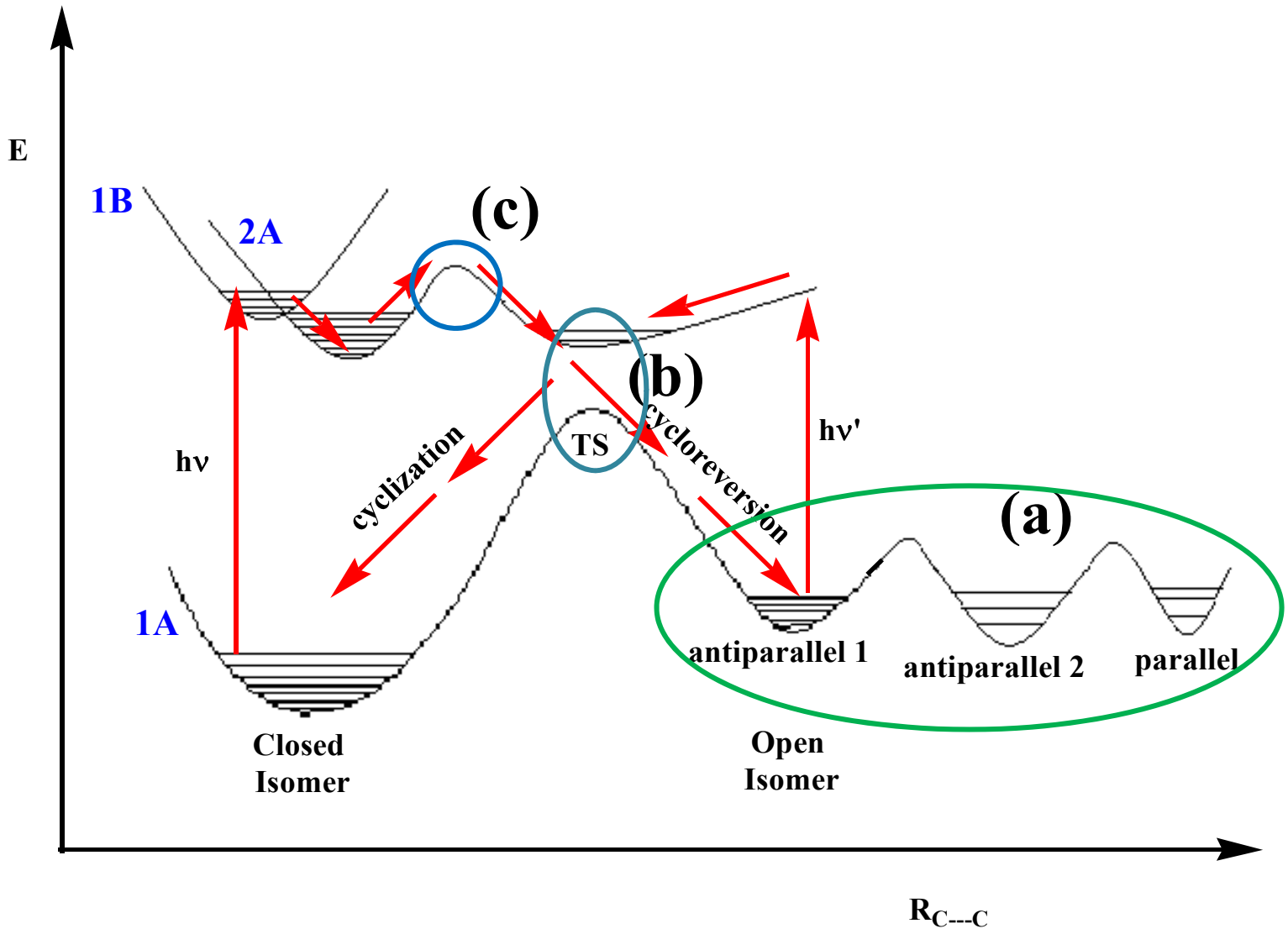

Scheme 4: Potential energy surface for cycloreversion reaction; (a), (b) and (c) mark the features of the potential energy surface relevant to the three hypotheses in the text.

3.4.3 Hypothesis a): QY is Determined by the Ground State Conformation

We investigated the population distribution of different conformers using canonical Boltzmann statistics at the ground state geometries. In this case, we considered the three different conformers of the open isomer of Diarylethenes: antiparallel 1 (ap1), antiparallel 2 (ap2) both of which have C_2 symmetry and parallel (par) conformer which has C_1 symmetry (**Figure 3.10**).

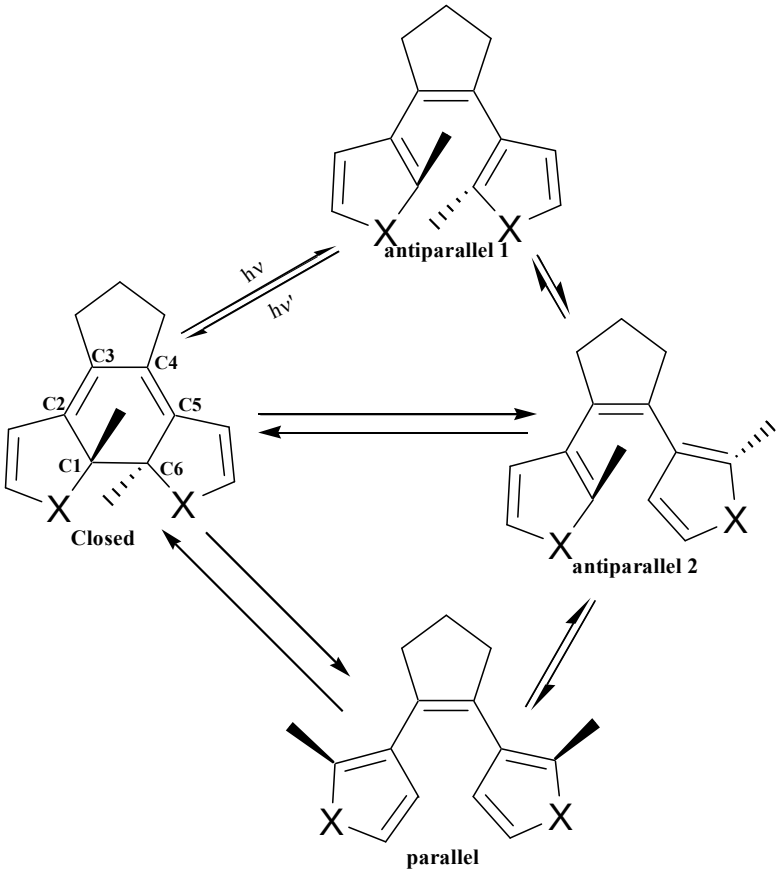

Figure 3.10: Conformers in the ground state of diarylethenes, out of the three open forms only antiparallel 1 can undergo reversible photochromism.

In crystal, the most stable conformer appears exclusively. Out of the three open conformers, only the ap1 form exists in crystal. However, under solvent conditions all the three conformers of the isomer can co-exist. The cyclization under solvent conditions depends on the relative availability of this reactive conformer, which is determined by finding the Boltzmann Distribution of the open conformers under equilibrium conditions. The Boltzmann distribution function for the open conformers was calculated as:

$$BD = \frac{ap1}{ap1 + ap2 + p} \qquad \text{(eq. 20)}$$

$$BD = \frac{1}{\exp\left(-\frac{\Delta G_{ap2}}{RT}\right) + \exp\left(-\frac{\Delta G_{p}}{RT}\right)} \qquad \text{(eq. 21)}$$

Where ΔG_{ap2} and ΔG_p are the Gibbs free energy differences of antiparallel 2 and parallel conformers relative to the antiparallel 1 conformer respectively. R is the universal gas constant, and T is the room temperature. **Table 3.9** shows the calculated photocyclization QY for the ground state geometries of the possible conformers from **Figure 3.10** in solution. Complete optimizations and frequency calculations were performed without symmetry constraint for the open conformers.

Table 3.9: Ground state relative free energies (in kcal/mol) at RM05-2X/6-31G* level for antiparallel2 (ΔG_{ap}) and parallel (ΔG_p) conformers in solution, calculated photocyclization quantum yield and experimental quantum yield.

	ΔG_{ap}	$\exp\left(-\frac{\Delta G_{ap}}{RT}\right)$	ΔG_p	$\exp\left(-\frac{\Delta G_p}{RT}\right)$	BD	QY	Exp. QY	Dev
DCN-1	1.30	0.111	0.35	0.56	1.49	0.60	0.06[a]	0.54
MA-1	0.09	0.852	-0.91	4.63	0.18	**0.15**	**0.27**[b]	-0.12
MA-1-A	0.30	0.607	-1.44	11.31	0.08	**0.08**	**0.13**[c]	-0.05
MA-2	-25.69	>>>	-25.09	>>>	0.00	0.00	0.06[a]	-0.06
PFC-1	6.44	0.000	1.67	0.06	16.62	**0.94**	**0.54**[d]	0.40
PFC-1-A	3.99	0.001	0.08	0.88	1.14	**0.53**	**0.40**[e]	0.13
PFC-1-B	1.66	0.061	1.74	0.05	8.81	0.90	0.28[e]	0.62
PFC-1-C	1.68	0.059	-0.41	2.00	0.49	**0.33**	**0.21**[f]	0.12
PFC-2	5.12	0.000	-0.49	2.27	0.44	**0.31**	**0.59**[g]	-0.28
PFC-2-A	-3.66	>>>	-7.51	>>>>	0.00	0.00	0.46[f]	-0.46
PFC-2-B	-0.65	3.003	-2.30	48.58	0.02	0.02	0.37[f]	-0.35
PFC-2-et	-36.15	>>>	-41.36	>>>	0.00	0.00	0.52[h]	-0.52
PFC-8	0.01	0.979	-1.08	6.15	0.14	**0.12**	**0.35**[i]	-0.23
							RMSD	**0.10**

(a) Ref[11] ; (b) Ref[34]; (c) Ref[13]; (d) Ref[17]; (e) Ref[35]; (f) Ref[19]; (g) Ref[7]; (h) Ref[8]; (i) Ref[22];

It is evident from the data above that in some cases (in bold), the deviation from the calculated QY is in good agreement with the experimental photocyclization QY. In cases where the deviation is unreasonable, it can be explained by the evaluation of Number of Imaginary frequencies (NImag=0 for minima, NImag=1 for transition state) given in **Table 3.10**. In such cases the final optimized geometry of the ap2 form or the par conformer is not a ground state.

Table 3.10: Optimized symmetry, reactive carbon-carbon bond distance (RC—C, in Å) and Number of Imaginary frequencies (NImag) for ap1, ap2 and par conformers.

	ap1			ap2			par		
Mol.	**Symm**	**$R_{C—C}$**	**NImag**	**Symm**	**$R_{C—C}$**	**NImag**	**Symm**	**$R_{C—C}$**	**NImag**
DCN-1	C1	3.41	0	C1	5.48	1	C1	4.07	1
MA-1	C2	3.56	0	C2	5.63	0	C1	4.28	1
MA-1-A	C2	3.55	0	C2	5.62	2	C1	4.31	0
MA-2	C1	3.14	0	C1	5.72	1	C1	4.27	1
PFC-1	C1	3.52	0	C2	5.30	2	C1	4.22	0
PFC-1-A	C2	3.52	1	C2	5.32	1	C1	4.23	0
PFC-1-B	C1	3.51	0	C1	5.23	1	C1	4.12	0
PFC-1-C	C1	3.62	0	C2	5.25	1	C1	4.04	0
PFC-2	C2	3.49	1	C2	5.67	1	C1	4.33	0
PFC-2-A	C2	3.56	1	C2	5.22	1	C1	4.03	0
PFC-2-B	C2	3.57	2	C2	5.22	2	C1	4.02	1
PFC-2-et	C2	4.19	1	C1	5.67	0	C1	4.32	0
PFC-8	C2	3.86	0	C2	3.86	0	C1	4.05	0

Table 3.10 illustrates the reactive bond distances ($R_{C—C}$) for all the conformers. In the case of ap1 conformers, which is the reactive open isomer, the $R_{C—C}$ is shorter than 4.0 Å (except for PFC-2-et), while for both ap2 and par form this distance is longer ~5.0 (except for PFC-8) and ~4.0 Å respectively. Experimentally it is known that the cyclization reaction is difficult when the $R_{C—C}$ is longer than 4.0 Å. From the above data it is also clear that in some cases the ground state ap1 conformer not necessarily has C_2 symmetry (except DCN-1, MA-2, PFC-1B: non-symmetric molecules); in such cases the higher symmetry geometry would be a transition state. Thus, hypothesis a) provides a good quantitative prediction only in certain cases.

3.4.4 Hypothesis b): Cycloreversion Quantum Yield

We employed TD-ΔSCF formalism to study the detailed potential energy surface (PES) analysis of the excited state profile and the locations of the pericyclic minimum to reproduce the experimental QY for cycloreversion reactions. For the cycloreversion reactions of photochromic compounds, the energy profile should depict the photoexcitation of the closed isomer to 1B excited state from where it should relax to one of the vibrational levels on the 2A state. After crossing a small barrier the system moves to the pericyclic minimum at the 2A state, it converts into the ground state 1A and form the open isomer (**Scheme 4**).

Table 3.11 gives the relative energies for the ground state (1A), singly excited state (1B) and the doubly excited state (2A) for 11 of the molecules in the dataset (DCN-1, MA-2, PFC-1-B: non-symmetric molecules). All the geometry optimizations were done using symmetry constrained to C_2. **Table 3.12** gives the $R_{C—C}$ distances for all the optimized structures in all three states.

Table 3.11: Relative energies (in kcal/mol) for the optimized ground state (1A), singly excited state (1B) and the doubly excited state (2A) for closed (c), open (o), transition state (TS) and pericyclic minimum (pm) on the PES for the data set of diarylethenes. All calculations were done at UM05-2X/6-31G* level

	1A State			2A State			1B State		
	c	o	TS	c	o	pm	c	o	pm
	ΔE	ΔE	ΔE	ΔE	ΔE	ΔE	ΔE	ΔE	ΔE
MA-1	6.09	0.00	50.92	79.07	185.23	77.47	54.32	75.76	57.27
MA-1-A	0.86	0.00	50.47	74.75	178.19	74.72	56.73	73.18	56.71
PFC-1	21.11	0.00	62.66	86.01	196.80	86.01	71.61	87.50	71.60
PFC-1-A	17.99	0.00	60.77	83.98	191.01	83.97	69.67	84.51	69.66
PFC-1-C	8.41	0.00	51.03	84.19	245.62	78.45	56.02	118.08	60.29
PFC-1-D	8.32	0.00	50.28	87.98	210.14	79.76	56.11	93.31	61.75
PFC-2	9.47	0.00		89.38	207.94		47.95	92.99	
PFC-2-A	5.20	0.00	47.95	89.59	109.14	76.43	46.96	89.14	54.73
PFC-2-B	4.52	0.00		87.64	206.56		43.22	87.56	87.64
PFC-2-et	10.57	0.00		87.46	208.64		46.64	93.61	
PFC-8	3.78	0.00	50.74	76.02	220.40	76.03	58.95	98.61	58.97

Table 3.12: Reactive C—C distance ($R_{C—C}$, in Å) for the optimized ground state (1A), singly excited state (1B) and the doubly excited state (2A) for closed (c), open (o), transition state (TS) and pericyclic minimum (pm) on the PES for the data set of diarylethenes. All calculations were done at UM05-2X/6-31G* level.

	1A State			2A State			1B State		
	c	o	TS	c	o	pm	c	o	pm
MA-1	1.530	3.561	2.057	1.776	3.561	2.046	1.827	3.561	2.046
MA-1-A	1.534	3.551	2.073	2.028	3.592	2.091	2.088	3.551	2.091
PFC-1	1.542	3.525	2.019	2.085	3.515	2.086	2.085	3.525	2.086
PFC-1-A	1.544	3.433	2.043	2.106	3.518	2.105	2.106	3.433	2.105
PFC-1-C	1.528	3.775	2.002	1.797	3.771	2.053	1.824	3.775	2.053
PFC-1-D	1.534	3.495	2.012	1.798	3.496	2.066	1.798	3.495	2.066
PFC-2	1.535	3.494		1.628	3.494		1.628	3.494	
PFC-2-A	1.530	3.560	1.993	1.667	3.560	2.012	1.592	3.560	2.012
PFC-2-B	1.528	3.565		1.752	3.565		1.567	3.565	1.823
PFC-2-et	1.543	3.503		1.632	3.503		1.632	3.503	
PFC-8	1.532	3.859	2.004	2.095	3.859	2.048	2.095	3.859	2.048

Nakamura *et al.*[35] proposed two different PES for normal-type (N) and inverse-type (I) frame molecule. From the data set (**Figure 3.9**) except for PFC-1 and PFC-1-A all are (N)-type frame PMs. They suggested that the large QY for the (I)-type molecule can be attributed to the absence of the barrier on the 2A surface from closed to open isomer, while in case of (N)-type molecule, they observed a short barrier. **Figure 3.11**, shows the PES for (a) (I)-type – PFC-1-A molecule and (b) (N)-type – PFC-1-C. On comparison of the two PESs, one can see that in case of PFC-1-A the closed isomer in the excited 2A state ($2A_c$) optimizes completely to the pericyclic minimum (**Figure 3.11 (a)**), which means that there is no barrier between the closed isomer and the pericyclic minimum ($2A_{pm}$) on the 2A PES. Hence, PFC-1-A will undergo cycloreversion with ease and this is evident from higher experimental cycloreversion QY for PFC-1-A, which is an (I)-type molecule. In the case of PFC-1-C, the closed isomer on the 2A state optimizes closer to the pericyclic minimum but does not overlap it. This suggests that there may be a short barrier on going from the $2A_c$ state to the $2A_{pm}$ and hence the quantum yield of PFC-1-C is lower.

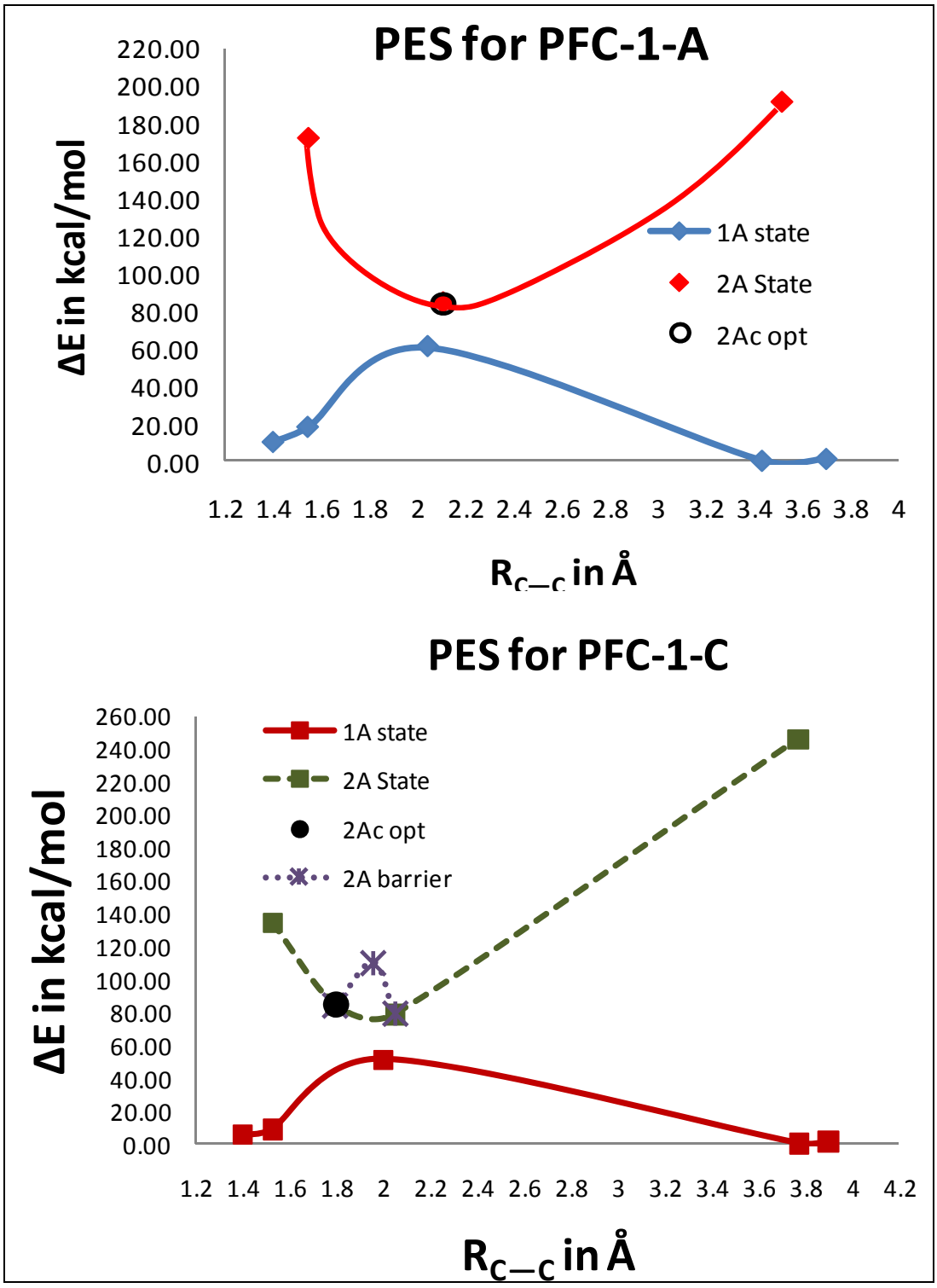

Figure 3.11: Potential Energy Surface depicting the ground 1A state and excited 2A state for (a) (I)-type – PFC-1-A molecule and (b) (N)-type – PFC-1-C

3.4.5 Hypothesis c) Empirical Correlations

The increase in the quantum yield of certain molecules can be correlated with other calculated properties, such as the energy difference (ΔE) between the 2A state closed isomer ($2A_c$) and the pericyclic minimum ($2A_{pm}$) and the internuclear distance $R_{C—C}$ in the optimized $2A_c$ (**Table 3.12**).

Table 3.13: Optimized distance $R_{C—C}$ (Å) in the 2A state, Energy Difference ΔE (kcal/mol) between 2A state closed isomer and the pericyclic minimum and the experimental quantum yield $\varphi_{c\rightarrow o}$ for the cycloreversion reaction.

Mol.	ΔE ($2A_c$ -$2A_{pm}$)	$R_{C—C}$ ($2A_c$)	$R_{C—C}$ ($2A_{pm}$)	$\varphi_{c\rightarrow o}$
MA-1	1.60	1.776	2.046	0.07[(a)]
MA-1-A	0.03	2.028	2.091	0.21[(b)]
PFC-1	0.00	2.085	2.086	0.37[(c)]
PFC-1-A	0.00	2.106	2.105	0.58[(d)]
PFC-1-C	5.74	1.797	2.053	0.13[(e)]
PFC-1-D	8.22	1.798	2.066	0.12[(e)]
PFC-2		1.628		0.013[(f)]
PFC-2-A	13.16	1.667	2.012	0.015[(e)]
PFC-2-B		1.752	1.823	0.0025[(e)]
PFC-2-et		1.632		0.0081[(g)]
PFC-8	-0.01	2.095	2.048	0.35[(h)]

(a) Ref[34]; (b) Ref[13]; (c) Ref[17]; (d) Ref[36]; (e) Ref[19]; (f)Ref[7]; (g) Ref[8]; (h) Ref[22];

A higher quantum yield is associated with a lower ΔE of the model systems. Both PFC-1 and PFC-1-A are (I)-type molecules and have a high quantum yield and the ΔE is 0.00 kcal/mol in their case (since closed isomer in 2A state fully optimizes to the pericyclic minimum). In contrast the low quantum yield of 0.015 for PFC-2-A is

associated with higher ΔE of 13.16 kcal/mol (**Figure 3.11**). The high quantum yields can also be associated to the longer, internuclear distance $R_{C—C}$ of the respective 2A state closed isomers of MA-1-A, PFC-1, PFC-1-A and PFC-8 and they show a linear correlation (**Figure 3.12**).

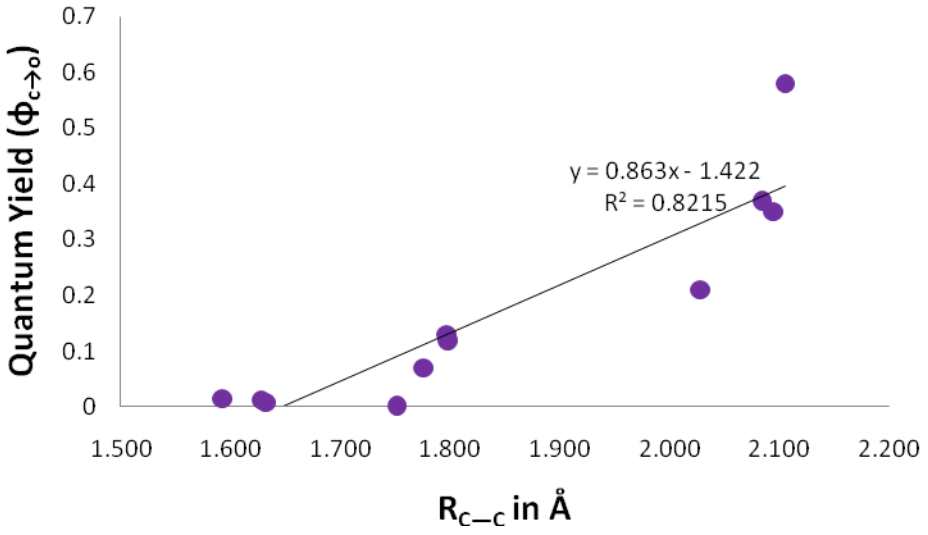

Figure 3.12: Correlation of the experimental quantum yield with the optimized RC—C in the 2A state closed isomer.

3.4.6 Conclusions

The TD-DFT study to predict the quantum yield for a set of 14 diarylethene derivatives is presented. Photocyclization quantum yield was evaluated based on the Boltzmann distribution of the equilibrium ground state reactive and non-reactive conformations and the result was in a quantitative agreement with the experimental QY. Correlation of experimental cycloreversion quantum yield with various properties of the excited state isomers on the potential energy surface was made. We concluded that the relative position of the pericyclic minimum on the 2A excited state surface with that of the transition state on the ground state can be used to explain the high or low QY for (I)-type and (N)-type molecules. The linear correlation of the reactive C—C distance and the QY indicates that greater the internuclear distance, higher is the quantum yield and vice-versa. We also conclude that low energy difference between the 2A state closed isomer and the pericyclic minimum is associated with the higher QY.

3.5 Design of Template Nanostructure Materials

3.5.1 Data Set

DNA presents a highly ordered polymer capable of forming oriented thin films. [37] It is also known to form intercalation complexes with many planar molecules. These properties can be used to design nanostructured photochromic materials. In order to verify the protocol to model the DNA based nanostructured photochromic diarylethenes, we performed MD simulations of DNA intercalation for benchmark series polyamine-anthracene conjugates. Unlike diarylethenes they were extensively studied by Wang *et al*.[38] (**Figure 3.13**) using fluorescence, circular dichroism and normal absorption spectroscopy in an attempt to correlate the effect of the polyamine chain length on the biological activity.

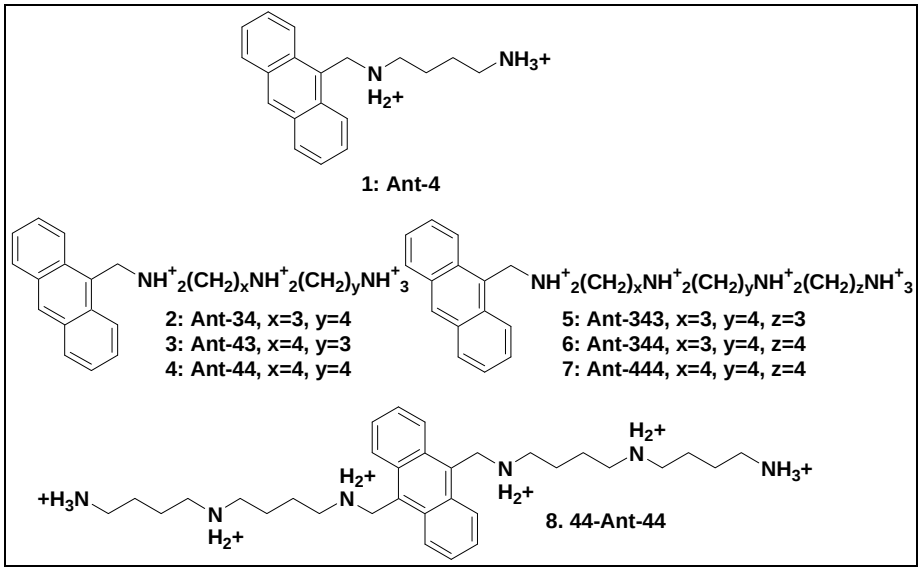

Figure 3.13: Anthracyclin drugs with different polyamine chains.

3.5.2 Modeling Approach

In case of ligand-DNA intercalating systems, the following properties have been identified as important for the successful modeling of ligand-DNA interaction: (i) *degrees of freedom of the drug ligand* and as a rule, the more intercalating sidechains are linked within a single ligand structure, the stronger the expected binding affinity; (ii) *role of base pair sequence,* where different specific base pair sequence for different drugs (GC base pair most common); (iii) *counter ion effects*, since the presence of small counter ion affect ligand binding, since the counter ions can screen and shield the negative backbone surface allowing non-electrolytes as well as positively charged ligand to interact more strongly with the DNA target; (iv) *role of solvent.*

3.5.3 Simulation Approach

All MD simulations have been carried out using the AMBER 10[39] suite of programs with the parmff99SB force field [40] for the DNA and general amber force field (gaff) [41]for the ligand. A consensus protocol was adopted for simulation in which the solute molecule is an ant-PA-DNA system was first ionized with sodium ions to neutralize the overall charge of the system. The ionized complex was then simulated in a truncated octahedral box having solvent shell extending for at least 8 Å around it. The neutral ion-oligomer complex is solvated with a layer of TIP3P water molecules. [42] Simulations are performed with periodic boundary conditions in which the central cell box contains 8000 water molecules. Considering the DNA, ant-PA conjugates, counterions, and solvent water, the total system consists of around 20,000 atoms.

The MD simulations consist of an initial minimization under constant pressure. The equilibration was done by first by slow heating to 310 K at constant volume over a period of 250-ps using restraints on the ant-PA-DNA and ions. These restraints are slowly relaxed from 4 to 1 kcal/mol/$Å^2$ during a series of three segments of 5000 steps of energy minimization using constant temperature. The final two unrestrained equilibrations were done at constant temperature (300 K) and constant pressure (1 bar). The simulations were then continued for a total of 5 ns at constant temperature, using the Berendsen algorithm. [43] Electrostatic interactions were treated using the particle mesh

Ewald (PME) algorithm [44] with a real space cutoff of 8 Å. SHAKE constraints [45]were applied to all bonds involving hydrogen atoms. The trajectories were extended to 5 ns for each system and conformations of the system were saved every 2 ps for further analysis.

3.5.4 Results

Table 3.14 lists the 8 different polycationic anthracene-PA (ant-PA) conjugates and 1 neutral anthracene constructed used for the drug-DNA interaction studies with the 12-mer 5′(GCGCGCGCGCGC)$_2$3′ Z-DNA. **Figure 3.14** shows the ant-PA-DNA intercalated complexes used for the starting conformation, in which the drug lies in parallel conformation w.r.t the base-pair hydrogen bonds.

Table 3.14: Different ant-PA conjugates and ant-PA-DNA complexes constructed with corresponding overall charges.

Structure	Charge	Structure	# of Na^+ions
Ant	0	GC--Ant	22
Ant-4	+2	GC-Ant-4	20
Ant-34	+3	GC-Ant34	19
Ant-43	+3	GC-Ant-43	19
Ant-44	+3	GC-Ant-44	19
Ant-343	+4	GC-Ant-343	18
Ant-344	+4	GC-Ant-344	18
Ant-444	+4	GC-Ant-444	18
44-Ant-44	+6	GC-44-Ant-44	16

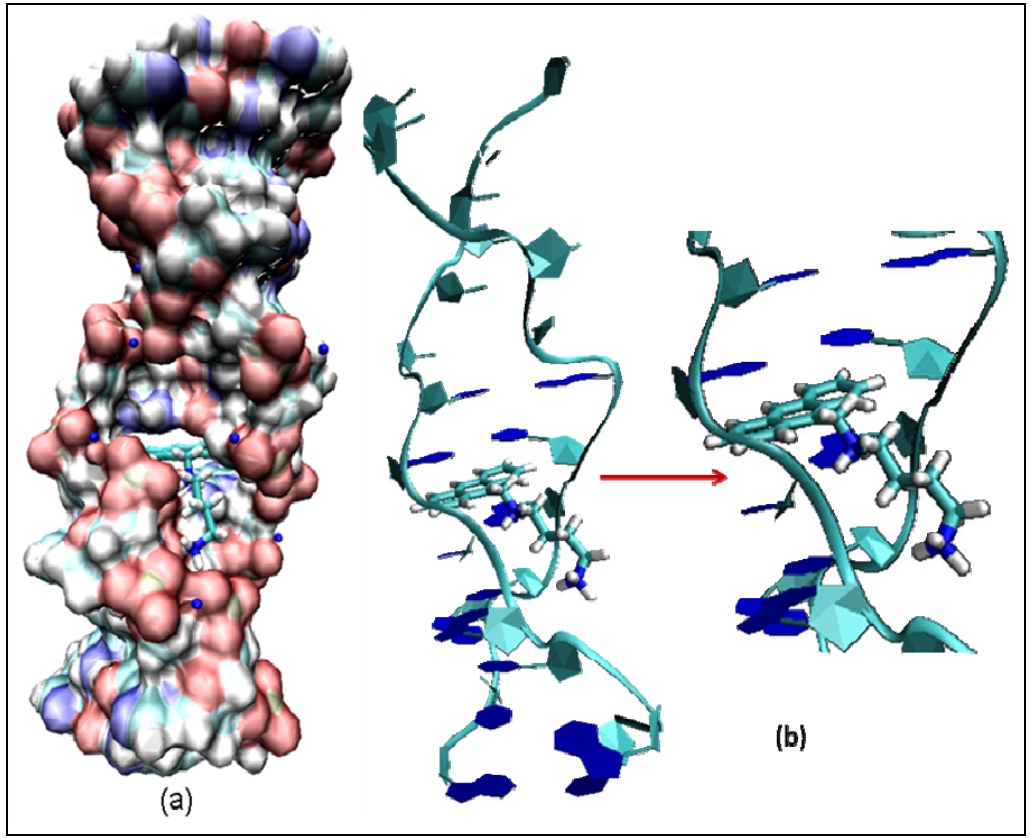

Figure 3.14: Constructed and minimized structures of the intercalated state of 12-mer 5′(GCGCGCGCGCGC)23′ Z-DNA with Ant-4 drug where the anthracene is intercalated in parallel conformation between GC base pairs (G-7-C-8 and G-17-C-18) and the polyamine chain in the inside of the minor groove. The figures are made by VMD.[46] ; (a) DNA is shown in a metallic pastel surface representation including licorice atom models and element-based color (White for Hydrogen, green for Carbon, red for Oxygen and blue for Nitrogen), whereas Ant-4 is represented via a licorice model with element-based color. b) DNA and base pairs are shown in a ribbon model and Ant-4 is represented via a licorice model with element-based color.

The aromatic ring is stacked into the DNA bases and the polyamine chain lies in the minor groove. The perpendicular and 45° angle twist conformation of anthracene drug w.r.t. the base-pair hydrogen bonds were also tried, which after equilibration became parallel. Hence for all other ant-PA –DNA complexes the parallel conformation was considered as the intercalated state and used for MD simulations.

The final intercalated structures after the 5ns production run were then used for probability density analysis and Binding Free Energy calculations using the MMPBSA.py tool of Amber software. **Figure 3.15** (a and b) shows the probability density plots for GC—Ant (orange) and GC—Ant4 (green) systems.

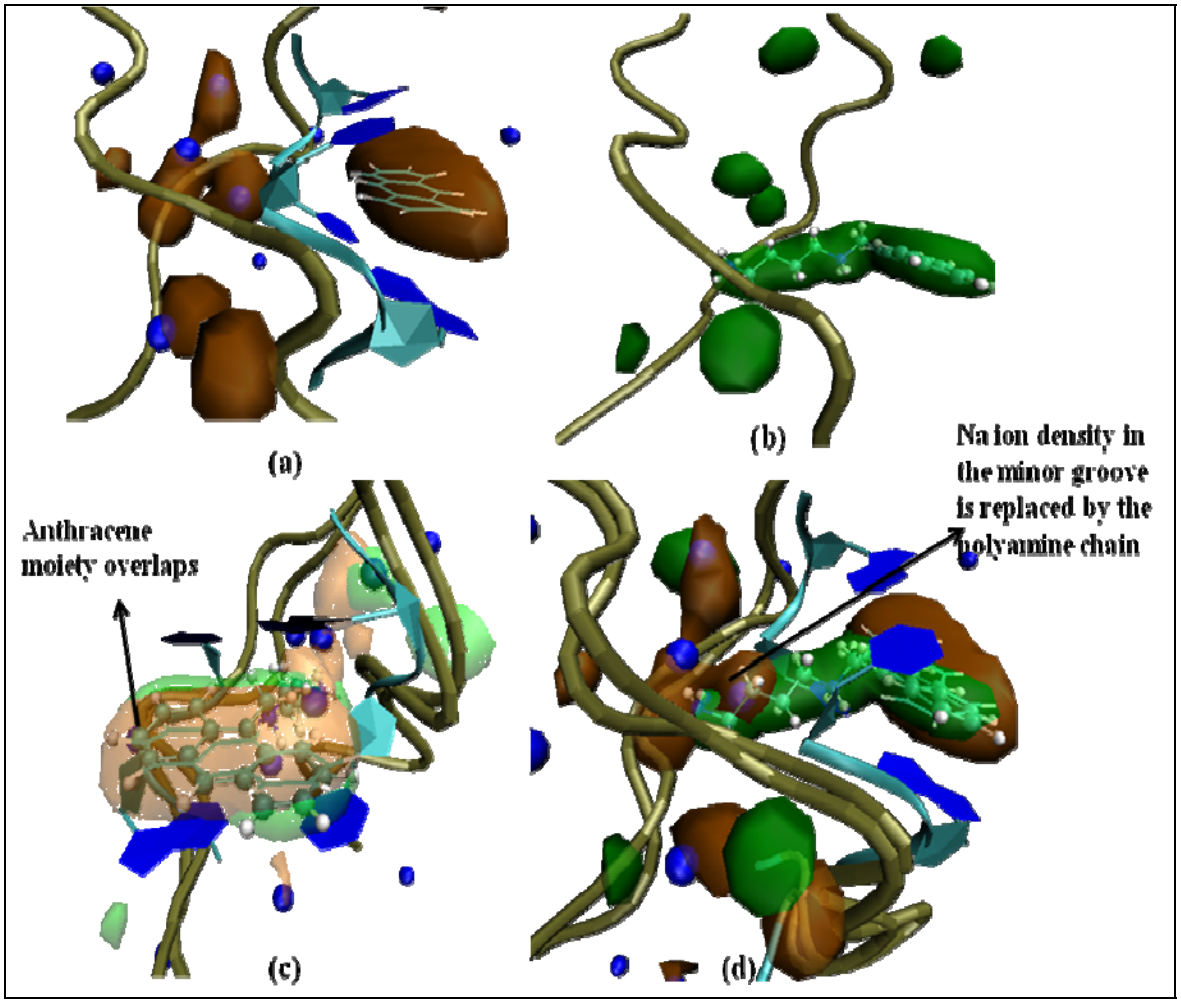

Figure 3.15: (a-d) Probability density plots for GC—Ant (orange) and GC—Ant4 (green). DNA and base pairs are shown in a ribbon model and the drugs Ant and Ant-4 are represented via a licorice model with element-based color.

From the probability density analysis for the above two systems, it can be clearly seen that there is no covalent bond formation between the anthracene moiety and the base pairs involved in intercalation. In the case of GC-Ant system there is a large Na^+ ion density within the minor groove of the DNA dodecamer, which is believed to stabilize the Z-DNA form (**Figure 3.15 (a)**). When there is a polyamine vectored anthracene, this Na^+ ion density is now replaced by the polyamine chain (**Figure 3.15 (d)**), which suggests the involvement of polyamines in stabilizing the Z-DNA form in cellular system. Similar overlapping of the Na^+ ion density and the polyamine density was observed for all the ant-PA systems.

The binding free energy ($\Delta G_{b,solv}$) for the intercalated systems is given in **Table 3.15**. The dissociation constant (k_d) was then evaluated using eq. 22 and compared to the experimental k_d values.

$$k_d = \exp^{\frac{\Delta G}{RT}} \qquad \text{(eq. 22)}$$

Table 3.15: Thermodynamic Gibb's free energy of binding ($\Delta G_{b,solv}$ in kcal/mol) for the intercalated ant-PA-DNA systems and dissociation constant (k_d in μm) at 300K.

Structure	$\Delta G_{b,solv}$	k_d	Exp. k_d
GC-Ant-4	-45.01	2.64E-27	3.5
GC-Ant34	-44.92	3.06E-33	3.5
GC-Ant-43	-52.16	1.75E-38	1.1
GC-Ant-44	-53.95	8.90E-40	3.3
GC-Ant-343	-69.23	7.70E-51	4.0
GC-Ant-344	-70.53	8.92E-52	4.0
GC-Ant-444	-64.94	9.95E-48	4.0
GC-44-Ant-44	-76.91	2.15E-56	4.0

From the **Table 3.15** it is evident that although the free energy of binding are all negative, which is qualitatively correct for the stable complexes and suggests that intercalation of the polyamine based anthracyclin derivatives to the DNA is thermodynamically favorable process. The calculated dissociation constant values are also orders of magnitude higher than the experimental values. This indicates that MM/PBSA protocol is not well suited for the interactions between the charged species, and a different approach is needed.

3.5.5 Conclusions

Molecular Dynamics simulations on a set of 8 polyamine based anthracyclin drug candidates intercalating with 12 mer 5′(GCGCGCGCGCGC)$_2$3′ Z-DNA were performed. Probability density analysis of the intercalated ant-PA-DNA versus Z-DNA demonstrated that the cationic polyamine chain replaces the Na^+ ions inside the minor groove of DNA which is important for the stability of the Z-DNA form. It was also noted that the drug intercalates between the base pairs based on pure dispersive interactions and no bond is formed. The Free Energy of binding for all the structures suggested that intercalation is a thermodynamically favorable process. These energies were then used to evaluate the dissociation constant of the drugs which can be compared to the experimental values. These studies were performed to model DNA based nanocomposites of photochromic materials.

3.6 References

1. Shirinyan, V. Z.; Krayshkin, M. M.; Belenkii, L. I., Photochromic dihetarylethenes. 8. A new approach to the synthesis of 3, 4-bis (2, 5-dimethyl-3-thienyl)furan-2, 5-dione as potential photochrome (january, pg 81, 2001). *Khimiya Geterotsiklicheskikh Soedinenii* **2001**, (3), 426-426.
2. Cave, R. J.; Zhang, F.; Maitra, N. T.; Burke, K., A dressed tddft treatment of the 2ag states of butadiene and hexatriene. *Chemical Physics Letters* **2004,** 389, (1-3), 39-42.
3. Gross, E. K. U.; Kohn, W., Local density-functional theory of frequency-dependent linear response. *Physical Review Letters* **1985,** 55, (26), 2850-2852.
4. Romaniello, P.; Sangalli, D.; Berger, J. A.; Sottile, F.; Molinari, L. G.; Reining, L.; Onida, G., Double excitations in finite systems. *Journal of Chemical Physics* **2009,** 130, (4), 11.
5. Kobatake, S.; Yamada, T.; Uchida, K.; Kato, N.; Irie, M., Photochromism of 1,2-bis(2,5-dimethyl-3-thienyl)perfluorocyclopentene in a single crystalline phase. *Journal of the American Chemical Society* **1999,** 121, (11), 2380-2386.
6. Yamada, T.; Kobatake, S.; Irie, M., Single-crystalline photochromism of diarylethene mixtures. *Bulletin of the Chemical Society of Japan* **2002,** 75, (1), 167-173.
7. Irie, M.; Lifka, T.; Kobatake, S.; Kato, N., Photochromism of 1,2-bis(2-methyl-5-phenyl-3-thienyl)perfluorocyclopentene in a single-crystalline phase. *Journal of the American Chemical Society* **2000,** 122, (20), 4871-4876.
8. Kobatake, S.; Shibata, K.; Uchida, K.; Irie, M., Photochromism of 1,2-bis(2-ethyl-5-phenyl-3-thienyl)perfluorocyclopentene in a single-crystalline phase. Conrotatory thermal cycloreversion of the closed-ring isomer. *Journal of the American Chemical Society* **2000,** 122, (49), 12135-12141.
9. Yamaguchi, T.; Irie, M., Photochromism of bis(2-alkyl-1-benzofuran-3-yl)perfluorocyclopentene derivatives. *Journal of Organic Chemistry* **2005,** 70, (25), 10323-10328.
10. Peters, A.; McDonald, R.; Branda, N. R., Regulating pi-conjugated pathways using a photochromic 1,2-dithienylcyclopentene. *Chemical Communications* **2002**, (19), 2274-2275.
11. Nakayama, Y.; Hayashi, K.; Irie, M., Thermally irreversible photochromic systems - reversible photocyclization of nonsymmetrical diarylethene derivatives. *Bulletin of the Chemical Society of Japan* **1991,** 64, (3), 789-795.
12. Irie, M.; Mohri, M., Thermally irreversible photochromic systems - reversible photocyclization of diarylethene derivatives. *Journal of Organic Chemistry* **1988,** 53, (4), 803-808.
13. Uchida, K.; Nakayama, Y.; Irie, M., Thermally irreversible photochromic systems - reversible photocyclization of 1,2-bis(benzo[b]thiophen-3-yl)ethene derivatives. *Bulletin of the Chemical Society of Japan* **1990,** 63, (5), 1311-1315.
14. Irie, M., Photochromism: Memories and switches - introduction. *Chemical Reviews* **2000,** 100, (5), 1683-1683.
15. Nakayama, Y.; Hayashi, K.; Irie, M., Thermally irreversible photochromic systems - reversible photocyclization of 1,2-diselenenylethene and 1,2-diindolylethene derivatives. *Journal of Organic Chemistry* **1990,** 55, (9), 2592-2596.
16. Uchida, K.; Kido, Y.; Yamaguchi, T.; Irie, M., Thermally irreversible photochromic systems. Reversible photocyclization of 2-(1-benzothiophen-3-yl)-3-(2 or 3-thienyl)maleimide derivatives. *Bulletin of the Chemical Society of Japan* **1998,** 71, (5), 1101-1108.
17. Fukaminato, T.; Kawai, T.; Kobatake, S.; Irie, M., Fluorescence of photochromic 1,2-bis(3-methyl-2-thienyl)ethene. *Journal of Physical Chemistry B* **2003,** 107, (33), 8372-8377.

18. Irie, M.; Uchida, K.; Eriguchi, T.; Tsuzuki, H., Photochromism of single-crystalline diarylethenes. *Chemistry Letters* **1995**, (10), 899-900.
19. Irie, M.; Sakemura, K.; Okinaka, M.; Uchida, K., Photochromism of dithienylethenes with electron-donating substituents. *Journal of Organic Chemistry* **1995,** 60, (25), 8305-8309.
20. Peters, A.; Branda, N. R., Electrochemically induced ring-closing of photochromic 1,2-dithienylcyclopentenes. *Chemical Communications* **2003**, (8), 954-955.
21. Moriyama, Y.; Matsuda, K.; Tanifuji, N.; Irie, S.; Irie, M., Electrochemical cyclization/cycloreversion reactions of diarylethenes. *Organic Letters* **2005,** 7, (15), 3315-3318.
22. Hanazawa, M.; Sumiya, R.; Horikawa, Y.; Irie, M., Thermally irreversible photochromic systems - reversible photocyclization of 1,2-bis(2-methylbenzo[b]thiophen-3-yl)perfluorocycloalkene derivatives. *Journal of the Chemical Society-Chemical Communications* **1992**, (3), 206-207.
23. Gilat, S. L.; Kawai, S. H.; Lehn, J. M., Light-triggered molecular devices - photochemical switching of optical and electrochemical properties in molecular wire type diarylethene species. *Chemistry-a European Journal* **1995,** 1, (5), 275-284.
24. Irie, M.; Lifka, T.; Uchida, K.; Kobatake, S.; Shindo, Y., Fatigue resistant properties of photochromic dithienylethenes: By-product formation. *Chemical Communications* **1999**, (8), 747-748.
25. Boese, A. D.; Martin, J. M. L., Development of density functionals for thermochemical kinetics. *Journal of Chemical Physics* **2004,** 121, (8), 3405-3416.
26. Zhao, Y.; Schultz, N. E.; Truhlar, D. G., Design of density functionals by combining the method of constraint satisfaction with parametrization for thermochemistry, thermochemical kinetics, and noncovalent interactions. *Journal of Chemical Theory and Computation* **2006,** 2, (2), 364-382.
27. Wodrich, M. D.; Corminboeuf, C.; Schreiner, P. R.; Fokin, A. A.; Schleyer, P. V., How accurate are dft treatments of organic energies? *Organic Letters* **2007,** 9, (10), 1851-1854.
28. Zhao, Y.; Truhlar, D. G., Assessment of density functionals for pi systems: Energy differences between cumulenes and poly-ynes; proton affinities, bond length alternation, and torsional potentials of conjugated polyenes; and proton affinities of conjugated shiff bases. *Journal of Physical Chemistry A* **2006,** 110, (35), 10478-10486.
29. Celani, P.; Ottani, S.; Olivucci, M.; Bernardi, F.; Robb, M. A., What happens during the picosecond lifetime of 2a(1) cyclohexa-1,3-diene - a cas-scf study of the cyclohexadiene hexatriene photochemical interconversion. *Journal of the American Chemical Society* **1994,** 116, (22), 10141-10151.
30. Higashiguchi, K.; Matsuda, K.; Kobatake, S.; Yamada, T.; Kawai, T.; Irie, M., Fatigue mechanism of photochromic 1,2-bis(2,5-dimethyl-3-thienyl)perfluorocyclopentene. *Bulletin of the Chemical Society of Japan* **2000,** 73, (10), 2389-2394.
31. Garashchuk, S.; Rassolov, V. A., Semiclassical nonadiabatic dynamics of nafh with quantum trajectories. *Chemical Physics Letters* **2007,** 446, (4-6), 395-400.
32. Mikhailov, I. A.; Belfield, K. D.; Masunov, A. E., Dft-based methods in the design of two-photon operated molecular switches. *Journal of Physical Chemistry A* **2009,** 113, (25), 7080-7089.
33. Asano, Y.; Murakami, A.; Kobayashi, T.; Kobatake, S.; Irie, M.; Yabushita, S.; Nakamura, S., Theoretical study on novel quantum yields of dithienylethenes cyclization reactions in crystals. *Journal of Molecular Structure-Theochem* **2003,** 625, 227-234.
34. Irie, M.; Mohri, M., Thermally irreversible photochromic sysytems- reversible photocyclization of diarylethene derivatives. *Journal of Organic Chemistry* **1988,** 53, (4), 803-808.
35. Nakamura, S.; Kobayashi, T.; Takata, A.; Uchida, K.; Asano, Y.; Murakami, A.; Goldberg, A.; Guillaumont, D.; Yokojima, S.; Kobatake, S.; Irie, M., Quantum yields and potential energy surfaces: A theoretical study. *Journal of Physical Organic Chemistry* **2007,** 20, (11), 821-829.

36. Uchida, K.; Irie, M., A photochromic dithienylethene that turns yellow by uv irradiation. *Chemistry Letters* **1995**, (11), 969-970.
37. Saito, M.; Musha, K.; Ikejima, T.; Ozawa, S.; Yokoyama, Y., Photochromism of diarylethenes in DNA-quaternary ammonium ion complex. *Kobunshi Ronbunshu* **2003,** 60, (10), 581-589.
38. Wang, C. J.; Delcros, J. G.; Biggerstaff, J.; Phanstiel, O., Molecular requirements for targeting the polyamine transport system. Synthesis and biological evaluation of polyamine-anthracene conjugates. *Journal of Medicinal Chemistry* **2003,** 46, (13), 2672-2682.
39. D.A. Case, T. A. D., T.E. Cheatham, III, C.L. Simmerling, J. Wang, R.E. Duke, R. Luo,; M. Crowley, R. C. W., W. Zhang, K.M. Merz, B.Wang, S. Hayik, A. Roitberg, G. Seabra, I.; Kolossváry, K. F. W., F. Paesani, J. Vanicek, X.Wu, S.R. Brozell, T. Steinbrecher, H. Gohlke,; L. Yang, C. T., J. Mongan, V. Hornak, G. Cui, D.H. Mathews, M.G. Seetin, C. Sagui, V. Babin,; Kollman, a. P. A. *Amber 10*, University of California, San Francisco., 2008.
40. Hornak V, A. R. O. A., Strockbine B, Roitberg A , Simmerling C Comparison of multiple amber force fields and development of improved protein backbone parameters. *Proteins-Structure Function and Bioinformatics* **2006,** 65, (3), 712-725.
41. Wang JM, W. R., Caldwell JW, Kollman PA, Case DA Development and testing of a general amber force field. *Journal of Computational Chemistry* **2004,** 25, (9), 1157-1174.
42. Jorgensen, W. L., Quantum and statistical mechanical studies of liquids.10. Transferable intermolecular potentail functions for water, alcohols, and ethers - application to liquid water. *Journal of the American Chemical Society* **1981,** 103, (2), 335-340.
43. Berendsen, H. J. C., Postma, J. P. M., Vangunsteren, W. F., Dinola, A., Haak, J. R., Molecular-dynamics with coupling to an external bath. *Journal of Chemical Physics* **1984,** 81, (8), 3684-3690.
44. Essmann, U., Perera, L., Berkowitz, M. L., Darden, T., LEE, H., Pedersen, L.G. , A smooth particle meah ewald method. *Journal of Chemical Physics* **1995,** 103, (19), 8577-8593.
45. Ryckaert, J. P., G. Ciccotti, and H. J. C. Berendsen., Numerical integration of the cartesian equations of motion of a system with constraints: Molecular dynamics of n-alkanes. *Journal of Computational Physics* **1977,** 23, (3), 327-341.
46. Humphrey, W., Dalke, A. and Schulten, K., Vmd - visual molecular dynamics. *Journal of Molecular Graphics* **1996,** 14, (1), 33-38.

SUMMARY

This Thesis describes the theoretical study aimed to predict various essential properties for the functional organic molecules that belong to diarylethene (DA) family of photochromic compounds. These photochromic materials can be used for optical data storage, photoswitching, and other photonic applications. We applied Density Functional Theory methods to predict 6 of the relevant properties: (i) molecular geometry; (ii) resonant wavelength; (iii) thermal stability; (iv) fatigue resistance; (v) quantum yield and (vi) nanoscale organization of the material.

We started with a benchmark set of 28 diarylethenes and optimized these structures and calculated their vertical absorption spectra. Bond length alternation (BLA) parameters and maximum absorption wavelengths (λ_{max}) were compared to the experimental data from X-ray diffraction studie and spectroscopy experiments. We validated TD-M05/6-31G*/PCM//M05-2X/6-31G*/PCM level of theory to give the best predictions for both parameters (RMSDare below 0.014 Å for the BLAs and 25 nm for λ_{max}). We also found that the polarization functions in the basis set and use of polarizable continuum model to account for solvent effects are both important for good agreement.

Next we considered thermal stability for a set of 7 photochromic compounds. From our studies we found out that both UB3LYP and UM05-2X functionals predict the activation barrier for the cycloreversion reaction within 3-4 kcal/mol from experimental value. We also investigated the mechanism of by-product formation in photochromic

compounds, defined as the rate of undesirable photochemical side reactions. It has been established experimentally that the by-product is formed from the closed isomer; however, the mechanism was not known. We found that the thermal by-product pathway involves the bicyclohexane (BCH) ring formation as a stable intermediate, while the photochemical by-product formation pathway may involve the methylcyclopentene diradical (MCPD) intermediate. At UM05-2X/6-31G* level, the calculated barrier between the closed form and the BCH intermediate is 51.2 kcal/mol and the barrier between the BCH intermediate and the by-product 16.2 kcal/mol.

Next we investigated two theoretical approaches to predict the quantum yield (QY) for a set of 14 diarylethene derivatives at the validated M05-2X/6-31G* theory level. Photocyclization quantum yield was evaluated based on the Boltzmann distribution of the equilibrium ground state reactive and unreactive conformations and the result was in qualitative agreement with the experimental QY. Correlation of experimental cycloreversion quantum yield with various properties of the excited state isomers on the potential energy surface was made. We concluded that the relative position of the pericyclic minimum on the 2A excited state surface with that of the transition state on the ground state can be used to explain the high or low QY for (I)-type and (N)-type molecules. We confirmed that the internuclear distance (longer C—C bond) correlates with high quantum yield. We also concluded that low energy difference between the 2A state closed isomer and the pericyclic minimum is associated with the higher QY.

Finally, we investigated the possibility of nanoscale organization of the photochromic material based on DNA template, as an alternative to the amorphous

polymer matrix. We performed molecular dynamics simulations on a series of ligand-DNA systems in which the ligand was intercalated in the DNA. The free energy binding calculations indicate ligand-DNA intercalation complex to be stable. However, the dissociation constant values exceeded the experimental values by an order of magnitude.

In summary, we conclude that Density Functional Theory methods could be successfully used as an important component of material design strategy in prediction of accurate molecular geometry, absorption spectra, thermal stability of isomers, fatigue resistance and quantum yield. The photophysical properties of nanocomposites are a subject to future studies.

LIST OF PUBLICATIONS

1. Patel, P. D.; Masunov, A. E., Theoretical Study of Photochromic Compounds. 1. Bond Length Alternation and Absorption Spectra for the open and Closed Forms of 29 Diarylethene Derivatives. *Journal of Physical Chemistry A* **2009,** 113, (29), 8409-8414.

2. Patel, P. D.; Mikhailov, I. A.; Belfield, K. D.; Masunov, A. E., Theoretical Study of Photochromic Compounds, Part 2: Thermal Mechanism for Byproduct Formation and Fatigue Resistance of Diarylethenes Used As Data Storage Materials. *International Journal of Quantum Chemistry* **2009**, 109, (15), 3711-3722.

3. Patel, P. D.; Masunov, A. E., Time-dependent density functional theory study of structure-property relationships in diarylethene photochromic compounds. In *Computational science – ICCS 2009, part ii, lecture notes in computational science (LNCS).* Seidel, E.; Allen, G.; Nabrzyski, J.; van Albada, D.; Dongarra, J.; Sloot, P., Eds. Springer: Baton Rouge, Louisiana, USA, **2009**; Vol. 5545, pp 211-220

4. Patel, P. D.; Masunov, A. E., Theoretical Study of Photochromic Compounds. 3. Thermal Stability of Diarylethene Derivatives. *To be submitted to Journal of Molecular Modeling.*

5. Patel, P. D.; Masunov, A. E., Theoretical Study of Photochromic Compounds. 4. Quantum Yield of Diarylethene Derivatives. *in preparation: Journal of Physical Chemistry C*

6. Patel, P. D.; Roitberg, A. E.; Masunov, A. E.; Archer, J. Phanstiel IV, O., Molecular Dynamics Simulations of interactions between anthracene-polyethyleneamine conjugates with DNA. *To be submitted to Journal of Biophysical Chemistry.*